On the Electronic Structure and Properties of Boron Allotropes and Boron-Rich Solids

A Thesis
Submitted for the Degree of
Doctor of Philosophy

by

Dasari L. V. K. Prasad

School of Chemistry
University of Hyderabad
Hyderabad – 500 046
INDIA

December 2008

To my parents, grand parents, sisters, brothers, brother-in-law, uncles, aunts, cousins, niece, nephew and the entire kinship

CONTENTS

STATEMENT

I hereby declare that the work embodied in this thesis is the result of investigations carried out by me in the School of Chemistry, University of Hyderabad, Hyderabad, India, under the supervision of Prof. E. D. Jemmis and Prof. T. P. Radhakrishnan.

In keeping with the general practice of reporting scientific observations, due acknowledgements have been made whenever the work described is based on the findings of other investigators.

Dasari L. V. K. Prasad

CERTIFICATE

Certified that the work included in this thesis entitled “On the Electronic Structure and Properties of Boron Allotropes and Boron-Rich Solids” has been carried out by Dasari L. V. K. Prasad under my supervision and the same has not been submitted elsewhere for any degree.

Prof. E. D. Jemmis
(Thesis Supervisor)

Prof. T. P. Radhakrishnan
(Thesis Co-Supervisor)

Dean
School of Chemistry

ACKNOWLEDGEMENTS

I would like to thank my doctoral supervisor, Prof. E. D. Jemmis for his guidance, insight, and invaluable help during the course of research on boron allotropes. I am also grateful to him for his kindness and encouragement. I thank my co-supervisor Prof. T. P. Radhakrishnan for his prompt help and support.

I thank the Dean and all the faculty members of the School of Chemistry, University of Hyderabad (UoH); especially I wish to express my appreciation to the quantum group, Prof. K. D. Sen, Prof. M. Durga Prasad, and Prof. S. Mahapatra. My special thanks to Prof. M. Periasamy, Prof. D. Basavaiah, Prof. A. K. Bhuyan, and Prof. Lalita Guruprasad for their affection. I also wish to thank the faculty at IPC and SSCU, Indian Institute of Science (IISc) for their seminars, discussions and wishes, whom I met when we transferred from UoH to IISc. I also thank the faculty at TSU/CPMU, Jawaharlal Nehru Centre for Advanced Scientific Research for organizing excellent symposia and workshops. I wish to thank Prof. A. Chatterjee at Physics, UoH & Prof. C. Dasgupta at Physics, IISc, for their introductory lectures on Solid State Physics.

I wish to thank the non-teaching staff both at UoH and IISc for their assistance. I thank the Center for Modelling Simulation and Design (CMSD) at UoH and Supercomputer Education and Research Center (SERC) at IISc for computational resources. I am grateful to Mr. Vinod Kumar and Mr. Kiran for their valuable technical help in running the calculations and Dr. Greg, Dr. Phil, and Dr. Reuti for rectifying the errors in the programs. I thank Council of Scientific and Industrial Research (CSIR) and Department of Science and Technology (DST) for research fellowship and international travel grant.

I am indebted to Prof. Pavel D'yachkov for his gracious help during my stay in Russia. I also thank the support from Dr. Nina, Evgeny, Vesnyan, Natalia, and Natasha without them the trip may not be a memorable. I am also grateful to Dr. A. L. Tchougreeff, Dr. Alex, and all the speakers and participants of 11th V.A. Fock Meeting.

I would like to thank the members of EDJ group. Thanks to Anoop for long discussions on solving chemical problems using computers. I thank the electron counting group Balu, Pancharatna, and Jayasree for helpful discussions. I wish to thank Usha who introduced biology to the group and I also thank her son, Chandrasekhar for his school tales. I also would like to thank Aswini, Deshigan, Param, Bishu, Jorly, Susmita, and the newbies at IISc, Shameema, Hari, Dibyendu and Subhendu for all their enthusiastic discussions. My special thanks to Anne for her helpfulness. I thank Dr. B. V. Prasad, Dr. G. N. Sastry, Dr. Pankaz, Prof. Hynk, Prof. N. Hosmane, Prof. Sason Shaik and Prof. Wesley D. Allen for their helpful discussions when they visited the group. I also thank the summer students Gopan, Rajesh, Shanthi, Cláire, Umayal, Deepti and Jyoti. It is my great delight to meet my monsoon friend Marc when he visited the group and I thank for his wishes. The group social gatherings are unforgettable. I especially wish to thank Prof. E. D. Jemmis' family for cordial support and for delicious dishes on the eve of Christmas get-togethers.

I thank my well-wishers at IISc, S.S.Rao, K.P.Rao, Naresh, Koti, Basu, V.S.Rao, Manju, Praveen, Sundar, Santhosh, Kotesh & team; and Vijay, G.Srinivas, Anjan, Koushik, Vasu, Suresh, Murthy, Prio, Debojyoti, Patra, Nagaraj, Devaraj, Bani, Animesh, Ramkumar, Viswanath, B.Ragavendra, Rakshit, Dipak, Vikranth, Rajesh, Suresh Babu, Kiran, Phani, Kola, Chakrapani, Udishnu, Arun, Raj, Venkat, Basha, Venkteswarlu, Hembram, Bargava, Srijan, Anki, Raghavendra, Chandrashekar, Jagadheesh, V.Prakash, Shekar, Kiran, Naveen, Shailesh, and Jovan at Pune, for their help and wishes.

I thank my friends at UoH, Karunakar, Sundar, Ravi, Israel, Jaya Prakash, Durga Rao, Chinni-Krishna, Sateesh, Muthu, Chinna, Praveen, Shiva, KK, Suneel, Kishore(3), K.Rao, S.Rao, Venkatrao, Sakhi, Salmon, for their support, affection, grace, and concern. I also would like to thank Raghavaiah, Lincoln, Swathi, Supriaya, Prabhakar, Satyam, Prashanth, Vijay, Lenin, Subba Rao, Harish, Kanakaraj, Khatema, Koti-Kamal, Raghunanth Babu, Prabhakar-Dhanaraj, Koti, Bheem, David, Ramesh, Santhosh, A.P.Venkat, Yedukondalu, Santaiah, Sundaraiah; the alumni of I-203, Ratnakar, Shankar, Bhushan, Sheshubau; Chiru, Anwar, Bhuvan, N.Hari, Veeru, D.K.Rao, Kavita, Yadi & friends; Sharath, G.K.Prasad, Abhijit, Armugham, S.Prasanth, Ravi, Nagaraj, Ramu, Vikram, Rajesh, Ramesh, Hariprasad, Gupta, and [a-z]* for all their wishes.

I cordially thanks to my Ongole – school, college friends, Jayasimha, Jagadheesh, Venkat, J.Narayana, Chakrapani, Iliyas, Ramu, Ramana, Suresh, Anand, Vital, Rajesh, Madhava Rao, Vasanth and team and the elderly friends for their splendid support and wishes. Its my great pleasure to have such wonderful friends.

I would like to thank my school college, and fellowship teachers, Balakotaiah, Syamala Devi, Bhaskara Rao, Ramalingam, Samadanam, Sarojini Devi, Jhansirani, Badari, Srinivasa Rao, Venkateswarlu, K.V.Subramanyam, Appa Rao, Prasada Rao, Ramanaiah, Salmon, YSPS, Seetaramaiah, Chiranjeevi Prasad, Sadu, Abishekam, Isaac, and Florence for the lessons they taught me and for their guidance and affection.

It is entirely inadequate to thank my parents, grand parents, sisters, brothers, brother-in-law, uncles, aunts, cousins, niece, nephew, and the entire kinship – who have always been my biggest admirers. No words can possibly express my gratitude for everything they have given me. I am grateful for their affection, continuing support, motivation, and for the sacrifices they have made for me. Thank you all, thank you very much. Finally, my endless thanks to the source of light, may your name be exalted, honored and glorified.

ABSTRACT

This thesis entitled “On the Electronic Structure and Properties of Boron Allotropes and Boron-Rich Solids” consists of five chapters. Chapter 1 gives an overview of the thesis which includes a brief history of chemical bonding in boron compounds followed by the summary of the problems discussed in the later chapters and quantum mechanical methods that are employed to understand the electronic structure, bonding, and properties of boron clusters, allotropes of boron, and boron-rich solids. Electronic structure, thermodynamic stability, and defects of the allotropes of boron using cluster fragment approach and macropolyhedral borane skeletal electron counting rules (*mno*) are presented in Chapter 2. Fullerene-like boron and boron carbide clusters stuffed with icosahedral B_{12} units are described in Chapter 3, where the viability of the clusters is appraised by the polyhedral skeletal electron counting, valence, topological charge stabilization, and orbital overlap compatibility rules. Chapter 4 covers electronic structure and conducting properties of boron and boride sheets, nanotubes, and fullerenes analogous to low dimensional allotropes of carbon. In Chapter 5, electronic and structural origin of mechanical stability and properties of boron allotropes and boron-rich icosahedral cluster solids are presented.

Chapter 1

Overview

1.1 Chemical Bonding in Boron Compounds

Boron compounds such as boric acid (H_3BO_3) and sodium borate ($Na_2B_4O_7.10H_2O$) have been known since ancient times as cleaning agent, glassifier, and potter glaze. However, the discovery of elemental form of boron has taken quite a long time. It was discovered in 1808 by the trio Joseph-Louis Gay-Lussac, Louis-Jacques Thenard, and Humphrey Davy. This year marks the bicentenary year of the elemental boron. By the middle of the 20th century many of its allotropes have been uncovered. Among them α- and β-rhombohedral (α-B_{12} and β-B_{105}) and α- and β-tetragonal boron (α-B_{50}, β-B_{192}) were crystallized with reasonable purity and refined fairly well with the available X-ray diffraction techniques. Subsequently boron-rich solids evolved. The structures are found to be dominated by the distinctive deltahedral skeletons (polyhedron with triangular faces) associated with unusual chemical bonding.[1-8] Parallelly plenty of hydrides of boron

called boranes and their derivatives were actively synthesized. The structure, bonding, and properties of these compounds were a puzzle to understand in comparison to the known hydrocarbons and allotropes of carbon.[9-14] However, with the aid of developing quantum chemistry the chemical bonding in boranes were interpreted as electron deficient.[15-17] That is a pair of electron can share more than two atoms, for example, three atomic centers sharing two electrons (3c-2e). This differs from the conventional wisdom of two electrons forms a chemical bond between two atomic centers (2c-2e). In a more general way the electron deficiency is: the number of valence electrons is less than the valence orbitals. This created novel vistas in understanding the chemical bond and propelled to explain the structural details of boranes and allotropes of boron and consequently the diverse chemical and physical properties of them.

The predicted structure and bonding in boron compounds was later successfully proved by low temperature X-ray diffraction and infrared spectroscopic techniques.[4-8,18] The simplest 3c-2e borane is diborane (B_2H_6), which is much like ethylene having two bridged hydrogens in the middle of molecule as shown in Figure 1.1a. How this 3c-2e bond can explain the bridged structure of B_2H_6? The formula B_2H_6 composed of eight atoms conventionally requires at least seven 2c-2e bonds to form a molecule of the kind of C_2H_6 (Figure 1.1b). Then the seven 2c-2e bonds need fourteen valence electrons. But in B_2H_6 the number of valence electrons is only twelve. Therefore B_2H_6 does not have enough electrons for every bond to be associated with two electrons and hence an electron deficient molecule. It suggests some atoms in B_2H_6 should share less than a pair of electron to be associated. The two boron atoms in B_2H_6 are bonded to two hydrogen atoms each by the formation of four electron sufficient 2c-2e B-H bonds (terminal bonds)

which demands eight electrons. The remaining two hydrogen atoms are bridged between the two boron atoms with electron deficient 3c-2e B-H_μ-B bridge bonds which require only four electrons (Figure.1.1a). This completes the total usage of 12 valence electrons of B_2H_6. Thus the deficiency of two electrons is ingeniously compensated by the formation of bridged electron deficient B-H_μ-B bonds in B_2H_6. This is the first structure with 3c-2e bridged B-H_μ-B bond formulated by Longuet-Higgins by introducing the concept of electron deficient chemical bond.[15-17]

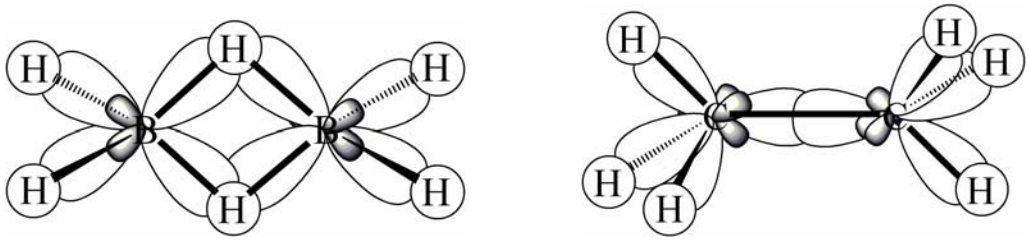

Figure 1.1. left **(a)** The structure of B_2H_6 and right **(b)** structure of C_2H_6

The higher boranes (generally called as borane clusters) acquired deltahedral structures which are highly complex in terms of their many 3c-2e bonding.[19-25] The boranes are mainly classified as *closo*-B_nH_{n+2} (closed polyhedral clusters), *nido*-B_nH_{n+4} (opened polyhedral clusters), and *arachno*-B_nH_{n+6} (more opened polyhedral clusters) as shown in Figure 1.1c-e.[26-27] Owing to their topological resemblances with solid geometries graph theoretical methods also played an immense role in understanding their structures.

The expanded version of the valence chemical bond and the availability of many boron compound structures further led to propose qualitative valence, skeletal electron

counting, and topological rules to generalize and explain the structure and bonding in boranes, allotropes of boron and their compounds. It is Lipscomb who started in generalizing the structure and stability by introducing a valence description of boranes (B_nH_m) in terms of the semi-topological scheme, "*styx* numbers".[27-30] Here *s* is the number of B-H_μ-B bridging bonds, *t* is the number of 3c-2e B-B-B bonds, *y* is the number of 2c-2e B-B bonds, and *x* is the number of BH_2 terminal groups. According to this scheme the structure and stability of B_nH_m can be evaluated by equating the sum of *styx* value to the half of the total number of atoms [(*s*+*t*+*y*+*x*) = (N)/2]. The sum of *styx* value is also equivalent to the number of framework or skeletal electrons. The number of skeletal electrons can be calculated as: each BH_2 and BH terminal groups gives one and two electrons and the remaining *m*-*n* bridged hydrogens (H_μ) supplies one electron each. For example, in B_2H_6 the *styx* value is *2002* where the sum of *s*+*t*+*y*+*x* = 4 = N/2 and also equal to the number of skeletal electrons [2(BH_2) + 2(H_μ) = 2 + 2 = 4] which satisfies the structure of B_2H_6 (Figure 1.1a). Similarly the *styx* rule can be applied to several other open borane structures such as B_4H_{10} (*styx = 4012*), B_5H_9 = (*styx = 4120*), B_6H_{10} (*styx = 4220*) etc.

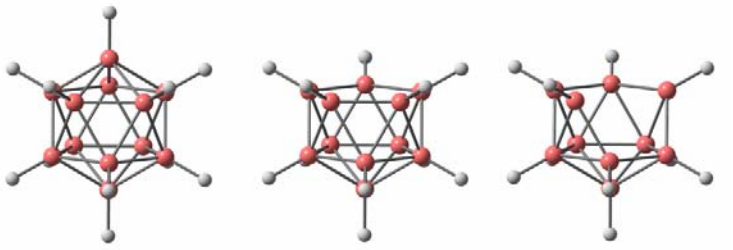

Figure 1.1. (left) **(c)** *closo*-$B_{12}H_{12}$, (middle) **(d)** *nido*-$B_{11}H_{11}$, and (right) **(e)** *arachno*-$B_{10}H_{10}$ boranes. The extra hydrogen atoms are not shown for clarity in *nido*- and *arachno*- boranes whereas in *closo*- borane though the general formula given as B_nH_{n+2} later it was modified to B_nH_n.

However, for *closo*- boranes and larger open cluster boranes the *styx* scheme became tedious in assigning the group values. Later on Wade proposed a set of skeletal electron counting rules called Wades rules based on linear combination of atomic orbitals (LCAOs) or molecular orbitals (MOs) approach.[31-34] These rules had explained many mono-polyhedral borane structures. According to these rules stable mono *closo*-, *nido*- and *arachno*- boranes requires *n*+1, *n*+2, and *n*+3 skeletal electron pairs respectively. The requirement of skeletal electrons can be explained by taking an icosahedral *closo*-$B_{12}H_{12}$ borane as an example. Here, the boron atomic orbitals (AOs) are divided into four. Two of them are *sp* hybrid orbitals directed radially outwards and inwards of the icosahedron. The rest of the two pure *p* orbitals are oriented tangentially to the icosahedron as shown in Figure 1.1f. These set of radial and tangential orbitals from each boron of icosahedron combines according to symmetry and generates 48 MOs. Out of 48 MOs 13 are skeletal bonding MOs, 12 are 2c-2e B-H terminal σ bonds, and the remaining 23 are antibonding. Among the 13 skeletal bonding MOs 12 MOs are belongs to the different combinations of radially outward *sp* orbitals and the remaining one MO is the in phase combination of radially inward *sp* orbitals. In order to fill all the 25 bonding MOs [13 skeletal MOs + 12 2c-2e B-H terminal σ bonds] it requires 50 valence electrons. But $B_{12}H_{12}$ has only 48 valence electrons (three electrons from each boron and one from each hydrogen = 12(3) + 12(1) = 48]. Therefore, $B_{12}H_{12}$ requires extra two electrons for the stability of the icosahedral structure. Wade has observed this similar trend in all the *closo*- polyhedral boranes where the number of skeletal bonding MOs are *n*+1 (*n* = number of vertices in polyhedron), number of 2c-2e B-H terminal σ bonds are *n*, and the remaining MOs are antibonding. Leaving the 2c-2e B-H terminal σ bonds as they are satisfied with electron

sufficient bonds, the skeletal *n*+1 electron pairs are necessary to stabilize the *closo*-polyhedra. Hence Wade proposed a general *n*+1 rule as the requirement of skeletal electrons for stable *closo*- polyhedral boranes. The *n*+1 rule can be crosschecked by counting back the total available skeletal electrons in *closo*- polyhedral borane. For example, in $B_{12}H_{12}$ we have 12 (BH) groups and each BH group provides two skeletal electrons i.e. altogether 12 skeletal electron pairs. But according to the Wade's *n*+1 rule $B_{12}H_{12}$ is short of two electrons and hence stable $B_{12}H_{12}$ is a dianionic species ($B_{12}H_{12}^{-2}$).

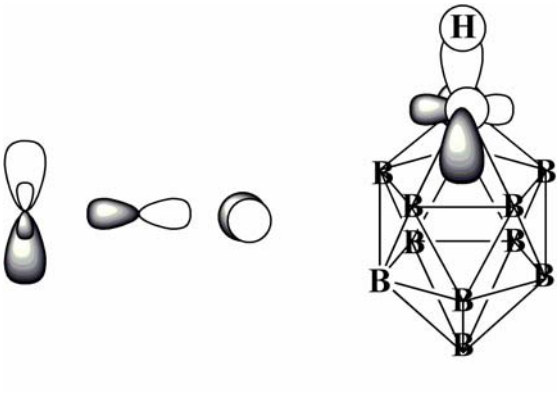

Figure 1.1(f). The atomic orbitals of boron, two *sp* hybrid orbitals (radially inward and outward), two pure *p* orbitals (tangential) centered on the boron vertex is depicted here. The radially inward *sp* and the two tangential *p* orbitals are skeletal orbitals which forms cluster bonding whereas the radially outward *sp* orbital forms 2c-2e σ bond with the terminal (or *exo*-) hydrogen.

Wade has extended the general applicability of the *closo*- *n*+1 rule to other classes of boranes, *nido- and arachno*- boranes where a stable *nido*- and *arachno*- boranes requires *n*+2 and *n*+3 skeletal electrons.[33,34] The rules can be explained easily by taking the examples given in Figure 1.1c-e. According to *closo*- *n*+1 rule $B_{12}H_{12}$ is dianionic

($B_{12}H_{12}^{-2}$). Removal of a BH group from $B_{12}H_{12}^{-2}$ we get the *nido*-$B_{11}H_{11}$ (Figure 1.1d) which is tetraanionic ($B_{11}H_{11}^{-4}$) since the removed BH group takes two electrons from the skeletal bonding. Similarly removal of another BH group from $B_{11}H_{11}^{-4}$ gives the *arachno*-$B_{10}H_{10}$ which is hexaanionic ($B_{10}H_{10}^{-6}$). In other words removal of a BH group from stable *closo*- polyhedra further requires those many electrons to stabilize the resultant structure within in the polyhedron skeleton as shown in Scheme 1. In the known experimental structures of boranes the extra anionic charge is compensated either by the counter cations or by the bridging hydrogens.

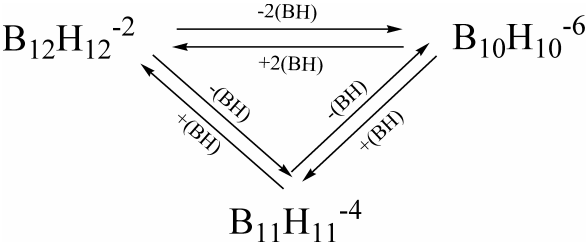

Scheme 1

The successful applicability of Wades rules are further verified by Stone tensor surface harmonic (TSH) theory[35] and graph theoretical approach of Aihara, King, and Rouvray.[36,37] Rudolph and Mingos had discussed paradigm for the electron requirements of clusters and polyhedral skeletal electron pair approach to unify these aspects.[38-41]

Here we must remember that before generalizing the concepts of bonding in polyhedral boranes by Wade and others, the deficiency of the two electrons in B_{12} fragment of α-rhombohedral boron (α-B_{12}) and boron carbide crystals ($B_{12}C_3$) had already been conceived by the pioneering work of Longuet-Higgins.[42,43] He also

suggested the possibility of $B_{12}H_{12}^{-2}$ before it got synthesized. This is quite similar to the structural links between hydrocarbons and allotropes of boron, where the terminal CH σ bonds condense to build up the carbon allotropes or the vice versa.

Lipscomb states in his Noble lecture (December 11, 1976)[44] about this missing structural link between the molecules and solids

"A B_6 octahedron was known in certain crystalline borides and the B_{12} icosahedron was found in boron carbide, but no one realized that a systematic description of the boron arrangements in these hydrides might be based on fragments of these polyhedra."

Though the idea of relating fragments of boron allotropes to boranes was envisaged, the electron counting rules introduced so far are not suitable in explaining the electronic requirements for elemental β-rhombohedral boron and its fragments. Because the fragments are not mono polyhedral skeletons they are condensed macropolyhedral skeletons where Wade's rules will not be applicable. Few of the condensed macropolyhedral boranes also have been synthesized whose electronic requirements are beyond the Wades rules. This gap was recently fulfilled by Jemmis and co-workers who introduced a unified electron counting rule called *mno* macropolyhedral borane skeletal electron counting rule.[45-48] According to the *mno* rule a condensed macropolyhedral borane requires $m+n+o$ (where n= number of vertices, m= number of condensed polyhedrons, and o= number of single vertex sharing) skeletal electron pairs for the stability. As an example here we will consider $B_{21}H_{18}$ which is derived from the condensation of two $B_{12}H_{12}^{-2}$ via triangular face sharing as shown in Figure 1.1g.

According to the *mno* rule, the number of polyhedra, m = 2, the number of vertices n = 21, and the number of single vertex sharing o = 0. The total number of skeletal electron pairs should be 2 + 21 + 0 (m+n+o) = 23. Therefore the *mno* rule suggests $B_{21}H_{18}$ should have 23 skeletal electron pairs for stability. We could calculate the number of available skeletal electron pairs in $B_{21}H_{18}$ in the same manner that we have done previously for Wade's rules. In $B_{21}H_{18}$, there are 18 BH groups each providing an electron pair. The three bridging boron atoms together provide 4.5 electron pairs. This leads to a total number of available electron pairs = 22.5 (18 + 4.5) which is one electron less than the required number of electron pairs (23). Hence a stable $B_{21}H_{18}$ is an anionic species. Similarly we can apply the *mno* rule on variety of condensed macropolyhedral boranes to evaluate their electronic requirement and hence their stability. This had led Jemmis and coworkers to propose a complete electronic requirement for the most complex crystal structure of elemental β-rhombohedral boron using *mno* electron counting rule. Thus the *mno* electron counting rule facilitated in relating boranes with allotropes of boron much similar to the connection between hydrocarbons and allotropes of carbon.

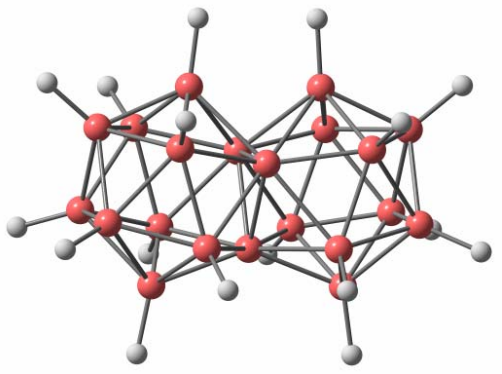

Figure 1.1(g). Structure of $B_{21}H_{18}$ derived from the condensation of two $B_{12}H_{12}^{-2}$ units via triangular face sharing.

The general understanding of the chemical bonding in boranes, allotropes of boron, and boron-rich solids structures are still evolving. Their unusual structures, chemical and physical properties like catalysis, large neutron absorption cross section (760 barn), low density (2.47 g/cm^3), high melting point (~2300 °C), thermo electric, high mechanical strength, ability to withstand to hostile conditions, etc prompted many people to chose as one of the promising area to explore the unknown details of structure, stability, and properties. In this thesis we presented few such unknown details using the established chemical bonding ideas and electron counting rules of boranes and verified by the *ab initio* (or also called first principles) density functional theory calculations. The details of the problems discussed in this thesis and the computational methods that are used to solve the problems are outlined in the next two sections.

1.2 Outline of the Problems Discussed in the Thesis

Over the years the structure, bonding, and properties of boranes and their derivatives are largely understood. However, the allotropes of elemental boron and boron-rich solids are still underway. It is because of their rather complex crystal structures outfitted with disorders in the form of partially occupied lattice and interstitial sites (intrinsic defects) which originated from the electron deficiency and the five-fold symmetry of the ubiquitous icoashedral B_{12} bonding network. In particular, the elemental β-rhombohedral boron and boron-rich icosahedral cluster solids (BRICS) are mystifying with their complex three dimensional (3D) condensations of icoashedral B_{12} skeletons.

The complexity has prevented the realization of the detailed electronic structure, stability, and properties. A certain reduction of this complexity was achieved by relating condensed polyhedral boranes to elemental β-rhombohedral boron just as condensed benzenoid aromatics are related to graphene using *mno* macropolyhedral borane skeletal electron counting rules introduced in our lab earlier.[49] However, the role of the intrinsic defects in thermodynamic stability, electronic conduction, and mechanical stability of β-rhombohedral boron are not clear.

In Chapter 2, we make use of the structural connections between boranes and elemental boron and the *mno* macropolyhedral borane skeletal electron counting rule to investigate the role of the intrinsic defects in thermodynamic stability and electronic conduction of β-rhombohedral boron using *ab initio* density functional theory calculations. The calculations show that ideal i.e intrinsic defect-less β-rhombohedral boron (β-B_{105}) is less stable than α-rhombohedral boron (α-B_{12}) and the band structure of β-B_{105} indicates valence electron deficiency and hence metallic behavior. This is in contrast to the experimental result that β-rhombohedral boron is the thermodynamically most stable allotrope of boron with semiconducting nature. The inconsistency of the results is mainly because the ideal β-B_{105} does not represent the real structure which is β-$B_{106.83}$ having intrinsic defects. Therefore it is necessary to study the electronic structure of β-rhombohedral boron crystal structure with intrinsic defects. Unfortunately, incorporating these intrinsic defects would lead to a large unit cell which forbids computing. In order to overcome this problem we proposed model solids based on cluster fragment approach using macropolyhedral borane skeletal electron counting rules to

closely represent the electronic structure of β-$B_{106.83}$. The analysis suggests that the defects in the real β-rhombohedral boron ($B_{106.83}$) are necessary to stabilize the structure and also for its semiconducting property.

On the other hand boron is not known to form allotropes with varied dimensions (D) like its next neighbor carbon, "fullerenes (0D), nanotubes (1D), and graphene (2D)" due to intrinsic electron deficiency. Of course, no other element like carbon is known to form allotropes with range of dimensions. In Chapter 3, we show that 0D boron clusters B_{98}, B_{100}, B_{101}, and B_{102} based on electron deficient stuffed fullerene-like icosahedral B_{84} fragment of elemental β-rhombohedral boron are viable using *ab initio* density functional theory calculations. These are envisaged as an icosahedral B_{12} each vertex of which is connected to the apex of a pentagonal pyramid (B_6) via radial 2*c*-2*e* σ bonds. The resulting B_{84} ($B_{12}@B_{12}@B_{60}$) retains the same symmetry as C_{60}, and the B_n (n= 84 to 116) clusters are generated around it. The stability of these clusters is estimated as a function of electron count using the Wade's polyhedral skeletal electron counting rules. This has further prompted us to propose fullerene-like boron carbide clusters $C_{50}B_{34}$ and its isomers based on B_{84} skeleton akin to the process of stabilizing borane dianions as carboranes. The structure and the stability of these clusters are compared with the standard *closo*- and *nido*- carboranes. The curvature of the $C_{50}B_{34}$ stuffed fullerene was found to play a vital role in achieving the most stable isomer of it. Further, three dimensional aromaticity, electron detachment energies, and IR, Raman active modes are calculated which can help experimental characterization.

The search for low dimensional allotropes of boron is further extended based on isoelectronic and structural similarities between carbon and known metal borides. The graphene analogue of magnesium diboride ($Mg^{+2}B_2^{-2}$~C_2) and polycarbyne analogue of lithium boride chain ($Li^{+}B^{-}$~C) are notable experimental examples. This view suggests that if boron were to adopt the carbon skeleton it would need an extra electron per atom for the stability. If the extra electrons are provided by the additional boron atoms properly then we would see boron allotropes analogous to carbon. In that prospect we show systematically the adaptation of carbon sheets, nanotubes, and fullerenes by boron and with respect to the electron count using *ab initio* density functional and semi-empirical tight-binding calculations in Chapter 4. The density of states calculations indicate boron sheets are metallic whereas graphene is a semi-metal. On the other hand boron nanotubes are metallic or semiconductor depending on the diameter of the tube but not on the chirality which differs from carbon nanotubes where the conductivity depends on both diameter and chirality. MgB_2 sheets and tubes are found to be metallic.

The allotropes of boron and boron-rich solids are known for their robust mechanical properties and greater hardness. However, the mechanical properties of these promising materials are not clear from theory and experiments due their intrinsic defects and lack of large pristine samples respectively. In Chapter 5, we presented complete list of elastic constants and their derived properties such as bulk modulus, shear modulus, and young's modulus of α-B_{12}, β-B_{105}, and bulk modulus of boron carbide ($B_{12}C_3$), and boron suboxide ($B_{12}O_2$) using *ab initio* density functional theory calculations. The elastic constants and their derived properties are compared with the available experimental results. The available experimental results are in good agreement with α-B_{12}, $B_{12}C_3$, and

$B_{12}O_2$ but not with β-B_{105}. The results presented in Chapter 2 indicate the absence of the intrinsic defects in β-B_{105} could be the reason for the disagreement of theoretical results with the experiments. Therefore we have calculated elastic constants and their derived properties for the solids modeled in the Chapter 2 which closely represent the electronic structure of experimental β-rhombohedral boron (β-$B_{106.83}$). The results of the modeled solids nearly match with the β-$B_{106.83}$. This analysis suggests that the intrinsic defects in β-rhombohedral boron are necessary for their mechanical stability. We further calculated bulk properties of $B_{12}C_3$ and $B_{12}O_2$ as a function of electrons by doping different atoms. We found that the electron precise solids are harder than the deficient ones.

1.3 Outline of the Computational Methods

Various quantum mechanical methods starting from semi-empirical extended Hückel (eH)[50] to *ab intio* density functional theories (DFT) are employed to study the above problems. Broadly, the molecular clusters have been dealt with localized Gaussian (Pople and Dunning) and numerical (Delley) basis sets.[51-53] The solids are studied with plane-wave basis sets and Vanderbilt ultrasoft pseudopotentials[54,55] (in eH, YAeHMOP parameters are used). The local density approximation (LDA) of Ceperley and Alder–Perdew and Zunger (CA-PZ),[56,57] generalized gradient approximation (GGA) of Perdew-Burke-Ernzerhof (PBE) exchange-correlation functionals,[58] and Becke three parameter exchange and Lee-Yang-Parr local and non-local correlation hybrid DFT functional, B3LYP are used.[59] The respective computational methods used are presented in the

individual chapters under the section of computational methods. The theoretical basis of these computational methods is briefly outlined here.

1.3.1 Extended Hückel Method

The extended Hückel method (eHM) also called as tight-binding method is based on one electron approximation.[50] The valence electron Hamiltonian is taken as some of one-electron Hamiltonian

$$H_{val} = \sum_i H_{eff}(i) \qquad \text{---------- (1)}$$

where the $H_{eff}(i)$ Hamiltonian is not specified explicitly.

The wavefunction (ψ_i) or molecular orbital is approximated in terms of linear combination of valence atomic orbitals (LCAO) of the atoms.

$$\psi_i = \sum_\mu C_{\mu i}\, \chi_\mu \qquad \text{---------- (2)}$$

where $C_{\mu i}$ are coefficients of atomic orbitals (χ_μ) which are expanded as Slater-type orbitals (STOs) with fixed orbital exponents.

$$\chi_\mu (r, \theta, \phi) = N r^{n-1} \exp(-\zeta r)\, Y^l_m(\theta, \phi) \qquad \text{---------- (3)}$$

where N is normalization constant, r is distance between nucleus to electron, n is principle quantum number, ζ is the orbital exponent, and $Y^l_m(\theta, \phi)$ spherical harmonics.

For the simplified one electron Hamiltonian, $H_{val,}$ the problem can be separated in to several one-electron problems.

$$H_{eff}(i)\ \psi_i = e_i\ \psi_i \qquad \text{---------- (4)}$$

$$E_{val} = \sum_i e_i \qquad \text{---------- (5)}$$

Since the effective Hamiltonian, H_{eff}, is not specified explicitly, the Schrödinger equation will be solved using the variational method. Applying variational principle using ψ_i as a trial function (equation 2) generates the following secular determinant and corresponding equations for the molecular orbital coefficients.

$$\det (H_{\mu\nu} - e_i S_{\mu\nu}) = 0 \qquad \text{---------- (6)}$$

$$\sum_\mu (H_{\mu\nu} - e_i S_{\mu\nu})\, C_{\mu i} = 0 \quad ; \nu = 1,2,3, \ldots..n. \qquad \text{---------- (7)}$$

where e_i's are the roots of the secular equation.

The matrix elements $H_{\mu\mu}$, $H_{\mu\nu}$, and $S_{\mu\nu}$ are as follows

$$H_{\mu\mu} = \langle \chi_\mu | H_{eff} | \chi_\mu \rangle = \alpha \text{ (coulomb integral)} \qquad \text{---------- (8)}$$

$$H_{\mu\nu} = \langle \chi_\mu | H_{eff} | \chi_\nu \rangle = \beta \text{ (resonance integral)} \qquad \text{---------- (9)}$$

$$S_{\mu\nu} = \langle \chi_\mu | \chi_\nu \rangle = \delta_{ij} \text{ (overlap integral)} \qquad \text{---------- (10)}$$

The overlap integrals $S_{\mu\nu}$ (equation 10) are strictly considered based on AOs which are STOs here, whereas the Hamiltonian is not specified explicitly. So the matrix elements $H_{\mu\mu}$ and $H_{\mu\nu}$ (equation 8 and 9) are chosen in the following way.

The diagonal elements $H_{\mu\mu}$ are chosen as valence state ionization potentials (VSIP). The off-diagonal matrix elements $H_{\mu\nu}$ (equation 9) are approximated as

$$H_{\mu\nu} = 0.5\ K\ (H_{\mu\mu} + H_{\nu\nu})\ S_{\mu\nu} \quad \text{---------- (11)}$$

The value of K was parameterized using the experimental ethane barriers and considered as 1.75. Thus, having the values of orbital exponent (ζ) and the diagonal matrix element ($H_{\mu\mu}$), the secular determinant will be solved by matrix diagonalization techniques using computers.

1.3.2 Density Functional Theory

Density functional theory (DFT) does not attempt to calculate the wave function but calculates the electron probability density, $\rho(r)$. Hohenberg and Kohn states that all ground-state properties are functionals of the ground-state charge density $\rho(r)$.[60] According to Hohenberg and Kohn theorem the total energy E_{tot} can be written as

$$E_{tot} = T[\rho] + U[\rho] + E_{xc}[\rho] \quad \text{---------- (12)}$$

where $T[\rho]$ is the kinetic energy of a system of noninteracting particles of density ρ, $U[\rho]$ is the classical electro static energy due to the Coulombic interaction, and $E_{xc}[\rho]$ is the exchange and correlation energy which includes all many-body contributions to the

total energy. But how do we determine the electron density? The electron density was constructed from a single electron wavefunction as in typical molecular orbital approach.

$$\psi \quad = \quad A(n) \mid \phi_1(1),\ \phi_2(2), \phi_3(3), \ldots\ldots \phi_n(n) \mid \qquad \text{---------- (13)}$$

Since the molecular orbitals are orthonormal $\langle\ \phi_i \mid \phi_j\ \rangle = \delta_{ij}$ ------ (14)

The charge density at a point r can be calculated by the summing over the occupied molecular orbitals, $|\phi_i(r)|^2$.

$$\rho(r) = \sum_i \ | \phi_i(r) |^2 \qquad \text{---------- (15)}$$

Therefore, from the wave functions and charge density the total energy (E_{tot}) components in equation (12) can be written as

$$\text{The kinetic energy term } T = \left\langle \sum_i^n \phi_i \left| \frac{-\nabla^2}{2} \right| \phi_i \right\rangle \qquad \text{---------- (16)}$$

$$\text{The Coulomb interaction term } U = \sum_i^n \sum_\alpha^N \left\langle \phi_i(r) \left| \frac{-Z}{R_\alpha - r} \right| \phi_i(r) \right\rangle +$$

$$\tfrac{1}{2} \sum_i \sum_j \left\langle \phi_i(r_1)\phi_j(r_2) \frac{1}{r_1 - r_2} \phi_i(r_1)\phi_j(r_2) \right\rangle + \sum_\alpha^N \sum_{\beta<\alpha} \frac{Z_\alpha Z_\beta}{|R_\alpha - R_\beta|}$$

$$= -\sum_\alpha^N \left\langle \rho(r_1) \frac{Z_\alpha}{|R_\alpha - r_1|} \right\rangle + \tfrac{1}{2} \left\langle \rho(r_1)\rho(r_2) \frac{1}{|r_1 - r_2|} \right\rangle + \sum_\alpha^N \sum_{\beta<\alpha} \frac{Z_\alpha Z_\beta}{|R_\alpha - R_\beta|}$$

$$\therefore U = \left\langle -\rho(r_1) V_N \right\rangle + \left\langle \rho(r_1) \frac{V_e(r_1)}{2} \right\rangle + V_{NN} \qquad \text{---------- (17)}$$

In the final Coulomb interaction equation (equation 17) the term $\rho(r_1)V_N$ represents the electron-nucleus attraction. The second term $\rho(r_1)\frac{V_e(r_1)}{2}$ represents the electron-electron repulsion. The final term V_{NN} represents the nucleus-nucleus repulsion.

However, the exchange and correlation energy term (E_{xc}) is not known and hence approximated. There are now various approximations to obtain the E_{xc}. Local density approximation (LDA), local spin density approximation (LSDA), generalized gradient approximations (GGA). Under each approximation again there are many varieties of exchange and correlation functionals available, CA-PZ (LDA), PBE (GGA), and B3LYP (Hybrid) to name a few.

Let us proceed with LDA to look at how the total energy can be derived. In LDA the charge density varies slowly. Hohenberg and Kohn suggested[61] that the E_{xc} can be obtained by integrating the uniform electrons gas which is as follows

$$E_{xc}[\rho] = \langle \rho(r) | \varepsilon_{xc} | \rho(r) \rangle \qquad \text{---------- (18)}$$

where the $\varepsilon_{xc}[\rho]$ is the exchange-correlation energy per electron in a homogeneous electron gas with electron density ρ. Now, incorporating the ε_{xc} in E_{tot}, it can be written as

$$E_{tot} = \sum_i \left\langle \phi_i \left| \frac{-\nabla^2}{2} \right| \phi_i \right\rangle + \left\langle \rho(r_1) \left[\varepsilon_{xc}[\rho(r_1)] + \frac{V_e(r_1)}{2} - V_N \right] \right\rangle + V_{NN} \qquad \text{------- (19)}$$

In order to determine the actual energy, the variations in E_{tot} should be optimized with respect to the variations in ρ within the orthonormality (δ_{ij}). In other words the energy is optimized with respect to the density.

$$\text{Therefore, } \frac{\delta E_{tot}}{\delta \rho} - \sum_i \sum_j \varepsilon_{ij} \left\langle \phi_i \mid \phi_j \right\rangle = 0 \qquad \text{---------- (20)}$$

In Hohenberg and Kohn theorem the way the density was obtained without finding the wavefunction was not manifested. The Kohn-Sham equations filled this gap. The Kohn-Sham equations are

$$\left[\frac{-\nabla^2}{2} - V_N + V_e + \mu_{xc}(\rho) \right] \phi_i = \varepsilon_i \phi_i \qquad \text{---------- (21)}$$

where μ_{xc} is the exchange-correlation potential. This can be obtained from the differentiation of E_{xc}, $\mu_{xc} = \frac{\partial (E_{xc}[\rho])}{\partial \rho}$

$$\text{Therefore } E_{tot} = \sum_i \varepsilon_i + \left\langle \rho(r_1) \left[\varepsilon_{xc}[\rho] - \mu_{xc}[\rho] - \frac{V_e(r_1)}{2} \right] \right\rangle + V_{NN} \qquad \text{---------- (22)}$$

The atomic orbitals (ϕ_i) (basis set) in the Kohn-Sham equations in principle can be any type such as Gaussian functions [$(g_{ijk} = N x^i y^j z^k \exp(-\alpha r^2))$] where i, j, k are nonnegative integers, α is a positive orbital exponent, and x, y, z are Cartesian coordinates of the nucleus. Plane waves [exp(*i*k•r)], where k is the momentum vector and r run through the Bravais lattice.[62]

The other gradient corrected and hybrid approximations that we have used in our calculations are GGA and B3LYP. These approximations are found to be useful when the electron density varies with the position. The variation of the electron density with position obtained by including the gradients, in general, the exchange

$$E_{xc}^{GGA}[\rho^{\alpha},\rho^{\beta}] = \int f(\rho^{\alpha}(r),\rho^{\beta}(r),\nabla\rho^{\alpha}(r),\nabla\rho^{\beta}(r))dr \qquad \text{---------- (23)}$$

where *f* is some of the spin densities and their gradients and ρ^{α}, ρ^{β} are spin polarized density components.[63] The GGA functionals tend to improve the total energies, atomization energies in comparison with LDA. Especially, when the systems are under weak intermolecular interactions, van der Waals systems are problematic within LDA.[64]

The hybrid DFT functionals are widely used. B3LYP is one of such popular method. This method involves a combination of DFT correlation and Hartree-Fock exchange. It is defined as

$$E_{xc}^{B3LYP} = (1-a_a-a_x)E_x^{LSDA} + a_0E_x^{exact} + a_xE_x^{B88} + (1-a_c)E_c^{VWN} + a_cE_c^{LYP} \qquad \text{-------- (24)}$$

where E_x^{exact} is from the Hatree-Fock E_x^{HF}, $a_o = 0.20$, $a_x = 0.72$, and $a_c = 0.81$ are obtained by fitting with the experimental results.

Using the above general theoretical basis of eH and DFT methods the electronic structure and properties of boron compounds that are discussed in the thesis are calculated. When the systems under study are finite (molecules or clusters), the standard localized Gaussian and numerical basis sets are used. On the other hand in the case of solids the plane-wave basis sets with Vanderbilt ultrasoft pseudopotentials are used.

References

[1] *Boron Synthesis, Structure and Properties*, edited by J. A. Kohn, W. F. Nye, and G. K. Gaulé (Plenum, New York), 1960.

[2] *Boron*, edited by G. E. Gaude, Vol. II (Plenum Press, New York), 1965.

[3] *Boron and Refractory Borides*, edited by V. I. Matkovich (Springer-Verlag, Berlin), 1977.

[4] *Boron-Rich Solids*, edited by D. Emin, T. Aselage, C. L. Beckel, I. A. Howard, and C. Wood, AIP Conf. Proc. No. 140 (AIP, New York), 1986.

[5] *Boron-Rich Solids*, edited by D. Emin, T. L. Aselage, A. C. Switendick, B. Morosin, and C. L. Beckel, AIP Conf. Proc. No. 231 (AIP, New York), 1991.

[6] N. Greenwood, A. Earnshaw, *Chemistry of the Elements* (Buttreworth-Heinemann, UK), 1997.

[7] A. F. Wells, *Structural Inorganic Chemistry*, 5th ed., (Clarendon Press: Oxford), 1984.

[8] J. Donohue, *The Structure of the Elements*, (Wiley: New York), 1974.

[9] A. Stock, *Hydrides of Boron and Silicon*, (Cornell University Press, Ithaca, N.Y.), 1933.

[10] L. Pauling, *The Nature of the Chemical Bond*, (Ithaca, New York), 1939.

[11] V. Bartow, Advan. Chem. Ser. **32**, 5 (1961).

[12] E. Wiberg, Pure Applied. Chem. **49**, 691 (1977).

[13] N. V. Sidgewick, *The Chemical Elements and Their Compounds*, (Clarendon, London), 1950, pp. 338.

[14] D. F. Shriver, *The Manipulation of Air-sensitive Compounds*, (McGraw Hill, New York), 1969.

[15] R. P. Bell and H. C. Longuet-Higgins, Proc. Roy. Soc., (London) A. **183**, 357 (1945).

[16] H. C. Longuet-Higgins, J. Chim. Phys. **46**, 268 (1949)

[17] H. C. Longuet-Higgins, Quart. Rev. **11**, 121 (1957).

[18] W. N. Lipscomb. Adv. Inorg. Chem. Radiochem. **1**, 117 (1959).

[19] M. F. Hawthorne and A. R. Pitochelli, J. Am. Chem. Soc. **81**, 5519 (1959).

[20] M. F. Hawthorne and A. R. Pitochelli, J. Am. Chem. Soc. **82,** 3328 (1960).

[21] J. Wunderlich and W. N. Lipscomb, J. Am. Chem. Soc. **82**, 4427 (1960).

[22] J. L. Boone, J. Am. Chem. Soc. **86**, 5036 (1964).

[23] J. F. Ditter, J. R. Spielman, and R. E. Williams, Inorg. Chem. **5**, 118 (1966).

[24] F. Klanberg and E. L. Muetterties, Inorg. Chem. **5**, 1955 (1966).

[25] F. Klanberg, D. R. Eaton, L. J. Guggenberger, and E. L. Muetterties, Inorg. Chem., **6**, 1271 (1967).

[26] R. E. Williams, Inorg. Chem. **10**, 210 (1971).

[27] W. N. Lipscomb, *Boron Hydrides*, W. A. Benjamin, New York, 1963.

[28] R. E. Dickerson and W. N. Lipscomb, J. Chem. Phys. **27**, 212 (1957).

[29] W. N. Lipscomb, J. Phys. Chem. **62**, 381 (1958).

[30] W. N. Lipscomb, Adv. Inorg. Chem. Radiochem. **1**, 118 (1959).

[31] K. Wade, J. Chem. Soc. Chem. Commun. **792**, (1971).

[32] K. Wade, *Electron Deficient Compounds*, (Nelson, London), 1971.

[33] G. A. Olah, K. Wade, R. E. Williams, *Electron Deficient Boron and Carbon Clusters*, (Wiley, New York), 1991.

[34] M. A. Fox, K. Wade, Pure Appl. Chem. **75**, 1315 (2003).

[35] A. J. Stone, J. Mol. Phys. **41**, 1339 (1980).

[36] J-I. Aihara, J. Am. Chem. Soc. **100**, 3339 (1978).

[37] R. B. King, D. H. Rouvray, J. Am. Chem. Soc. **99**, 7834 (1977).

[38] R. W. Rudolph and W. R. Pretzer, Inorg. Chem. **11**, 1974 (1972).

[39] R. W. Rudolph, Acc. Chem. Res. **9**, 446 (1976).

[40] D. M. P. Mingos, Nature Phys. Sci. **99**, 236 (1972).

[41] D. M. P. Mingos, Acc. Chem. Res. **17**, 311 (1984).

[42] H. C. Longuet-Higgins and M. de V. Roberts, Proc. Roy. Soc., (London) **224A**, 336 (1954).

[43] H. C. Longuet-Higgins and M. de V. Roberts, Proc. Roy. Soc., (London) **230A**, 110 (1955).

[44] W. N. Lipscomb, Science **196**, 1047 (1997).

[45] M. M. Balakrishnarajan and E. D. Jemmis, J. Am. Chem. Soc. **122**, 456 (2000).

[46] E. D. Jemmis, M. M. Balakrishnarajan, and P. D. Pancharatna, J. Am Chem. Soc. **123**, 4313 (2001).

[47] E. D. Jemmis, M. M. Balakrishnarajan, and P. D. Pancharatna, Chem. Rev. (Washington, D.C.) **102**, 93 (2002).

[48] E. D. Jemmis, Chemtracts-Inorganic Chemistry, **18**, 620 (2005).

[49] E. D. Jemmis and M. M. Balakrishnarajan, J. Am. Chem. Soc. **123**, 4324 (2001).

[50] R. Hoffmann, J. Chem. Phys. **39**, 1397 (1963).

[51] P. C. Hariharan and J. A. Pople, Theor. Chim. Acta **28**, 213 (1973).

[52] T. H. Dunning, J. Chem. Phys. **53**, 2823 (1970).

[53] B. Delley, J. Chem. Phys. **92**, 508 (1990).

[54] M. C. Payne, M. P. Teter, D. C. Allan, T. A. Arias, and J. D. Joannopoulos, Rev. Mod. Phys. **64**, 1045 (1992).

[55] D. Vanderbilt, Phys. Rev. B **41**, R7892 (1990)

[56] D. M. Ceperley and B. J. Alder, Phys. Rev. Lett. **45**, 566 (1980).

[57] J. P. Perdew and A. Zunger, Phys. Rev. B **23**, 5048 (1981).

[58] J. P. Perdew, K. Burke, and M. Ernzerhof, Phys. Rev. Lett. **77**, 3865 (1996).

[59] A. D. Becke, J. Chem. Phys. **98**, 5648 (1993).

[60] P. Hohenberg and W. Kohn, Phys. Rev. **136**, B864 (1964).

[61] W. Kohn and L. J. Sham, Phys. Rev. **140**, A1133 (1965).

[62] M. D Segall, P. J. D. Lindan, M. J. Probert, C. J. Pickard, P. J. Hasnip, S. J. Clark, and M. C. Payne, J. Phys.: Condens. Matter **14**, 2717 (2002).

[63] Ira N. Levine, *Quantum Chemistry* (Prentice Hall, 5th edition), 1999.

[64] J. Kohanoff, *Electronic Structure Calculations for Solids and Molecules* (Cambridge University Press), 2006.

Chapter 2

Electronic Structure and Stability of α- and β-rhombohedral Boron

2.1 Introduction

Allotropes of boron have complex polyhedral structures associated with electron deficient chemical bonding. Among its numerous allotropes only α- and β-rhombohedral boron were crystallized with high quality. The other phases were mixed with several impurities like carbon, nitrogen, oxygen, silicon etc.[1-4] These crystal structures are mainly based on icosahedral B_{12} skeletons, a structural pattern most commonly observed in polyhedral boranes as well. The ubiquitous B_{12} icosahedron in the allotropes of boron establishes diverse exotic extended three dimensional B_{12} networks and makes it more complex to understand their electronic structure and properties. Especially, the partially occupied lattice and interstitial sites (intrinsic defects) in the elemental β-rhombohedral boron and boron-rich icosahedral cluster solids (BRICS) defy conversional modes of understanding. The electronic structure, relative stability, conducting and mechanical properties that

stems from the intrinsic defects of elemental β-rhombohedral boron and BRICS are still remains to be fully understood.

There have been several experimental and theoretical studies on the allotropes of boron and boron-rich solids.[5-14] However, the complexity of elemental β-rhombohedral boron in terms of unusual icosahedral B_{12} condensations and intrinsic defects has prevented detailed comparative theoretical studies of allotropes of boron so far. A certain reduction of this complexity is achieved by relating condensed polyhedral boranes to allotropes of boron just as hydrocarbons are related to the allotropes of carbon.[15,16] For example, the concept of condensation that gave graphite from benzene is applied to the structure of polyhedral boranes here (Figure 2.1). In polyhedral boranes, we could have a condensation similar to edge sharing seen in benzenoid aromatics. Further, we could have a triangular face sharing and there is also the possibility of a four vertex sharing between polyhedra and indeed a connection that could be possible through a single vertex sharing.

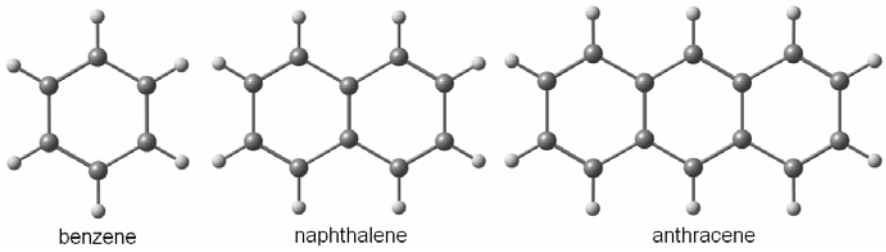

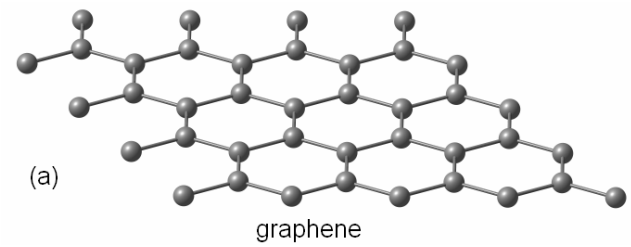

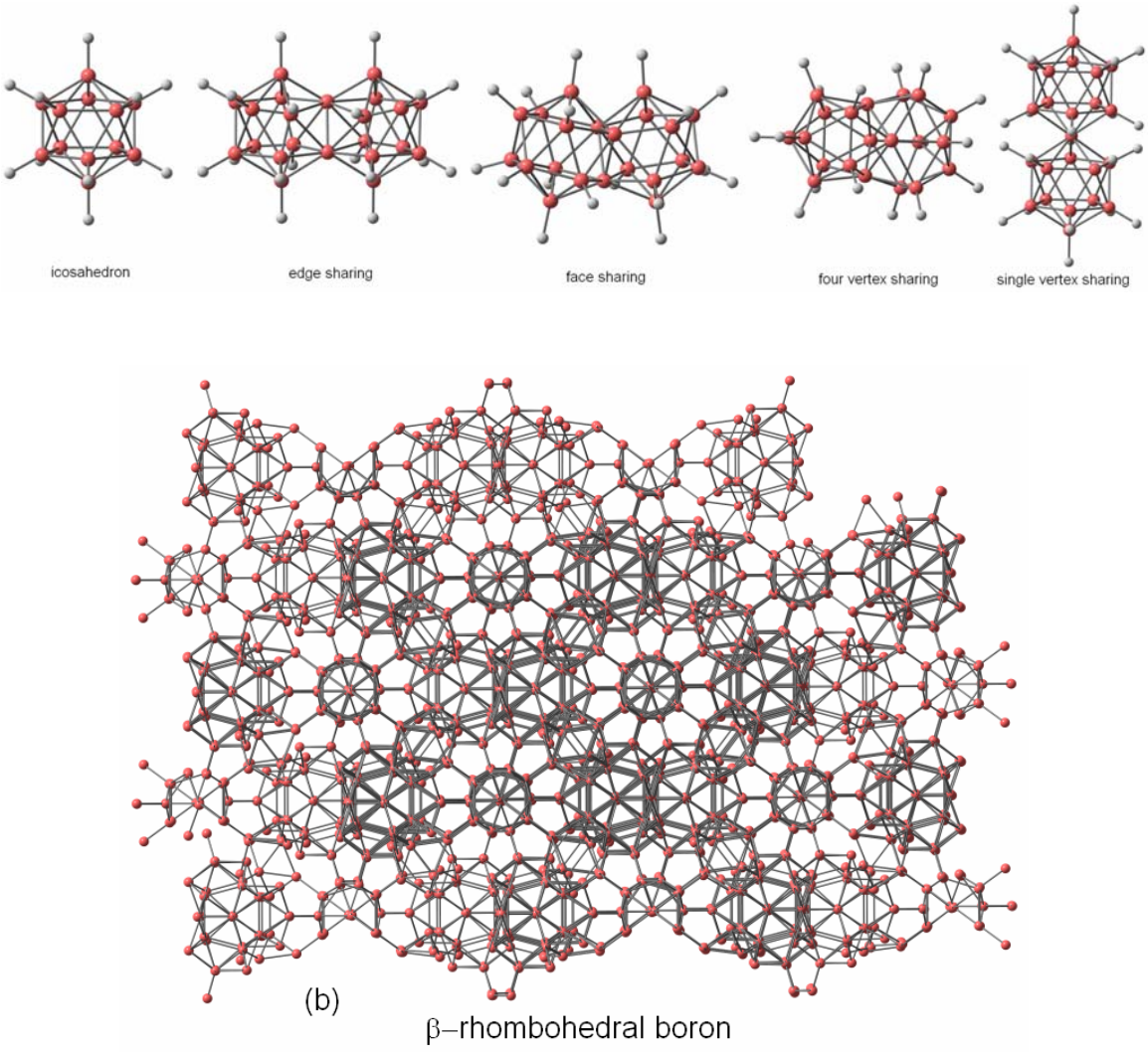

Figure 2.1. An example of cluster fragment approach: **(a)** Condensation of benzenoid aromatics such as benzene, naphthalene, and anthracene into a two dimensional graphene. **(b)** Different condensations of icosahedra presented in β-rhombohedral boron are shown with icosahedral borane. The detailed structure of β-rhombohedral boron will be discussed later.

Such condensed polyhedral boron compounds stability can be gauged by the *mno* polyhedral skeletal electron counting rule similar to the Hückel $4n+2$ π electron rule for benzenoid aromatics.[17-21] This has set the stage for detailed study of the electronic

structure, stability, origin of the intrinsic defects, and electronic properties of allotropes of boron using cluster fragment approach by *ab initio* DFT calculations.

2.2 Computational Methods

We have carried out first principles quantum mechanical calculations in the frame work of DFT. The ground state electronic structures were obtained using Cambridge Sequential Total Energy Package (CASTEP) code implemented in Materials Studio.[21,22] The total electronic energies of the solids are carried out with the effect of exchange and correlation (XC) using non local corrected generalized gradient approximation (GGA) based on the Perdew Burke Ernzerhof (PBE).[23] The ultra-soft pseudopotentials (USP) description was used for the elements that are presented in the crystal structures.[24] It describes the electron ion interaction and represents the electronic wavefunctions using a plane wave basis set. For the crystal lattice, integration over the symmetrised Brillouin zone was performed using k–points generated via the Monkhorst–Pack scheme.[25] Simultaneous optimization of crystal lattice parameters and atomic relaxation were performed under the space group symmetry constraints by Broyden-Fletcher-Goldfarb-Shanno (BFGS) method.[26] The density mixing was done by Pulay scheme.[27] Because of the large unit cell, we first optimized the unit cell and then set for properties calculation. The band and DOS curves (the number of energy levels between E and E+dE) are obtained by broadening discrete energy levels on a grid of k–points using Gaussian smearing functions of 0.2 eV Full Width Half Maximum (FWHM). The fragmented

molecular clusters of β-rhombohedral boron generated based on the cluster fragment approach are calculated by Amsterdam Density Functional (ADF) package.[28] The total electronic energies were included the effect of XC which is taken into account using GGA at Becke-Perdew level. Here, the Slater-type orbital (STO) basis set with double-zeta (DZ) is used and inner shells are treated within the frozen core approximation.

2.3 Results and Discussion

Before describing the structural details and DFT results of boron allotropes using cluster fragment approach let us look at why elemental boron favors icosahedral B_{12} skeleton? The overwhelming preference for icosahedral B_{12} skeleton cannot be accidental in the boron allotropes and boron-rich solids. In fact the many structural peculiarities of allotropes of boron appear to be the result of attempts at generating maximum number of boron atoms in the icosahedral environment. Thus it is important to know the reason for the preference as a beginning subject of boron allotropes.

Comparison of the fragments of icosahedral borane and the regular Archimedean icosahedron, leads to an explanation for the specific preference of elemental boron for icosahedron. According to the Wade's *closo*- n+1 and *nido*- n+2 (where n is the number of boron atoms) skeletal electron counting rules, *closo*- and *nido*- boranes requires two and four additional electrons for their stability respectively.[29,30] Therefore, the stable *closo*- icosahedral borane is $B_{12}H_{12}^{-2}$. The $B_{12}H_{12}^{-2}$ can be thought of as being constructed

from two *nido*- pentagonal pyramidal fragments (*nido*-B_6H_6). The *nido*-B_6H_6 requires an additional charge of -4 (Wade's *nido*- *n*+2 rule) to be stable. The charge can be compensated by adding four hydrogens to the $B_6H_6^{-4}$ which gives a neutral B_6H_{10}. The stable experimentally known neutral borane, B_6H_{10}, has four bridging hydrogens in the B_5 ring. The terminal ring B-H bonds are directed towards the capping BH group by about 25^o so that there is better overlap between the p orbitals of the capping BH group and the π MOs of the B_5 ring (Figure 2.3). This is due to the better ring-cap orbital overlap compatibility.[31-32] A similar angle can be calculated from solid geometry for the pentagonal pyramid obtained by dividing the Archimedean icosahedron into two. This angle of 26.6^o is nearly the same as what is needed naturally for the borane pentagonal pyramid as shown in the Figure 2.3. Thus while forming the icosahedral borane from the two pentagonal pyramids; there is no need to have any major compromise in overlap. This is not true for other polyhedral borane structures. For example, during the formation of a *closo*- pentagonal bipyramidal borane ($B_7H_7^{-2}$) from a pentagonal pyramidal borane -

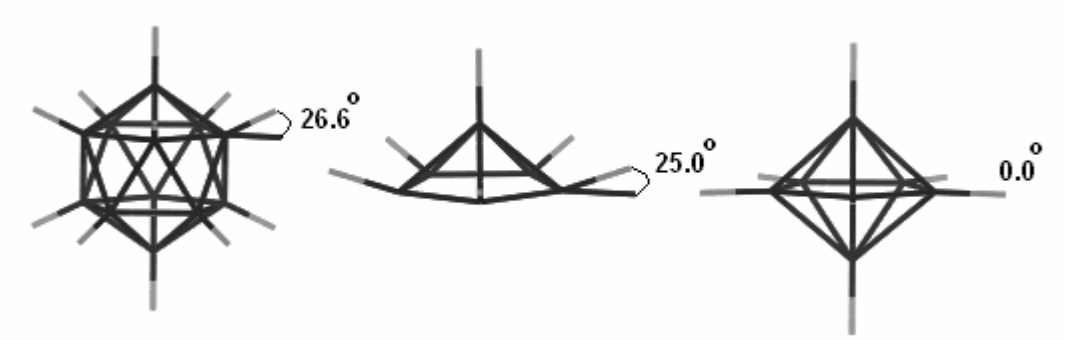

Figure 2.3. Schematic illustration of the angle that B-H makes with the B_5 ring plane in icosahedral $B_{12}H_{12}^{-2}$, pentagonal pyramidal B_6H_{10} (bridging hydrogens are removed for clarity), and pentagonal bipyramidal $B_7H_7^{-2}$ respectively.

and a B-H cap, the terminal B-H bond of the B_5 ring has to be brought from their optimum angle of 25^o in the pentagonal pyramidal borane to 0^o in $B_7H_7^{-2}$. Thus the structure is not relatively stable. Many experimental and theoretical calculations show that the icosahedral arrangement is indeed the most favored one for boranes.[33-36] Given that icosahedron is the most favored polyhedra of boron, it is easy to explain the structures of boron allotropes.

2.3.1 α-rhombohedral Boron

The α-rhombohedral boron (α-B_{12}) crystal structure was first proposed by McCarty and further described by Decker and Kasper.[37] Among the allotropes of boron α-B_{12} has the simplest form. It contains one B_{12} unit in the rhombohedral Bravais lattice in the space group $R\bar{3}m$ with lattice parameters a = 5.05 Å and α = 58.06^o (Figure 2.3.1a). It constitutes crystallographically two independent atomic sites, polar (**p**) and equatorial (**e**). Among the twelve vertices of B_{12}, six are polar and the rest of six are equatorial sites. The polar sites are connected to the neighboring B_{12} units through 2c-2e bonds. Each equatorial site is connected to two neighboring B_{12} units via 3c-2e bonds as shown in the Figure 2.3.1b. The 2c-2e B-B inter icosahedral bonds are almost aligned with the rhombohedral edges. The distortion from cubic close packing is found to be 1.94^o. A clear representation of the 2c-2e and 3c-2e B-B inter icosahedral bonding is depicted in Figure 2.3.1c and 2.3.1d respectively.

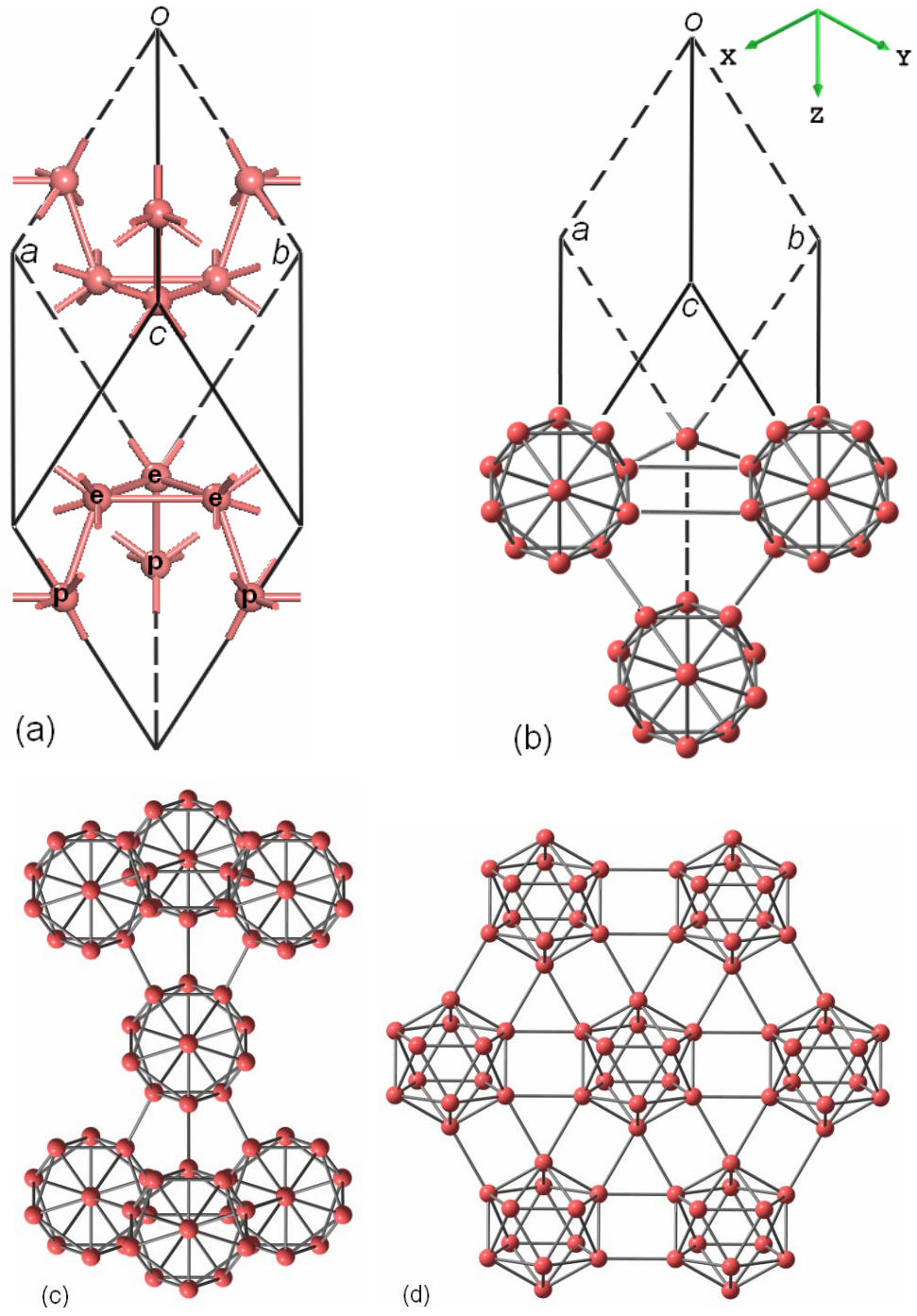

Figure 2.3.1. (a) Unit cell of α-rhombohedral boron crystal structure shown with the two independent atomic cites polar (**p**) and equatorial (**e**). In **(b)** formation of the 2c-2e and 3c-2e bonds between polar and equatorial cites of icosahedron is depicted. An extended view of 2c-2e bonding along the rhombohedral diagonal axis and 3c-2e bonding along the top view of the rhombohedral diagonal axis are shown in **(c)** and **(d)** respectively.

In principle all the 12 vertices can form 2c-2e bonds with the neighboring B_{12} units, but the five fold symmetry does not allow translational periodicity. In addition this needs two extra electrons per B_{12} unit to stabilize the unit cell. Hence it chooses a resourceful way of connectivity to avoid the extra electrons. A B_{12} unit needs 38 electrons to stabilize the unit cell, 26 electrons (n+1 electron pairs) for the cluster bonding and 12 electrons for *exo*-2c-2e bonds. But B_{12} contains only 36 valence electrons. The extra requirement of two electrons is met by the two electrons saved from the formation of the six 3c-2e bonds [6–(6×2/3)]. Thus the stability of the polyhedral boranes is governed by the Wade's n+1 skeletal electron pair rule and the stability of the B_{12} unit in the solid is anticipated by the work of Longuet-Higgins.[38]

2.3.2 β-rhombohedral Boron

The structure of β–rhombohedral boron involves clusters of B_{12} units condensed in novel ways.[2] It is necessary to analyze the rules that govern the condensation of polyhedral boranes akin to the condensed benzenoid aromatics. This can be done by the recently introduced *mno* polyhedral skeletal electron counting rule.[17-19] According to this rule, a polyhedral structure with m polyhedra, n vertices and o single atom bridges between polyhedra requires $m+n+o$ electron pairs for stability. Most of the atoms in β–rhombohedral boron form a part of an icosahedral or near icosahedral structure with many vacancies and extra occupancies. We discuss the β–rhombohedral boron crystal

structure with a view to understand the organization of the various clusters of boron atoms, in relation to the structure of boranes, and to find ways to model the structures.

The β–rhombohedral boron crystal structure was first proposed by Hoard et al,[39] and further studied by Geist et al,[40] Callmer,[41] and Slack et al.[3,42] The crystal structure of β–rhombohedral boron has a distorted face centered cubic (fcc) lattice (rhombohedral). It has 105 boron atoms with 15 crystallographically equivalent cites in its idealized unit cell (without the intrinsic defects), in the space group $R\bar{3}m$ with lattice constants a = 10.145 Å, $\alpha = 65.28^{o}$ (Figure 2.3.2a, b).

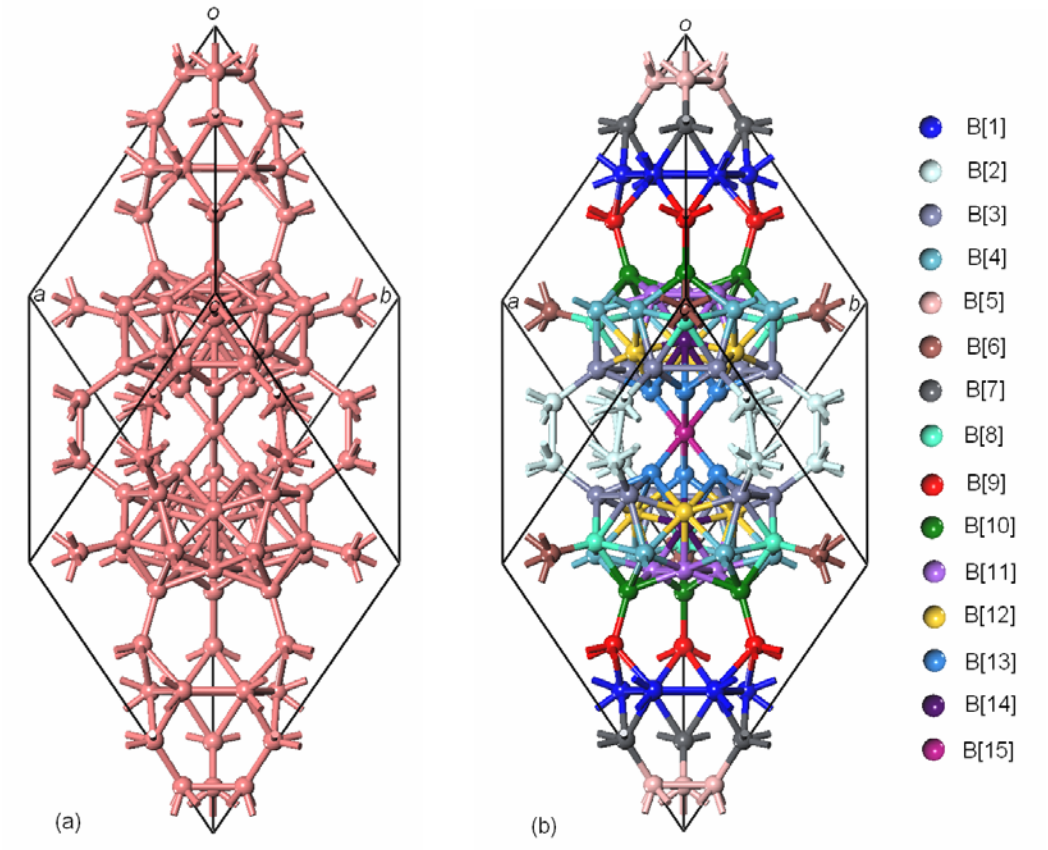

Figure 2.3.2. (a) Unit cell of β-rhombohedral boron crystal structure and its 15 crystallographically independent atomic cites are shown with different colors in **(b)**. The boron cites numbering is adopted from Slack et al.[3,42]

The main structural moiety in the β–rhombohedral boron unit cell is B_{84} polyhedron, where a central B_{12} icosahedron is surrounded by twelve half icosahedra (B_6 pentagonal pyramids). That is each vertex of B_{12} icosahedron is connected by the apex vertex of B_6 pentagonal pyramid ($B_{12}@B_{12}@B_{60}$). So the surface of the B_{84} is identical to the surface of C_{60} fullerene. These large B_{84} soccer ball clusters are placed at the points of the rhombohedral lattice as shown in Figure 2.3.2c. This allows six of the half icosahedra of each B_{84} unit to link together at midpoints of the edges of the cell forming further icosahedra. By this way the chain of B_{12} icosahedral units run through the structure along each of the rhombohedral cell edges (Figure 2.3.2c,d). This is similar to the polar 2c-2e –

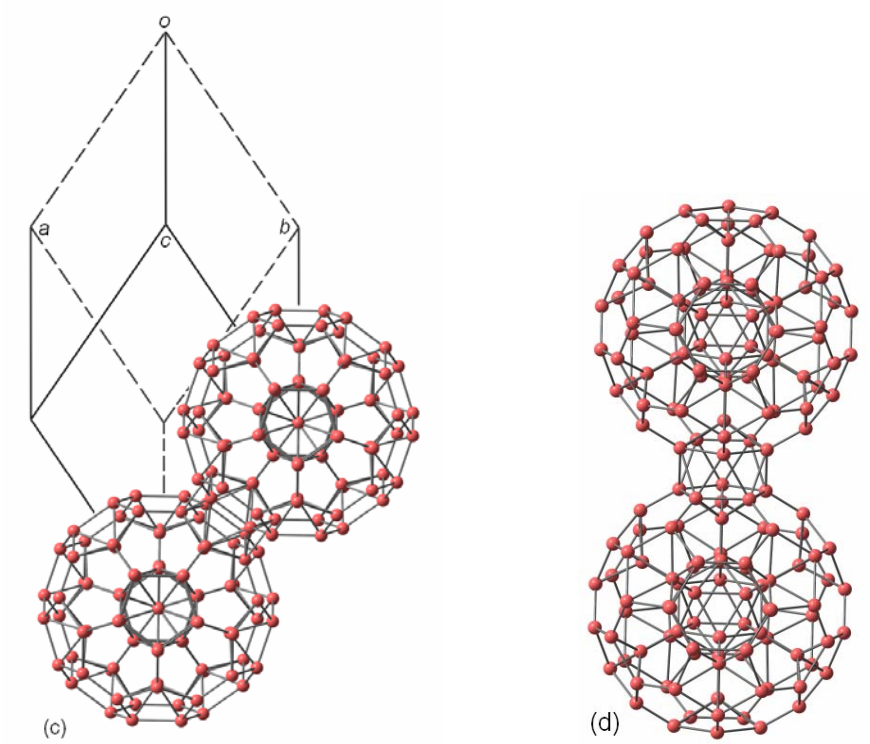

Figure 2.3.2. (c) β-rhombohedral boron crystal structure where the B_{84} soccer ball units occupy the vertices of the unit cell (for clarity only two B_{84} units are shown here). The pentagonal pyramids of B_{84} aligned along the edges of the unit cell will combine and forms other icosahedra at the midpoints of the edges. **(d)** The formation of the icosahedron between two B_{84} units is shown along the C_3 axis of the inner B_{12} of B_{84}.

B-B bonds between the icosahedra of α-B_{12} (Figure 2.3.1). The remaining six half icosahedra of B_{84} can not link to half icosahedron of another six B_{84} units. It is due the space constraints and the five fold symmetry of the B_{84} unit which does not translate the periodicity of the crystal.

However, the extension of the B_{84} network is further achieved by a B_{10} unit of C_{3v} symmetry. This B_{10} has three five membered rings viewed from three sides as shown in Figure 2.3.2e. The central atom present in this B_{10} unit together with the five membered rings provides three pentagonal pyramidal units even though some of the atoms are shared. So that the remaining six half icosahedra of B_{84} will link to the pentagonal pyramids of six different B_{10} units. Further the rest of the two pentagonal pyramids of B_{10} unit are surrounded by its near two pentagonal pyramids of different B_{84} soccer balls (Figure 2.3.2f). Such a condensation of three pentagonal pyramids of different B_{84} via a B_{10} generates a B_{28} unit [$(3\times B_6) + B_{10}$].

A B_{10} unit can also be viewed as three condensed icosahedra each mutually sharing one triangular face and one common vertex with the other two. Simply a B_{28} unit is $B_{10}@3(B_6)$. Two such B_{10} or B_{28} units are linked through an additional boron atom at the center of the rhombohedral cell (B[15] in Figure 2.3.2b). This is the only atom that is not part of any icosahedral arrangement in the entire unit cell. Therefore rhombohedral unit cell can be viewed as B_{84} which is centered at each vertex, plus B_{10}-B-B_{10} unit situated along the main body diagonal (β-B_{105} = B_{84} + B_{10}-B-B_{10}) as shown in the Figure 2.3.2g.

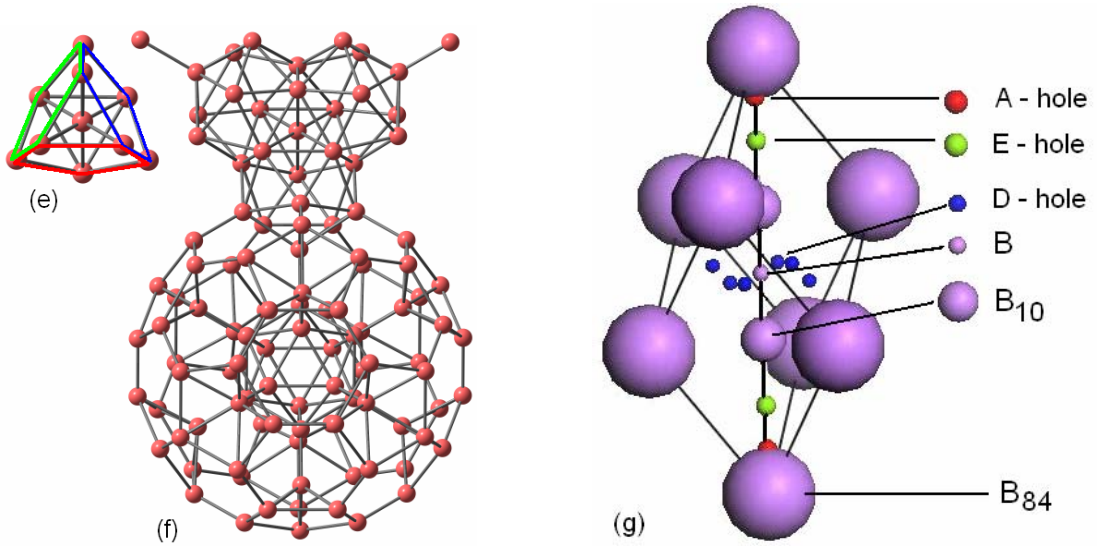

Figure 2.3.2. (e) The B_{10} unit where the three five membered rings are marked with three different colors. **(f)** A B_{84} soccer ball connected to lower pentagonal pyramid of B_{10} unit. The remaining two pentagonal pyramids of B_{10} are connected to the near two B_{84} units (only a part of B_{84} that is pentagonal pyramid connected to one of the vertex of inner B_{12} is shown here) which forms a B_{28} unit. **(g)** The crystal structure of β-rhombohedral boron, where the B_{84} soccer balls occupy the vertices of the unit cell is shown with a solid sphere. The B_{10}–B–B_{10} chain occupies the main body diagonal. The space between the polyhedral units is little expanded for a better view. The three types of major holes that are presented in the unit cell are also shown here.

The structure of the unit cell can also be considered in another way where each vertex and the edge center of the rhombohedral unit cell is occupied by a B_{12} icosahedron and a B_{28}-B-B_{28} (B_{57}) chain aligned along the main body diagonal of the unit cell as shown in Figure 2.3.2h. The B_{28}-B-B_{28} chain or B_{57} fragment connected by part of the icosahedral B_{12} units of B_{84} is also can be seen in Figure 2.3.2. In this view β-rhombohedral boron is effectively comprised of four B_{12} units (one from the vertex +

three from edge centers) and a B_{57} unit (β-B_{105} = $4B_{12}$ + B_{57}). However, this is not the complete story of β-rhombohedral boron crystal structure.

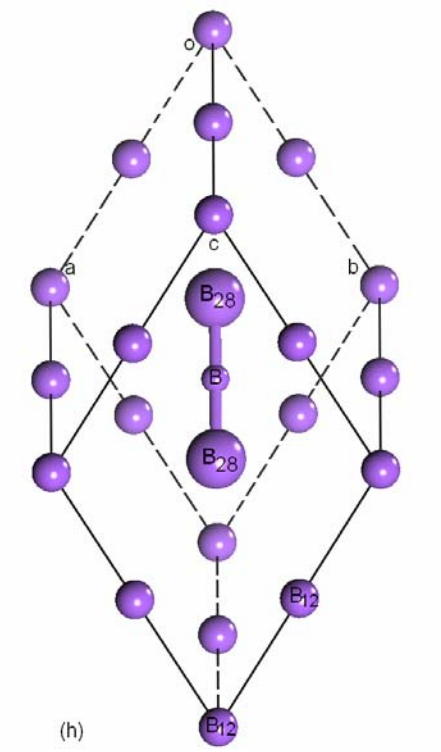

Figure 2.3.2. (h) Crystal structure of β-rhombohedral boron, where the B_{12} icosahedral units occupy the vertices and edge centers of the unit cell. The B_{28}-B-B_{28} (B_{57}) unit occupies the main body diagonal of the unit cell. This is similar to the view of Figure 2.3.2 **(g)** where the B_{10}-B-B_{10} chain aligns in the diagonal axis of the unit cell.

The model proposed by Hoard et al[39] constitutes 15 crystallographically independent atomic sites and these are fully occupied as shown earlier in the Figure 2.3.2b. The Figure 2.3.2b is extended with B_{84} attached to six B_{28} fragments for more visibility to understand the 15 crystallographically independent atomic sites as shown in Figure 2.3.2i. It is thought that one of these crystallographically independent sites

contains statistical vacancies. Slack, observed that the six symmetry equivalent B[13] sites connected by mean of the central B[15] site situated in B_{57} unit is partially vacant.[3,42] There are also five different symmetry equivalent interstitial sites, B[16] – B[20] are partially occupied. The partially occupied five intestinal sites are in the A, E, and D holes (Figure 2.3.2g). Hole A is situated out side the triangular faces of inner B_{12} of B_{84} and hole E is outer surface of the B_{84} along the diagonal axis of the rhombohedral unit cell. Hole D is roughly situated around the B[15] site. Comparatively the size of the hole A and E are larger than hole D. The observed occupancies of different β–rhombohedral boron samples are tabulated in Table 2.3.2a.

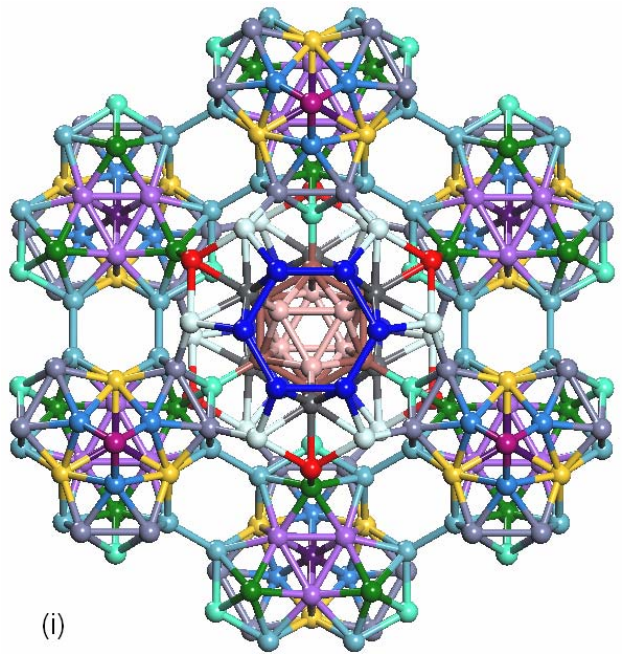

Figure 2.3.2. (i) The extended β-rhombohedral boron crystal structure, where B_{84} condense with near B_{84} units (only the B_{28} part is indicated) via B_{10} is shown along the top view of rhombohedral diagonal axis. The color code follows the crystallographically independent atomic cites of β-rhombohedral boron in Figure 2.3.2b.

Table 2.3.2a. Percentage of partially occupied lattice and interstitial sites of different β-rhombohedral boron crystal structure samples.

No	Crystal structure	Site No [symmetry multiplicity] % of occupancy						# of B / unit cell
		13[6]	16[6]	17[6]	18[6]	19[6]	20[12]	
1	Geist	100.0	0.000	0.000	0.000	0.000	0.000	105.00
2	Hoard	66.67	33.33	0.000	0.000	0.000	0.000	105.00
3	Callmer	73.40	24.80	0.000	0.000	0.000	0.000	104.89
4	Slack(i)	77.70	25.80	3.200*	5.800	7.200	0.000	106.37
5	Slack(ii)	73.00	28.40	9.700	7.400	7.000	2.50	106.83
6	Slack(iii)	74.50	27.20	8.500	6.600	6.800	3.70	106.86

*It has [12] symmetry multiplicity than the general [6].

We make use of this information presented in Table 2.3.2a to evaluate the electronic requirement of β-rhombohedral boron similar to α-rhombohedral boron using *mno* electron counting rule. In order to do that β-rhombohedral boron is divided where the *exo*- bonds represent nearly localized 2c-2e bonds. This gives a B_{57} and four B_{12} cluster fragments (as described in Figure 2.3.2h). The dangling valences in B_{57} and B_{12} fragments are saturated by hydrogen atoms to calculate their electronic requirements using *mno* rule which gives $B_{57}H_{36}$ and $B_{12}H_{12}$ boranes. The $B_{57}H_{36}$ is the combination of two $B_{28}H_{21}$ fragments connected via a boron atom as shown in Figure 2.3.2j.

Thus generated fragments can be tested for their stability with respect to the electron count and hence their condensed solids. According to the *mno* rule the $B_{57}H_{36}$ or the B_{57} unit in β-rhombohedral boron has 3 electrons more than necessary i.e. $B_{57}H_{36}^{+3}$ (B_{57}^{+3}) is the stable unit (Table 2.3.2b). One of the ways of removing the +3 charge is by expulsion of one boron atom from the six fold B[13] site since it is already partially occupied (~73.00 %). This gives a *nido*- structure with 56 boron atoms. It translates to

occupancy of 100× 5/6 = 83.33 %. But the percentage of occupancy of B[13] is lower than 83.33%. This is compensated by the partially occupied B[17] interstitial site which is clear from the experimental data shown in Table 2.3.2a. The B[17] site is near the D hole and is within bonding distance to B[13] and B[15] sites, which are involved in the capping. This site has an occupancy range 3.2 – 9.7 % in the three samples of Slack. It is as if the structure has overcorrected than what is required. The atoms removed by over correction is compensated by the B[17] sites not far from it. Hence the total percentage of occupancy of B[13] can be assumed as (80.9, 82.7, 83.0) respectively, which strongly indicates that one boron atom is missing at B[13] site in the β–rhombohedral boron. The rest of the four partially occupied interstitial sites B[16], B[18], B[19], and B[20] provide the extra electrons required for the individual icosahedral B_{12} units.

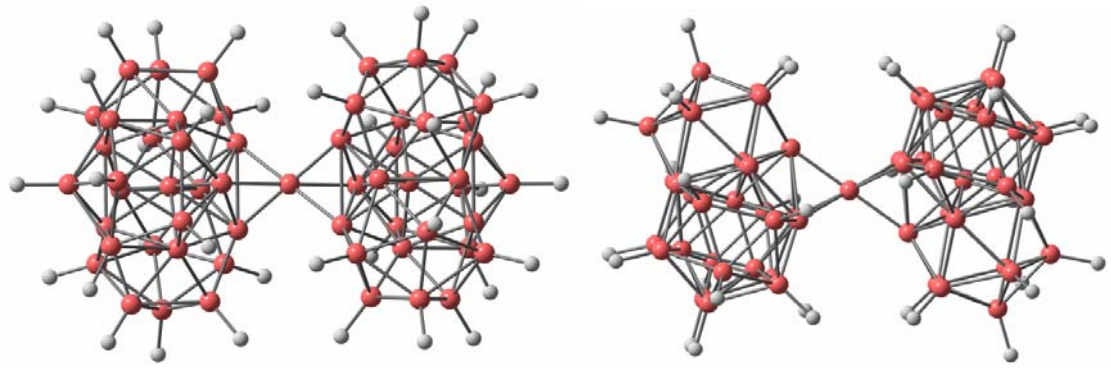

Figure 2.3.2. **(j)** $B_{57}H_{36}$ fragment connected by two $B_{28}H_{21}$ units through a single boron atom bridge (B_{28}-B-B_{28}) is shown in two orientations. The left $B_{57}H_{36}$ shows the octahedral coordination of central boron (B[15] site) with the six B[13] sites whereas the right one is shown mapping of the icosahedral units.

Table 2.3.2b. The electron counts for the clusters based on the *mno* rule. The third column gives count on total available skeletal electron pairs (ASEP) for the cluster bonding. The last but one column gives the required skeletal electron pairs for the cluster bonding according to the *mno* rule. The last column gives the required charge (RC) on the cluster [RC = (ASEP) - (*m*+*n*+*o*)]. The details of the polyhedral electron counting rules and its few examples are given in the Chapter 1.

No	Cluster	A.S.E.P	*m*	*n*	*o*	*m*+*n*+*o*	R.C
1	$B_{12}H_{12}$	12	1	12	0	13	-2
2	$B_{28}H_{31}$	31.5	3	28	0	31	+1
3	$B_{57}H_{36}$	67.5	8	57	1	66	+3

Electron count for $B_{57}H_{36}$: A.S.E.P = 36 (BH) + 21 (B) = 36 (2) + 21 (3) = 67.5 electron pairs. According *mno* rule: *m*+*n*+*o* = 8+57+1 = 66. So a stable $B_{57}H_{36}$ is a tri-cation.

The four icosahedra [(B[1], B[2], B[7], B[9] (edge center icosahedra) and B[5], B[6] (inner icosahedron of B_{84})] (Figure 2.3.2i) which are each two electron deficient are at the bonding distance of the interstitial sites B[16], B[18], B[19] and B[20]. The site B[16] is located in between A and E holes and B[18], B[19], and B[20] are located above the D hole (or F hole not shown in the Figure 2.3.2g). The partial occupancies of these interstitial atoms add up to 38.8%, 45.3%, and 44.3% in the three different samples (Table 2.3.2a). This translates to 7.0, 8.6, and 8.64 electrons not far from the 8 electrons that are necessary for the 4 B_{12} units. Thus the ideal unit cell (without the intrinsic defects) does not represent 105 atoms of β–rhombohedral boron. At the B_{57} unit, one boron atom is missing, so that three extra electrons are removed. At the same time, the interstitial boron atoms, 2.66 (= 8/3) of them provide eight electrons so that the unit cell has (105 -1 + 2.66) 106.66 boron atoms, which is near to 106.83 as proposed by Slack et al (Table 2.3.2a). The 106.66 boron atoms or 320 valence electrons per unit cell is also supported by the few metal doped β-rhombohedral boride experimental structures (Table

2.3.2c). Thus we have showed that the electron sufficient β-rhombohedral boron has non-stoichiometric formula unit, $B_{106.66}$ using *mno* electron counting rule and experimental results. However, we do not know how far these intrinsic defects (2.66 boron atoms) are essential in stabilizing the β-rhombohedral boron and its conducting properties. Therefore, we have analyzed the role of intrinsic defects in stability and conducting properties of β-rhombohedral boron using DFT calculations.

Table 2.3.2c. Percentage of partially occupied lattice and interstitial sites of experimental β-rhombohedral borides and their corresponding volumes.

No	Crystal structure	Site No [symmetry multiplicity] % of occupancy					# of e^-	Vol ($Å^3$)
		13[6]	16[6]	A[2]	E[2]	D[6]		
1	Li8 B103.44[a]	64.00	10.00	0.000	100.0	100.0	318.32	834.765
2	Cu3.72 B103.92[b]	61.10	20.90	6.100	50.50	22.1,10[*]	319.12	829.963
3	Cu4.14 B103.92[c]	69.00	13.00	8.000	61.00	22.0,12[*]	320.04	833.415
4	Fe2.12 B103.36[d]	72.60	0.000	50.70	0.000	18.50	316.44	826.105
5	Hf2.07 B103.42[e]	65.50	8.100	0.500	9.800	31.10	314.40	835.689
6	Zr2.04 B103.04[f]	52.80	14.50	0.000	18.10	27.90	313.20	832.377
7	Cr2.52 B103.30[g]	71.17	0.000	71.90	0.000	18.00	314.94	831.321

[*]It has [12] fold symmetry.
[a]Ref10, [b]Ref43, [c]Ref44, [d]Ref45, [e]Ref42, [f]Ref46, [g]Ref42.

2.3.3 Stability and Conducting Properties

Elemental β-rhombohedral boron is known to be the thermodynamically most stable allotrope of boron at normal temperature and pressure.[44-46] But the calculations suggest that the α-rhombohedral (α-B_{12}) boron is about 0.13 eV/atom more stable than the ideal β-rhombohedral boron (β-B_{105}). This is in contrast to the experimental results. Whereas the results on graphite reproduce it's long known greater thermodynamic

stability than diamond (Table 2.3.3a). The optimized lattice parameters, volume, and density of boron and carbon allotropes are comparable to the experimental results within in the GGA/PBE level of approximation. However, in ideal β-B_{105} the lattice parameters and volume have been relatively increased and hence decrease in the density when compare to the electron sufficient β-$B_{106.83}$.

Table 2.3.3a. Lattice parameters and cohesive energy of α-rhombohedral boron (α-B_{12}), ideal β-rhombohedral boron (β-B_{105}), diamond, and graphite calculated using GGA/PBE functionals. The available experimental values are also tabulated.

System	Space Group	Lattice parameters (A^o)			Vol ($Å^3$)	Density $g.cm^{-3}$	Cohesive[‡] energy (eV)
		a	b	c			
α-B_{12}	R-3M	4.973	4.973	4.973	83.35	2.584	6.67
α-B_{12}[a]	R-3M	5.057	5.057	5.057	87.37	2.465	5.81[*]
β-B_{105}	R-3M	10.14	10.14	10.14	823.4	2.288	6.54
β-B_{105}[b]	R-3M	10.17	10.17	10.17	826.8	2.279	5.31[*] (theory)
β-B_{105}[c]	R-3M	10.14	10.14	10.14	823.2	2.289	-
β-$B_{106.83}$[d]	R-3M	10.13	10.13	10.13	820.3	2.335	-
Diamond	FD-3M	3.534	3.534	3.534	44.16	3.612	9.13
Diamond[e]	FD-3M	3.566	3.566	3.566	45.38	3.515	7.37[†]
Graphite	P63/MMC	2.440	2.440	7.026	36.23	2.202	9.27
Graphite[f]	P63/MMC	2.464	2.464	6.711	35.29	2.261	7.40[†]

[a]Ref37, [b]Ref40, [c]Ref39, [d]Ref3, [e]Ref47, [f]Ref48, [*]Ref48, and [†]LBL Report 3720-Rev.
[‡]Cohesive energies should be considered within the GGA/PBE marginal convergence.

The band structure of α-B_{12} points to a semiconductor behavior with an indirect band gap from the top of the valence bands at Z to the bottom of conduction bands at G of 1.63 eV. The direct band gap at G is found to be 2.0 eV (Figure 2.3.3a). The band gap details are in good agreement with the available experimental and theoretical results.[49, 14] On the other hand the valence band of the ideal β-B_{105} is not completely filled (Figure 2.3.3b). It shows β-rhombohedral boron to be metallic which is contradictory to the

experimental observation that it is a semiconductor.[50] The top three bands of the valence region cross over to the Fermi level and are dispersed within the 0.67 eV near the Fermi region. A significant forbidden gap of about 1.47 eV from the Fermi region to the bottom of the conduction band at F is observed. The indirect gap between the top most band just above the Fermi region at G and the bottom of the conduction band at F is found to be 1.03 eV. This unit cell has 105 atoms. So there are 315 valence electrons available to fill the valence band. But the full valence band can accommodate 320 electrons. The three bands just above the Fermi region could accommodate the rest of the 5 electrons, if sufficient electrons were available. The deficiency of 5 electrons is in good agreement with the suggested electronic requirement of ideal β-B_{105} (B_{57}^{+3} + $4B_{12}^{-2}$) and previous theoretical results proposed by Bullet.[11] This indicates that the ideal β-B_{105} is electron deficient and unstable which contradicts the experimental results. It appears that the partial occupancies and vacancies which accounts for the extra five electrons (1.66 boron atoms) are required for the stability.

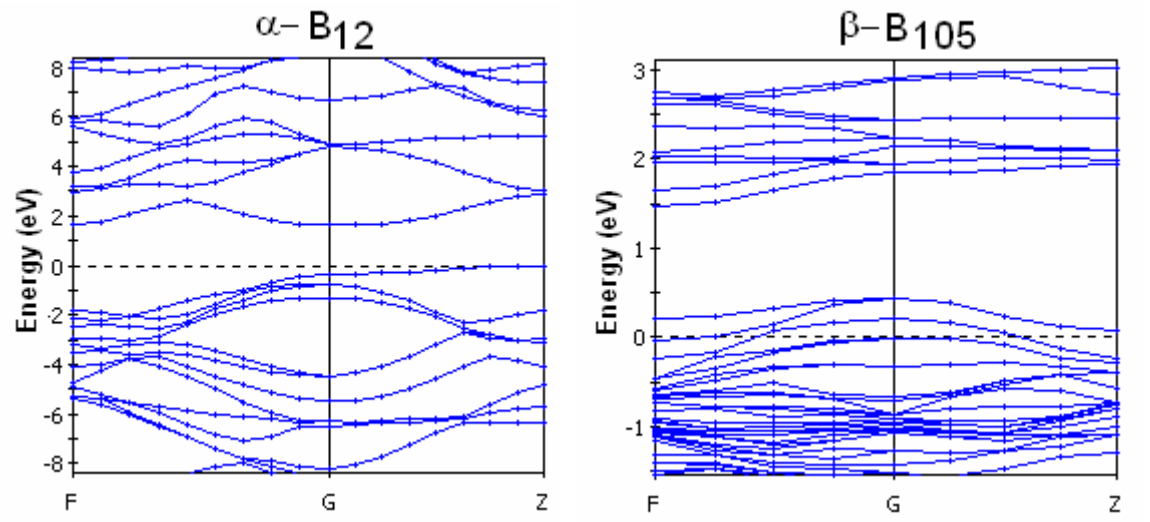

Figure 2.3.3. **(a)** The calculated band structure of α-B_{12} and **(b)** β-B_{105} along their high symmetry points of Brillouin zone. Fermi energy level is indicated by a dotted line.

Therefore, it is necessary to study the β-rhombohedral boron crystal structure with partially occupied sites in order to understand these experimental observations. Unfortunately we could not compute electronic structure of β-rhombohedral boron with partially occupied sites (β-$B_{106.66}$). The size of the unit cell that would have no fractional occupancy will be too large to compute. Instead, the requirement of additional five electrons can be met by adding or substituting appropriate atoms at proper sites of the β-rhombohedral boron unit cell without disturbing its symmetry. The proper cite locations are chosen in such a way that the local electronic requirement of the polyhedral cluster fragments of β-rhombohedral boron should be satisfied. As we have already seen the ideal β-B_{105} is five electrons deficient since a stable B_{57} fragment is B_{57}^{+3} and the four icosahedral B_{12} fragments require two electron each for the stability (β-B_{105}^{-5} = B_{57}^{+3} + $4B_{12}^{-2}$). But the elemental β-rhombohedral boron can not be a charged species. Therefore, The B_{57}^{+3} and the $4B_{12}^{-2}$ fragments are systematically made neutral by doping with proper atoms. These fragments dangling valences are saturated by hydrogens and are further validated for their stability using density functional calculations. This facilitates to model doped β-rhombohedral boron that closely represent the electron sufficient β-rhombohedral boron (β-$B_{106.66}$).

There are several justifications for the above approach. Metal doped endohedral borane clusters (B_{12}) are calculated to be stable.[10,51] As we know the B_{57} unit in the β–rhombohedral boron is having three electrons more than necessary (Table 2.3.2b), the only possibility to make B_{57} unit electron sufficient and yet retain symmetry of the β-rhombohedral boron solid is by substitution of boron by atoms with sufficient number of

electrons (Be, C, Li, Ca, Mg, etc.). It is found that there are three locations in B_{57} unit where one can substitute foreign atoms providing with reduction of 3 electrons. These sites are the two centers of the B_{28} units B[14] and the center of the B_{57} unit B[15] site. Therefore the following electron precise hydrogenated fragments are generated based on *mno* rule (Table 2.3.2b): $B_{28}H_{21}^{+1}$, $LiB_{27}H_{21}^{-1}$, $BeB_{27}H_{21}$, $CB_{27}H_{21}^{+2}$, $MgB_{27}H_{21}$, $SiB_{27}H_{21}^{+2}$, $B_{57}H_{36}^{+3}$, $Be_3B_{54}H_{36}$, $Li_2CB_{54}H_{36}$, $Be_2MgB_{54}H_{36}$ and $Mg_3B_{54}H_{36}$.

Among the many combinations examined the structures with Be, Li, and C as replacement atoms are found to be suitable (Table 2.3.3b). All structures except the clusters with Mg and Si atoms are found to be minima. But in the case of $B_{57}H_{36}^{+3}$, $Be_3B_{54}H_{36}$ and $Li_2CB_{54}H_{36}$ imaginary vibrational frequencies of -14.33, -31.16 and -48.38 cm^{-1} respectively are calculated. However in solids these small imaginary frequencies are known to be soft-modes, indicating a structural instability. As temperature decreases, the soft mode freezes and approaches to zero. The imaginary modes of vibrations in $B_{57}H_{36}^{+3}$, $Be_3B_{54}H_{36}$, and $Li_2CB_{54}H_{36}$ are A_{1u} and E_u type within D_{3d} symmetry. The A_{1u} is partial rotation of two B_{28} units in opposite direction (↑↓) about the B[15] center and the E_u is a bending mode of B_{28}-B-B_{28}. Even if these are not ground states as isolated molecules, these could be stable building blocks in a rigid rhombohedral framework. The stable clusters are found to have large HOMO-LUMO gaps. The bond lengths in these clusters are found to be similar to those of the *closo*- and stuffed polyhedral boranes.[51] There is an acceptable agreement between the bond lengths of the B_{57} skeleton of B_{105} and the calculated $B_{57}H_{36}^{+3}$ cluster. The B-B bond distance (1.988 Å) of the two triangles (B[13] sites) that connect the central boron atom (Figure 2.3.2 j) is very close value of

1.989 Å obtained from the X-ray structure. The B-B distance between the central boron atom (B[15]) to the boron atom of the adjacent B_3 ring (B[13] sites) in B_{105} of 1.735 Å is close to the distance of 1.785 Å calculated for $B_{57}H_{36}^{+3}$.

Table 2.3.3b. The average bond distances, lowest vibrational frequencies (min freq) and HOMO – LUMO (H-L) gaps at GGA Becke Perdew/DZ level for $B_{28}H_{21}^{+}$, $B_{57}H_{36}^{+3}$ and their isoelectronically substituted clusters.

S.No	Substituted Cluster	Average bond distances (Å)			min freq (cm^{-1})	H-L gap (eV)
		B-B	[14]-B ([13]-[15])	[14]-[15]		
1	$B_{28}H_{21}^{+1}$	1.854	1.849	-	146.1	3.375
2	$LiB_{27}H_{21}^{-1}$	1.887	1.864	-	156.6	2.404
3	$BeB_{27}H_{21}$	1.864	1.847	-	149.4	3.015
4	$CB_{27}H_{21}^{+2}$	1.882	1.912	-	6.4	3.331
5	$MgB_{27}H_{21}$	1.868	2.246	-	-201.6	1.133
6	$SiB_{27}H_{21}^{+2}$	1.834	2.122	-	-138.9	2.384
7	$B_{57}H_{36}^{+3}$	1.911	1.802 (1.785)	2.816	-14.3	3.427
8	$Be_3B_{54}H_{36}$	1.863	1.809 (1.843)	2.932	-31.1	2.494
9	$Li_2CB_{54}H_{36}$	1.862	1.815 (1.742)	2.744	-48.3	2.694
10	$Be_2MgB_{54}H_{36}$	1.869	1.806 (2.349)	3.545	-418.5	0.743
11	$Mg_3B_{54}H_{36}$	1.890	2.283 (-)	3.539	-137.2	0.388
12	$B_{106.66}$	1.799	1.768 (1.687)	2.726	-	-
13	$Li_8Be_3B_{102}$	1.805	1.765 (1.746)	2.790	-	-
14	$Li_{10}CB_{102}$	1.789	1.796 (1.703)	2.751	-	-

The specific combinations used are Be_3 and LiCLi at the B[14], B[15] and B[14] positions of β–rhombohedral boron to achieve the electron precise neutral B_{57} unit ($Be_3B_{54}H_{36}$ and $Li_2CB_{54}H_{36}$). Let us now look at the remaining part of the unit cell, the icosahedral B_{12} fragments. The four icosahedra here are electron deficient by two electrons each. It needs 8 electrons extra per unit cell to satisfy the electron requirements of the four icosahedra. The holes that are present in the β–rhombohedral boron are well

suited to add the extra electrons. Using the experimental information of metal doped β–rhombohedral boron, the preferred holes to dope the foreign atoms can be located. The sites near by A, E, and D holes can accommodate required number of electrons respectively. Adding appropriate atoms to these locations, one can design numerous β–rhombohedral borides with full occupancy and without disturbing its crystal symmetry. The hole A has six-fold symmetry and the hole E has two-fold symmetry as shown in Figure 2.3.3c. Therefore A and E holes can accommodate six and two Li atoms which provide eight electrons that are required for four icosahedra. Resultantly to accommodate five electrons (-8 for four B_{12} units +3 for B_{57} unit =5) we choose Li, Be, and C atoms in those particular positions. This generates unit cells A-Li_6-E-Li_2-Be_3B_{102} ($Li_8Be_3B_{102}$) and A-Li_6-E-Li_2-CLi_2B_{102} ($Li_{10}CB_{102}$). The viability of these model crystals is supported by the known boranes and the corresponding borides doped by Be, Li and C atoms.[52-55]

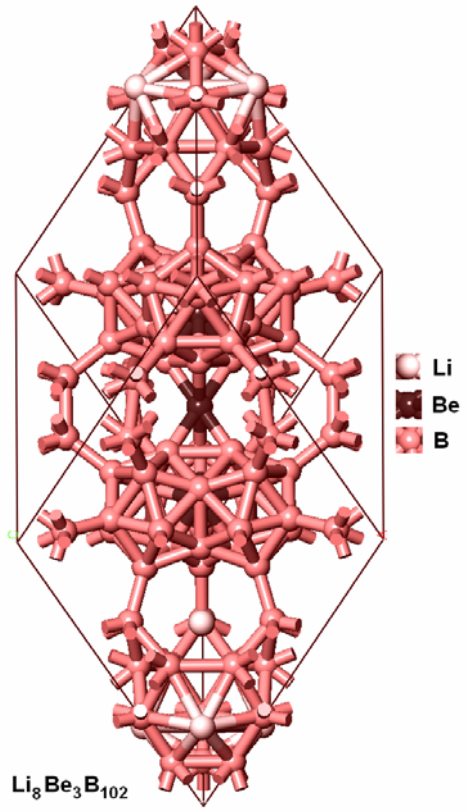

Figure 2.3.3. (c) The A and E holes of the optimized rhombohedral $Li_8Be_3B_{102}$ boride showing the Li positions. The substituted Be at B[14] and B[15] also can be seen.

The band structure justifies our anticipation that the valence band should be completely occupied by electrons. The valence and conduction bands of $Li_8Be_3B_{102}$ are well separated in the given Brillouins zone. An indirect band gap of about 1.7 eV is observed from the top of valence band at G and the bottom of conduction band at F zones as shown in Figure 2.3.3d. The PDOS of Be shows that the Be bands are present just below the Fermi region as shown in Figure 3.3.3f. The PDOS of center Be atom of B_{57} unit falls at the Fermi level. The rest of the two Be PDOS are 14 eV away from the Fermi region. The Li bands are located at the very bottom of the Fermi region, which indicated that these are localized. The valence and conduction bands of $Li_{10}CB_{102}$ are well separated. But a band can be seen very near to the Fermi surface in G-Z direction (2.3.3e). An indirect band gap of 1.88 eV from the top of the valence band at G and the bottom of the conduction band at F is observed.

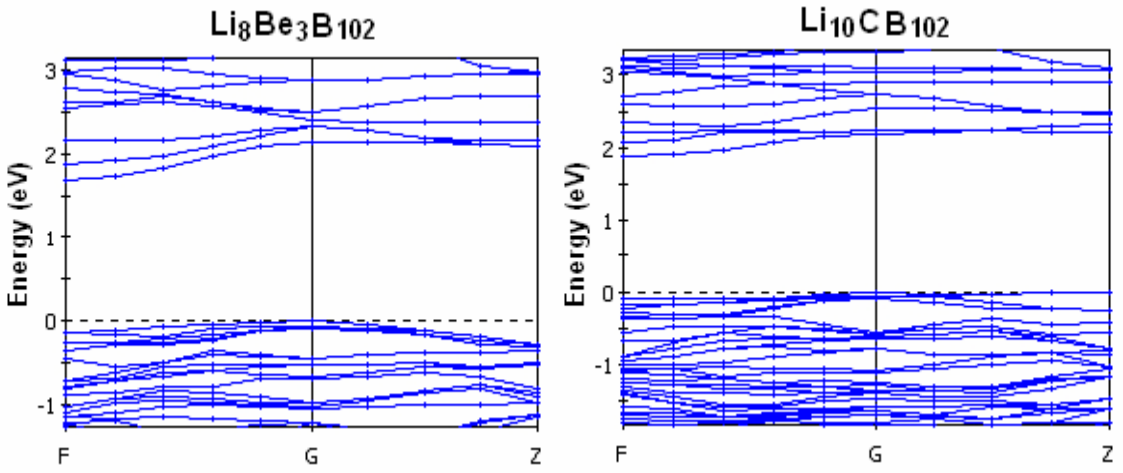

Figure 2.3.3. (d) The calculated band structure of $Li_8Be_3B_{102}$ and **(e)** $Li_{10}CB_{102}$ along their high symmetry points of Brillouin zone. Fermi energy is indicated by a dotted line.

The PDOS shows the presence of the carbon bands away from the Fermi region. These are dispersed in the range of 2-17 eV. Interestingly the bands generated by Li in any part of the unit cell are observed around the same energy (2.3.3f). In view of the low percentage of doping, the PDOS contribution from the hetero atom is small everywhere. The contribution of the two B_3 triangles to the band structure is substantial in the Fermi region and do not change in the doped structures. In the case of idealized B_{105}, these bands are not completely filled. In experimental β-$B_{106.83}$ these bands are filled using the electrons available from intrinsic defects. In the model systems the doped atoms provide these extra electrons. It shows that Li is almost completely Li^+ in the unit cell. The PDOS arising from the Be and C atoms are in the same region of energy as that obtained for the bands of the two central boron atoms of the B_{28} and the central boron atom of B_{57} (2.3.3f).

The reduction of volume of these model crystals (815.3 Å in A-Li_6-E-Li_2-Be_3B_{102}, 807.9 Å in A-Li_6-E-Li_2-CLi_2B_{102} from the ideal B_{105} (823.4 Å) indicates the extra stabilization obtained by doping (Table 2.3.3c). The mixing energies of these solids were evaluated by taking the standard binding energies of Li, Be, α-rhombohedral boron and graphite. According to this the stabilization energies of A-Li_6-E-Li_2-Be_3B_{102} and A-Li_6-E-Li_2-CLi_2B_{102} are 4.25 eV and 0.67 eV respectively. We have also modeled similar type of experimentally found ~Li_8B_{104} (Table 2.3.2c) where the Li atoms are occupied at E and D sites, generates E-Li_2-D-Li_6-Be_3B_{102}. And we have checked the A and D site preference with A-Li_2-D-Li_6-Be_3B_{102}. The mixing energies sows that the former is 5.49 eV and the later is 5.62 eV stable (Table 2.3.3c). If we look at the ~Li_8B_{104} the partial occupancy

nature is decreased from the experimental $B_{106.83}$. Perhaps tuning the electron count based on cluster fragments approach would still reduce the partial occupancy ($Li_8Be_3B_{102}$).

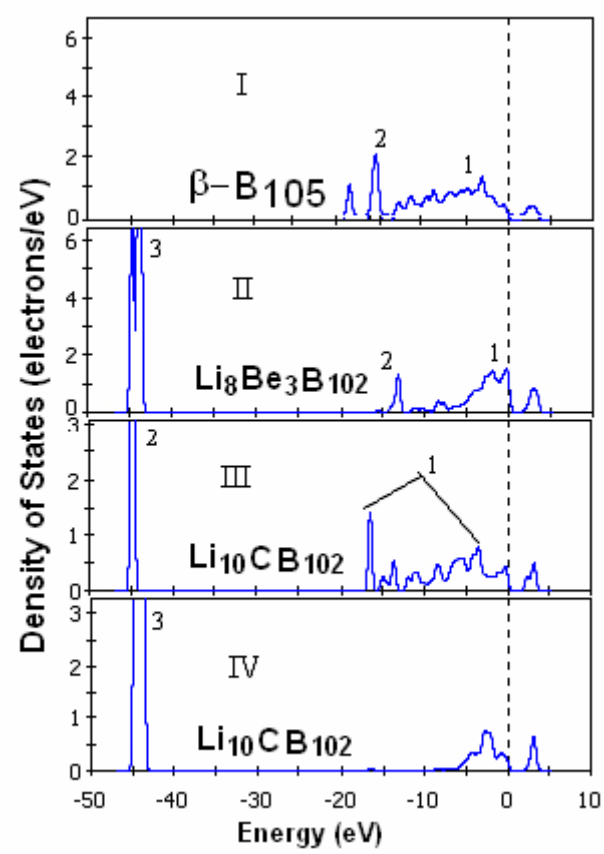

Figure 2.3.3f. The calculated PDOS for B_{105}, $Li_8Be_3B_{102}$ and $Li_{10}CB_{102}$. (I) The PDOS of three boron atoms located at the centers of B_{57} (1) B[15] and of two B_{28} (2) B[14] units in the B_{105}. (II) The PDOS of three Be atoms are located at B[14] and B[15] positions and Li atoms at A and E holes in $Li_8Be_3B_{102}$. (III) The PDOS of one C and two Li at B[15] and B[14] positions in $Li_{10}CB_{102}$. (IV) The PDOS of 8 Li at A and E holes of in $Li_{10}CB_{102}$.

Table 2.3.3c. Space groups, lattice parameters, volume (V), Density (D) and the total energy per atom calculated using GGA/PBE for Li and Be elemental solids and the model rhombohedral borides.

System	Space Group	Lattice parameters (Å)			Vol ($Å^3$)	D ($g.cm^{-3}$)	Total Energy (eV)
		a	b	c			
Lithium	IM-3M	3.424	3.424	3.424	40.17	0.573	-190.03[a]
Beryllium	P93/MMC	2.277	2.277	3.563	16.00	1.869	-30.89[a]
A-Li_6-E-Li_2-Be_3B_{102}	R-3M	10.13	10.13	10.13	815.3	2.413	-9548.05
E-Li_2-D-Li_6-Be_3B_{102}	R-3M	10.12	10.12	10.12	809.9	2.429	-9549.27
A-Li_2-D-Li_6-Be_3B_{102}	R-3M	10.12	10.12	10.12	810.7	2.427	-9549.40
A-Li_6-E-Li_2-CLi_2B_{102}	R-3M	10.08	10.08	10.08	807.9	2.433	-9987.81

[a]Total Energy per atom.

However many metal doped β-rhombohedral boron crystal structures reveal that, the doped atoms occupy the interstitial positions rather than substituting boron atoms. In order to maintain the electron count, it chooses partial occupancy as an intrinsic defect. The band gaps of the above model structures are similar to β-rhombohedral boron and some of the metal doped β-rhombohedral borides which are semiconductors.[12] This shows the essential similarity between β-rhombohedral boron ($B_{106.83}$), boron rich metal borides and the model systems studied. These results should help to understand the conducting properties of borides with respect to the intrinsic defects.

2.4 Conclusion

The structural details of α-rhombohedral boron and β-rhombohedral boron which are dominated by the icosahedral B_{12} unit are discussed in a view to understand their

electronic structure using cluster fragment approach. The stability of the fragmented clusters (mainly B_{12}, B_{28}, and B_{57}) of these allotropes is evaluated by *mno* electron counting rule. This has facilitated to understand the electronic requirements and the origin of the intrinsic defects in β-rhombohedral boron. The electron sufficient nature of α-rhombohedral boron is clear due its resourceful way of sharing electrons through 3c-2e bonds, where vacant or partially occupied sites are not seen in the lattice. The mystery of five missing electrons of the β-rhombohedral boron is understood through cluster fragment approach. That is the β-$B_{106.66}$ = β-B_{105}^{-5} (B_{57}^{+3} + $4B_{12}^{-2}$). The electronic requirement criterion of β-$B_{106.66}$ is verified by the DFT calculations. The calculations suggest that the ideal β-rhombohedral boron is less stable than α-rhombohedral boron. In addition the band structure indicates β-rhombohedral boron to be metallic which is contrary to the experimental results. These theoretical results, which are contrary to experiments, are explained using model solids where the five missing electrons are provided to the ideal β-rhombohedral boron by doping and substitution of strategic atoms like Li, Be and C. The nature and position of various doping atoms are inferred from the studies on fragments of β-rhombohedral boron designed using the *mno* rule such as $B_{12}H_{12}^{-2}$, $B_{28}H_{21}^{+1}$, $BeB_{27}H_{21}$, $LiB_{27}H_{21}^{-1}$, $CB_{27}H_{21}^{+2}$, $B_{57}H_{36}^{+3}$, $Be_3B_{54}H_{36}$ and $Li_2CB_{54}H_{36}$. This fragmented analysis generated electron sufficient β-rhombohedral borides $Li_8Be_3B_{102}$ and $Li_{10}CB_{102}$ are found to be stable. The band structure details shows $Li_8Be_3B_{102}$ and $Li_{10}CB_{102}$ are semiconductors similar to β-$B_{106.83}$ and many known β-rhombohedral borides. Finally, the entire structural and electronic analysis suggests that the vacancies and partial occupancies in β-rhombohedral boron are necessary to stabilize the structure and also for its semiconducting properties. We make use of the electron

sufficient $Li_8Be_3B_{102}$ and $Li_{10}CB_{102}$ solids to understand the role of intrinsic defects in mechanical properties of boron allotropes, which will be discussed in Chapter 5.

References

[1] G. H. Fetterly, in *Boron Synthesis, Structure and Properties*, edited by J. A. Kohn, W. F. Nye, and G. K. Gaulé (Plenum, New York), 1960.

[2] J. Donohue, *The Structure of the Elements*, (Wiley: New York), 1974.

[3] G. A. Slack, C. I. Hejna, M. F. Garbauskas, and J. S. Kasper, J. Solid State Chem. **76**, 52 (1988).

[4] S. Krishnan, S. Ansell, J. J. Felten, K. J. Volin, and D. L. Price, Phys. Rev. Lett. **81**, 586 (1998).

[5] R. Frang and H. Werheit, Europhys. Lett. **9**, 145 (1989).

[6] H. Werheit, M. Luax, and U. Kuhlmann, Phys. Status Solid B **176**, 415 (1993).

[7] R. Schmechel and H. Werheit, J. Phys.: Condens. Matter. **11**, 6803 (1999).

[8] *Boron-Rich Solids*, edited by D. Emin, T. L. Aselage, A. C. Switendick, B. Morosin, and C. L. Beckel, AIP Conf. Proc. No. 231 (AIP, New York), 1991.

[9] M. Fujimori and K. Kimura, J. Solid State Chem. **133**, 178 (1997).

[10] M. Kobayashi, I. Higashi, H. Matsuda, and K. Kimura, Journal of Alloys Compd. **221**, 120 (1995).

[11] D. W. Bullet, J. Phys. C **15**, 415 (1982).

[12] S. Lee, D. M. Bylander, and L. Kleinman, Phys. Rev. B **42**, 1316 (1990).

[13] Y. Imai, M. Mukaida, M. Ueda, and A. Watanabe, J. Alloys and Comp. **347**, 244 (2002).

[14] J. Zhao and J. P. Lu, Phys. Rev. B **66**, 092101 (2002).

[15] E. D. Jemmis and M. M. Balakrishnarajan, J. Am. Chem.Soc. **123**, 4324 (2001).

[16] E. D. Jemmis, Chemtracts-Inorganic Chemistry, **18**, 620 (2005).

[17] M. M. Balakrishnarajan and E. D. Jemmis, J. Am. Chem. Soc. **122**, 456 (2000).

[18] E. D. Jemmis, M. M. Balakrishnarajan, and P. D. Pancharatna, J. Am Chem. Soc. **123**, 4313 (2001).

[19] E. D. Jemmis, M. M. Balakrishnarajan, and P. D. Pancharatna, Chem. Rev. (Washington, D.C.) **102**, 93 (2002).

[20] E. Z. Huckel, Phys. **76**, 628 (1932).

[21] M. D Segall, P. J. D. Lindan, M. J. Probert, C. J. Pickard, P. J. Hasnip, S. J. Clark, and M. C. Payne, J. Phys.: Condens. Matter **14**, 2717 (2002).

[22] Accelrys Inc., Materials Studio CASTEP, San Diego, *Accelrys Inc*, 2001.

[23] J. P. Perdew, K. Burke, and M. Ernzerhof, Phys. Rev. Lett. **77**, 3865 (1996).

[24] D. Vanderbilt, Phys. Rev. B **41**, 7892 (1990).

[25] H. J. Monkhorst and J. D. Pack, Phys. Rev. B **13**, 5188 (1976).

[26] T. H. Fischer and J. Almlof, J. Phys. Chem. **96**, 9768 (1992).

[27] P. Pulay, J. Comput. Chem. **3**, 556 (1982).

[28] ADF2002.03, SCM, TheoreticalChemistry, Vrije Universiteit, Amsterdam, http://www.scm.com

[29] K. Wade, J. Chem. Soc. Chem. Commun. **792**, (1971).

[30] M. A. Fox, and K. Wade, Pure Appl. Chem. **75**, 1315 (2003).

[31] E. D. Jemmis, J. Am. Chem. Soc. **104**, 7017 (1982).

[32] E. D. Jemmis and P. V. R. Schleyer, J. Am. Chem. Soc. **104**, 4781 (1982).

[33] P.v.R.Schleyer and K. Najafian, Inorg. Chem. **37**, 3454 (1998).

[34] P.v.R. Schleyer, K. Najafian, and A.M. Mebel, Chem. **37**, 6765 (1998).

[35] E.D. Jemmis and M.M. Balakrishnarajan, Bull. Mater. Sci. **22**, 863 (1999).

[36] E. D. Jemmis, M. M. Balakrishnarajan, and P. D. Pancharatna, Chem. Rev. **102**, 93 (2002).

[37] B. F. Decker and J. S. Kasper, Acta Crystallogr.**12**, 503 (1959).

[38] H. C. Longuet-Higgins and M. de V. Roberts, Proc. Roy. Soc., (London) **230A**, 110 (1955).

[39] J. L. Hoard, D. B. Sullinger, C. H. L. Kennard, and R. E. Hughes, J. Solid State Chem. **1**, 268 (1970).

[40] D. Geist, R. Kloss and H. Follner, Acta Crystallogr. B**26**, 1800 (1970).

[41] B. Calmer, Acta Crystallogr. B**33**, 1951 (1977).

[42] G.A. Slack, C.I. Hejna, M.F. Garbauskas, and J.S. Kasper, J. Solid State Chem. **76**, 64 (1988).

[43] S. Andersson and B. Callmer, Journal of Solid State Chem. **10**, 219 (1974).

[44] I. Higashi, T. Sakurai, and T. Atoda, Journal of the Less-Common Metals. **45**, 283 (1976).

[45] B. Callmer and T. Lundstroem, Journal of Solid State Chem. **17**, 165 (1976).

[46] B. Callmer, L. E. Tergenius, and J. O. Thomas, Journal of Solid State Chem. **26**, 275 (1978).

[44] N. Greenwood, and A. Earnshaw, *Chemistry of the Elements* (Buttreworth-Heinemann, UK), 1997.

[45] J. L. Hoard, and A. E. Newkirk, J. Am. Chem. Soc. **82**, 70 (1960).

[46] P. Runow, Journal of Materials Science **7**, 499 (1972).

[47] T. Hom, W. Kiszenik, and B. Post, Journal of Applied Physics **8**, 457 (1975).

[48] M. Takeda, K. Kimura, A. Hori, H. Yamashita, and H. Ino, Phys. Rev **B** 48, 13161 (1993).

[49] F. H. Horn, J. Appl. Phys. **30**, 1611 (1959).

[50] R. Schmechel and H. Werheit, J. Solid State Chem. **154**, 61 (2000).

[51] E.D. Jemmis and M. M. Balakrishnarajan, J. Am. Chem. Soc. **122**, 7392 (2000).

[52] R. W. Rudolph, Acc. Chem. Res. **9**, 440 (1976).

[53] J. C. Calabrese, D. F. Gaines, S. J. Hildebrandt, and J. H. Morris, J. Am. Chem. Soc. **98**, 5489 (1976).

[54] D. F. Gaines, J. L. Walsh, and J. C. Calabrese, Inorg. Chem. **17**, 1242 (1978).

[55] A. Kirfel, A. Gupta, and G. Will, Acta. Crystallogr. B **35**, 1052 (1979).

Chapter 3

Stuffed Fullerene-like Boron and Boron Carbide Clusters

3.1 Introduction

Buckminsterfullerene, C_{60} – a truncated icosahedron with 12 pentagons and 20 hexagons (Figure 3.1a) – has been a promising molecule for its prodigious and spectacular chemical and physical properties.[1-8] This aesthetically pleasing hollow spherical molecule ascended as high temperature superconductor when doped with alkali metals.[9-13] Uses such as superhard fullerite,[14-16] catalyst,[17,18] drug carrier,[19-21] and hydrogen storage materials[22-24] have been suggested in recent years. These interesting properties and zero-dimensional (0D) chemical structure of C_{60} has motivated to search for fullerene-like molecules based on other elements in the periodic table. There has been considerable amount of success in generating substitutional doped fullerenes called *dopyballs* with boron ($C_{60-n}B_n$, n = 1–12), nitrogen ($C_{60-n}N_n$, n = 1–12) and few other heteroatoms soon after the discovery of C_{60} fullerene by Kroto *et al* in 1985.[25-42] Binary inorganic fullerene-

like structures (IFs) such as MoS_2, WS_2, BN, and several intermetallic phases such as $Ni@In_{10}@Na_{37}@In_{70}$, $As@Ni_{12}@As_{20}$ etc have been synthesized recently.[43-58] On the other hand a variety of computational methods have also been applied to predict vast numbers of inorganic fullerene-like structures.[31-39,52,53] However, there are many elements in the periodic table yet to uncover for elemental and inter-elemental inorganic fullerene-like structures.

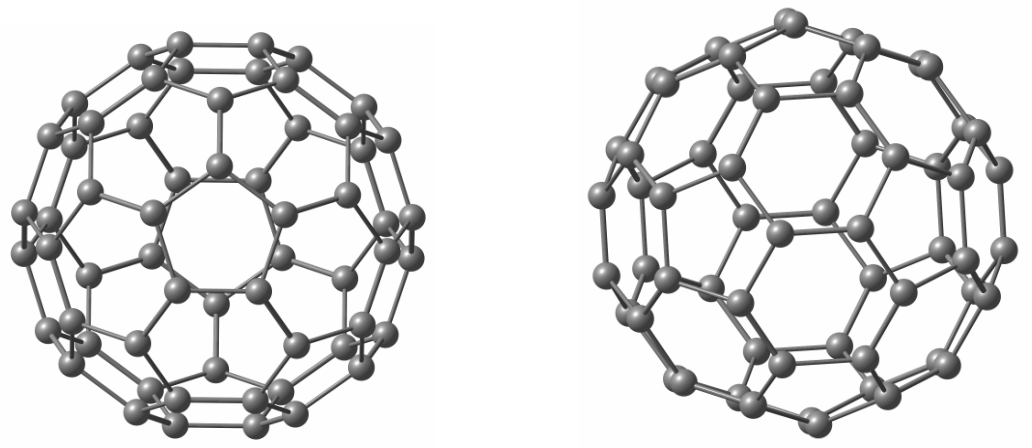

Figure 3.1. (a). Buckminsterfullerene, C_{60} shown in truncated icosahedron symmetry along the C_5 axis (left) and inclined C_2 axis (right).

Our earlier study on boranes, carboranes, and allotropes of boron shows that fullerene-like boron and boron carbide clusters based on an electron deficient icosahedral B_{84} fragment of elemental β-rhombohedral boron would be viable.[59-64] In this chapter we investigate modeling of boron and boron carbide fullerene-like structures based B_{84} fragment using qualitative electron counting and valence rules of boranes and carboranes.[63-77] The modeled fullerene-like boron and boron carbide clusters are then

analyzed for their electronic structure and stability using *ab initio* density functional theoretical calculations.

Let us begin with the structure of B_{84} fragment and the construction of stable fullerene-like boron and boron carbide clusters. A fullerene-like structure for boron as a distorted icosahedral B_{84} fragment can be seen in the complex extended covalent network of β-rhombohedral boron that we discussed in the previous chapter. But B_{84} is not hollow like C_{60}. It is stuffed with an icosahedral *closo*-B_{12} fragment and its 12 vertices are connected to 12 pentagonal pyramidal fragments (*nido*-B_6) via radial 2c-2e σ bonds as shown in Figure 3.1b. The space filling model can allow forming 20 hexagons in between the 12 surface pentagons of the B_6 units which resembles a C_{60} surface. Succinctly B_{84} can be described as $B_{12}@(B_6)_{12}$ or $B_{12}@B_{12}@B_{60}$ i.e. B_{60} is stuffed by an icosahedral B_{12} fragment and then the 12 pentagons of B_{60} and the 12 vertices of B_{12} are covalently interlinked by another 12 boron atoms. Hence B_{84} is formally a stuffed fullerene-like boron. However, B_{84} is not a finite cluster in β-rhombohedral boron. The surface of the B_{84} in β-rhombohedral boron crystal structure is three dimensionally connected by near polyhedral skeletons with electron deficient multi-center bonding (Chapter 2, Figure 2.3.2a-i). So the termination of the multi-center bonds between the B_{84} units in the β-rhombohedral boron leads to high electron deficiency and hence instability. The deficiency of the clusters can be calculated by applying Wade's *closo*- *n*+1 and *nido*- *n*+2 (*n* = number of vertices in a polyhedron) polyhedral skeletal electron counting rules[65] on the fragments of B_{84}, inner icosahedral *closo*-B_{12} units and the 12 pentagonal pyramidal *nido*-B_6 units. Accordingly the *closo*-B_{12} requires -2 and *nido*-B_6 requires -4 electrons for

their stability. That is a stable finite B_{84} cluster requires an additional 50 electrons [B_{84}^{-50} = *closo*-B_{12}^{-2} + 12(*nido*-B_6)$^{-4}$]. Therefore, the 50 electron deficient B_{84} should not be expected as a stable finite cluster.

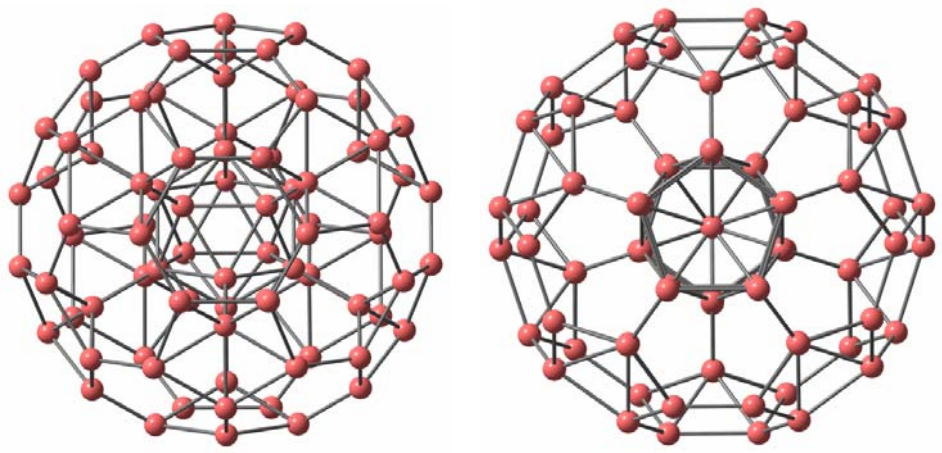

Figure 3.1. (b). Icosahedral B_{84} stuffed fullerene-like boron cluster shown along the C_3 axis (left) and C_5 axis (right). The inner icosahedral *closo*-B_{12} is connected to the outer 12 pentagonal pyramidal *nido*-B_6 units via radial 2c-2e σ bonds can be seen here.

However, the unstable B_{84} would be a stable species, if the required 50 electrons can be provided. As we have seen the B_{84} structure is highly stabilized in β-rhombohedral boron by compensating the required number of 50 electrons through the condensation and fractionally occupied interstitial boron atoms. For example a *nido*-B_6 pentagonal pyramid of B_{84} is four electrons deficient. Such two *nido*-B_6^{-4} units of two different B_{84} units condense together and produce a two electron deficient icosahedral *closo*-B_{12} unit (Chapter 2, Figure 2.3.2d) in between the two B_{84} units. The requirement of these two electrons for B_{12} units is further diminished by the formation of extra condensations and fractionally occupied interstitial boron atoms in the β-rhombohedral boron crystal

structure. Majority of the interstitial boron atoms are situated in the in-between gaps of *nido*-B_6 units i.e. near to the 20 hexagons of B_{84} unit. Therefore the condensation process of *nido*-B_6 units largely reduces the requirement of 50 electrons. Here we have adopted similar criteria where the requirement of 50 electrons of B_{84} can be compensated by capping the 12 *nido*-B_6 pentagonal pyramids with boron atoms, where boron provides three valence electrons. Let us see how the electron count goes here. The 12 *nido*-B_6 units require 48 electrons (12 × *nido*-B_6^{-4} = 48). Capping each *nido*-B_6 units by boron reduces the requirement of 48 electrons to 12 (3 × 12 B = 36). The remaining 12 electrons are provided by the extra 4 boron atoms which can be placed on the surface hexagons of B_{84} unit systematically. Thus the requirement of 48 electrons for the 12 *nido*-B_6 units is met. However, there is the inner icosahedral B_{12} unit of B_{84} which needs another two electrons. These two electrons further can be provided by a 0.66 boron (3 × 0.66 B = 2) atom on the surface of the hexagons. Totally we need to provide 16.66 boron atoms to the 50 electron deficient B_{84} cluster (3 × 16.66 B = 50) which gives an electron sufficient $B_{100.66}$ stuffed fullerene-like boron cluster. Therefore, the electron sufficient $B_{100.66}$ would be stable in a finite zero dimensional cluster and does not associate to form extended network that found in the β-rhombohedral boron (Chapter 2, Figure 2.3.2a,c).

But the fractional boron atom in $B_{100.66}$ is not possible to calculate. However, B_{84} can approach near electron sufficiency by adding close integer numbers of 16.66 i.e. 14 – 18 boron atoms on the surface pentagons and hexagons of the cluster systematically. This generates stuffed fullerene-like boron clusters, B_{98} (D_{3d}), B_{99} (C_{3v}), B_{100} (C_{2h}), B_{101} (C_s), and B_{102} (D_{3d}) as shown in Figure 3.1c-g respectively. In principle several combinations are possible to add 14 – 18 boron atoms on the surface pentagons and hexagons of B_{84}

unit. Out of several combinations possible, we have restricted to the ones built from the previous structure of high symmetry B_{96} (I_h). Thus we have qualitatively arrived first elemental stuffed fullerene-like boron clusters using skeletal electron counts.

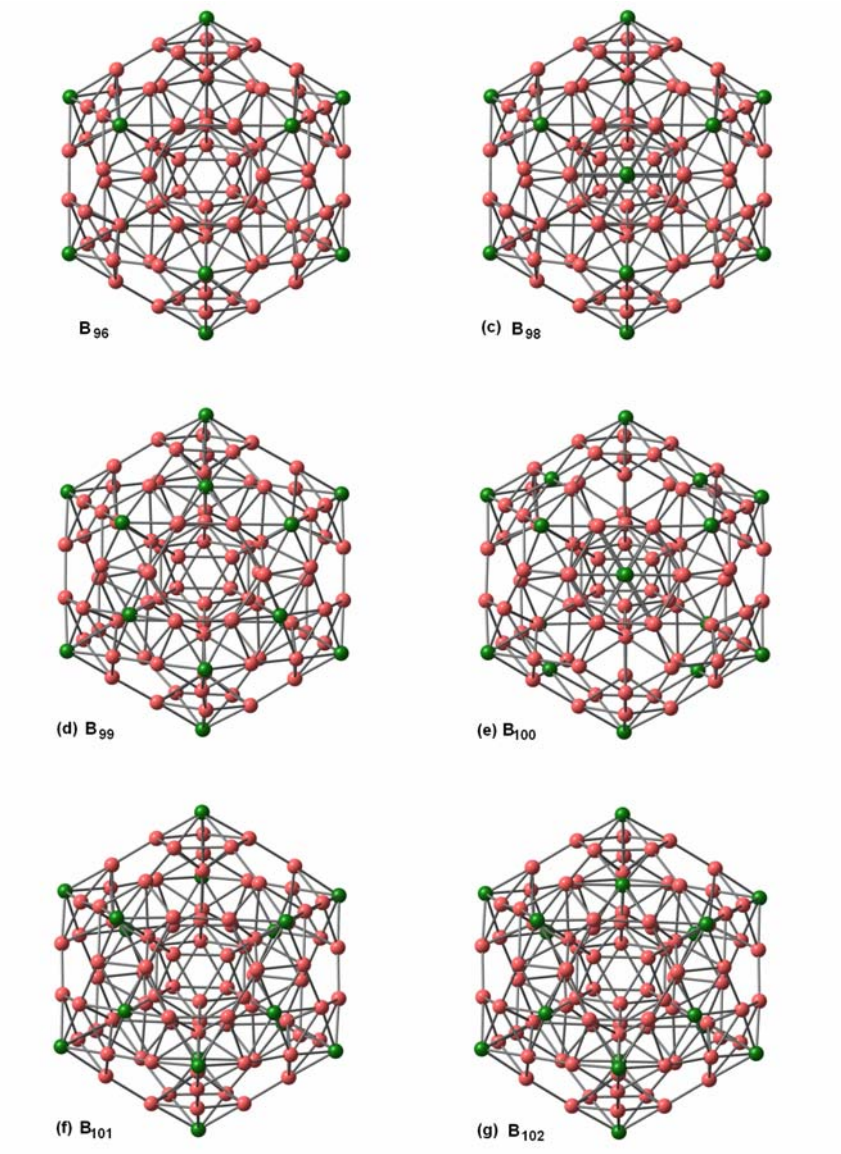

Figure 3.1. Stuffed fullerene-like boron clusters **(c)** B_{98} (D_{3d}), **(d)** B_{99} (C_{3v}), **(e)** B_{100} (C_{2h}), **(f)** B_{101} (C_s), and **(g)** B_{102} (D_{3d}) are constructed from B_{96} (I_h) cluster (top left) are shown. The added boron atoms are indicated in green colour (dark in B&W print).

The above process of stabilizing an electron deficient B_{84} cluster inquires us to look at a similar well known scheme that stabilizes polyhedral borane dianions as neutral carboranes.[66-78] For example an icosahedral borane dianion ($B_{12}H_{12}^{-2}$) can be stabilized by the substitution of two boron atoms by two carbon atoms which gives a neutral $C_2B_{10}H_{12}$. The substitution of boron by carbon is known to foster the stability of boron clusters due to the formation of strong B-C bonds.[70-76] This motivates us to look at the fragments of B_{84}, *closo*-B_{12}^{-2} and *nido*-B_6^{-4}. The dianionic and tetraanionic charges on *closo*-B_{12} and *nido*-B_6 units can be provided by the substitution of two and four carbon atoms respectively. So we get neutral *closo*-C_2B_{10} and *nido*-C_4B_2 units. Essentially, the neutral carboranes are isoelectronic analogues of borane anionic species. This view produces a neutral stuffed fullerene-like boron carbide cluster $C_{50}B_{34}$ = *closo*-C_2B_{10} + 12 (*nido*-C_4B_2). Here, we do not have the problem of fractional atoms as in stuffed fullerene-like boron clusters. But where do we place the carbons for better stability in $C_{50}B_{34}$? The substitution of two carbon atoms in *closo*-B_{12}^{-2} and four carbon atoms in *nido*-B_6^{-4} fragments of B_{84} generates three positional isomers each. They are 1,2-, 1,7-, and 1,12-*closo*-C_2B_{10} and 1,2,5,6-, 1,3,4,6-, and 2,3,4,5-*nido*-C_4B_2 as shown in Figure 3.1h-m respectively. The combination of three isomers of *closo*-C_2B_{10} and three isomers of *nido*-C_4B_2 produce a total number of nine isomers of $C_{50}B_{34}$ clusters. However, the well established experimental and theoretical chemistry of *closo*- and *nido*- carboranes (in our case *closo*-$C_2B_{10}H_{12}$ and *nido*-$C_4B_2H_6$)[66-78] would aid to screen the best possible isomers of $C_{50}B_{34}$. Therefore in order to compare the energetics of stuffed fullerene-like $C_{50}B_{34}$ isomers with respect to their fragments isomers we have created the hydrogenated isomers of *closo*-C_2B_{10} and *nido*-C_4B_2. The hydrogens are added to the dangling valences

of the fragments *closo*-C_2B_{10} and *nido*-C_4B_2. This gives 1,2-, 1,7-, and 1,12-*closo*-$C_2B_{10}H_{12}$ (**1A**, **1B**, **1C** respectively) and 1,2,5,6-, 1,3,4,6-, and 2,3,4,5-*nido*-$C_4B_2H_6$ (**2A**, **2B**, **2C** respectively) as shown in Figure 3.1h-m.

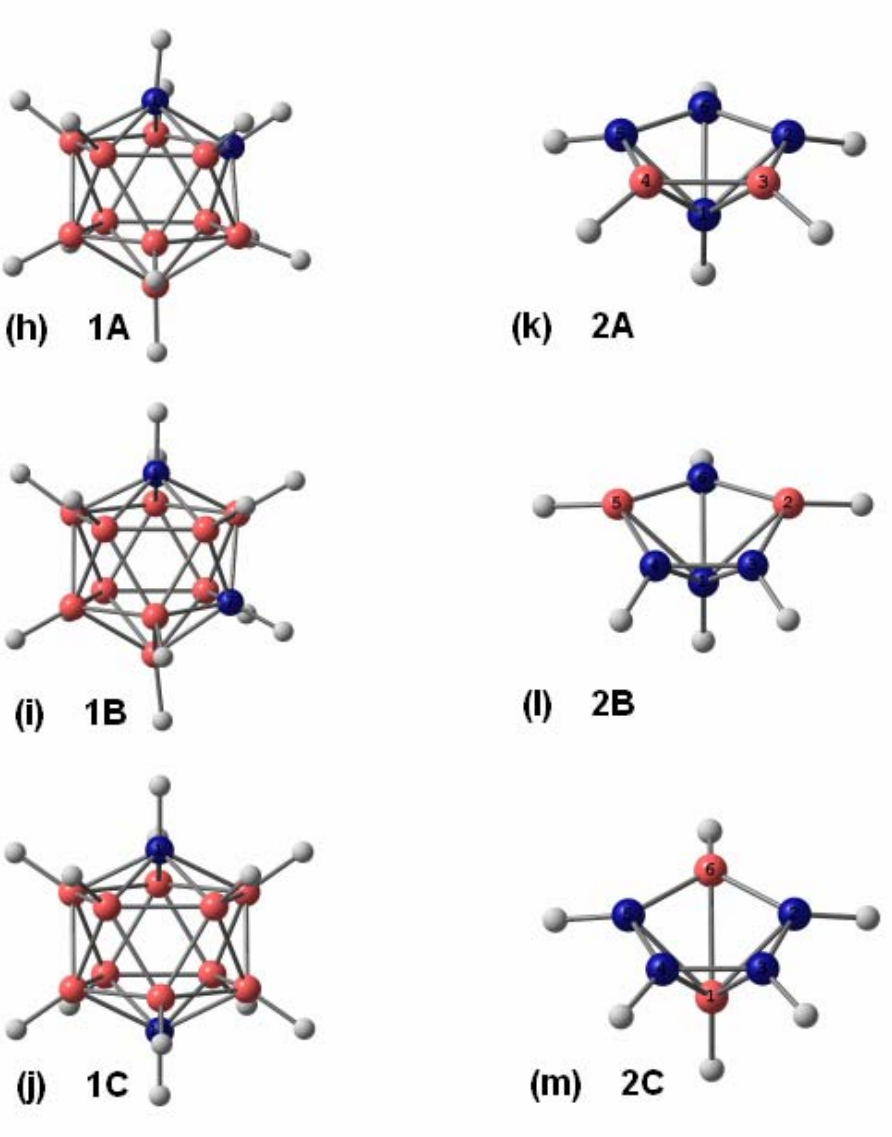

Figure 3.1. In the absence of hydrogens **(h)** 1,2-*closo*-C_2B_{10}, **(i)** 1,7-*closo*-C_2B_{10}, **(j)** 1,12-*closo*-C_2B_{10}, **(k)** 1,2,5,6- *nido*-C_4B_2, **(l)** 1,3,4,6-*nido*-C_4B_2, **(m)** 2,3,4,5-*nido*-$C_4B_2H_6$ and their hydrogenated analogues **1A**, **1B**, **1C, 2A, 2B,** and **2C** respectively. The substituted carbon atoms are shown in thick blue colour (dark in B&W print)

According to the valence rules of carboranes the high electronegative atom (carbon in carboranes) prefers low coordination number and less number of nearest neighbor bonds (C-C).[70-74] Therefore, among the isomers of *closo*-$C_2B_{10}H_{12}$ and *nido*-$C_4B_2H_6$, the 1,12-*closo*-$C_2B_{10}H_{12}$ and 2,3,4,5-*nido*-$C_4B_2H_6$ satisfies the above valence rules and hence the lowest energy isomers. Considering this stabilization criteria of these isomers the best possible stuffed fullerene-like boron carbide cluster would be the combination of 1,12-*closo*-C_2B_{10} and 12 (2,3,4,5-*nido*-C_4B_2) fragments which gives $C_{50}B_{34}$ structure (**3C**) as shown in Figure 3.1n.

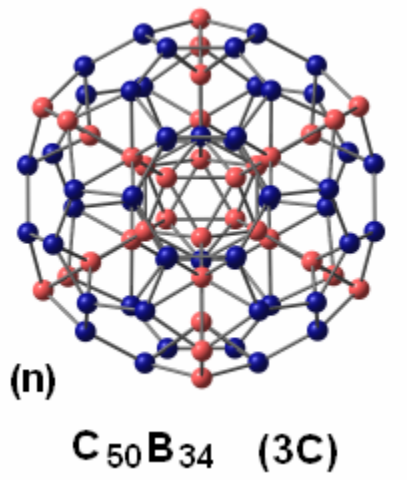

Figure 3.1. (n). Stuffed fullerene-like boron carbide cluster $C_{50}B_{34}$ (**3C**) generated out of the combinations of 1,12-*closo*-C_2B_{10} and 12 (2,3,4,5-*nido*-C_4B_2) fragments. The substituted carbon atoms are shown in thick blue colour (dark in B&W print).

Thus we have achieved stuffed fullerene-like boron and boron carbide clusters based on β-rhombohedral boron crystal structure and polyhedral electron counting rules. Despite these qualitative predictions and observations, we present here quantitative electronic structure and stability of these clusters using first-principles density functional

theory calculations and reason for their stability with respect to the electron counting and valence rules of boranes. We use density of states (DOS) to understand the chemical bonding and the presence of extra added boron and carbon atoms in these clusters. Further, infra-red and Raman active harmonic vibrational frequencies, aromaticity, and electron detachment energies are calculated and compared with C_{60} fullerene.

3.2 Computational Methods

First principles DFT calculations are carried out using DMOL3 and Gaussian 03 programs.[79-80] All the constructed clusters are initially optimized using DMOL3 within the generalized gradient approximation treated by Perdew-Burke-Ernzerhof exchange-correlation potential (GGA/PBE) with an all electron double numerical atomic orbitals augmented by d-polarization functions as basis set (DNP).[81] They are further optimized using Gaussian 03 within Becke three parameter exchange and Lee-Yang-Parr local and non-local correlation hybrid DFT functional, B3LYP/6-31G(d) level of theory for comparisons.[82] The fully relaxed clusters are calculated for harmonic vibrational frequencies by evaluating the matrix of second derivatives of energy with respect to the nuclear positions (Hessian or force constant matrix) at the same level of theories to verify the nature of the stationary point and for zero-point vibrational energy corrections. The infrared (IR) and Raman vibrational intensities have also been calculated by differentiation of dipole derivatives with respect to the electric field by which we can assign spectral activity. The absence of imaginary vibrational frequency confirms that the

clusters are minima on the potential energy surface. In order to understand the three dimensional aromatic character of these clusters, the nucleus-independent chemical shifts (NICS) for the ghost atoms at the center of the clusters has been calculated by employing gauge-independent atomic orbital (GIAO) approach at GIAO-HF/6-31G(d)//B3LYP/6-31G(d) level.[83,84] The calculated NICS values and the highest occupied and the lowest unoccupied molecular orbital energy differences (HOMO–LUMO) of the clusters are used to gauge their stability. For comparisons C_{60} fullerene is also calculated at the same level of theories as mentioned above.

3.3 Results and Discussion

Firstly, we will present the electronic structure and bonding of stuffed fullerene-like boron clusters and then the stuffed fullerene-like boron carbide clusters will be detailed.

3.3.1 Stuffed Fullerene-like Boron Clusters

The near electron sufficient clusters B_{98} (D_{3d}), B_{99} (C_{3v}), B_{100} (C_{2h}), B_{101} (C_s), and B_{102} (D_{3d}) (Figure 3.1c-g) obtained from the 50 electron deficient B_{84} cluster are fully optimized. They are found to retain in the spherical shape without any unusual bond distortions. The average B-B cluster bond distance is about 1.780 Å which is the typical

B-B distance in the borane compounds.[85] When compare to the 50 electron deficient B_{84} cluster the radial 2c-2e σ bonds are shortened from 1.844 to 1.579 Å in B_{98} to B_{102} clusters respectively. The average diameter (average distance between two opposite pentagons) of the nearly electron sufficient clusters is 8.2 Å whereas the B_{84} cluster diameter is about 8.16 Å (optimized in the I_h symmetry constraints) and 9.0 Å in experimental β-rhombohedral boron.[85] What could be the diameter of the hypothetical hollow B_{60} (without the stuffing B_{12} and the apex atoms of B_6 units)? The diameter of a truncated icosahedron can be calculated using solid geometry.[86] Here we consider the diameter (*d*) as 2 × inradius (the distance between the center of the polyhedron and to its face center) of the solid. The inradius of truncated icosahedron numerically can be taken as (2.377) *a*, where *a* is the edge length (B-B bond length). So the diameter of B_{60} is 8.5 Å ($d = 2 \times 2.377 \times a$, where $a = 1.787$ is taken from the most stable borane, $B_{12}H_{12}^{-2}$). The diameter 8.5 Å calculated from the solid geometry suggests that the inner B_{12} unit does not have any space problem to covalently interlink the apex atoms of the pentagonal pyramids (B_6 units) and hence can accommodate within the B_{60} skeleton.

The cohesive energy per atom (E_c) of the optimized stuffed fullerene-like boron clusters are calculated with respect to the electron count. The cohesive energy of these clusters suggests that the "B_{84} (I_h)" gets increasingly more stabilized while nearing electron sufficient structures (Table 3.3.1a). The B_{84} is 0.274 eV higher in energy when compare to 14 electron deficient B_{96} where all the 12 pentagons are capped with boron atoms. The B_{98} (D_{3d}), B_{99} (C_{3v}), B_{100} (C_{2h}), and B_{101} (Cs) are 0.324, 0.332, 0.343, and 0.375 eV lower in energy when compared to B_{84} (I_h) cluster. Among them B_{101} cluster is close to electron sufficient $B_{100.66}$ cluster. The high symmetric cluster near to $B_{100.66}$ is

B_{102} (D_{3d}) which has four electrons more than needed is only 0.006 eV higher than B_{101}. Clusters B_{104} (D_{3d}) and B_{106} (D_{5d}) also calculated by adding two and four boron atoms on the vacant hexagons of B_{102} (Figure 3.3.1a,b). They are found to be 0.091 and 0.168 eV higher than B_{102}. The HOMO-LUMO gap in B_{98} is only 0.062 eV and the gap increases in B_{99} (0.368 eV), B_{100} (0.356 eV), B_{101} (0.419 eV), and B_{102} (0.632 eV) (Table 3.3.1a).

Table 3.3.1a. Cohesive energies (eV/atom) and HOMO – LUMO (H – L) gaps (eV) for different stuffed fullerene-like boron clusters (B_n) along with point groups.

#	B_n Clusters	Point Group	$-E_c$ (eV/atom)	H – L gap (eV)
1	B_{84}	I_h	5.346	0.910
2	B_{96}	I_h	5.620	0.030
3	B_{98}	D_{3d}	5.670	0.062
4	B_{99}	C_{3v}	5.678	0.368
5	B_{100}	C_{2h}	5.689	0.356
6	B_{101}	C_s	5.721	0.419
7	B_{102}	D_{3d}	5.715	0.632
8	B_{104}	D_{3d}	5.626	0.314
9	B_{106}	D_{5d}	5.547	0.613

The harmonic vibrational frequencies for the lowest energy stuffed fullerene-like boron clusters B_{98}, B_{99}, B_{100}, B_{101}, and B_{102} are calculated using GGA/PBE/DNP (DMOL3) method. The clusters B_{100}, B_{101}, and B_{102} are found to be minima on the potential energy surface with significant lowest frequencies (123.2, 191.1, and 207.9 cm^{-1} respectively). The clusters B_{98} and B_{99} are on the first and third order saddle points with one imaginary frequency (-33.0 cm^{-1}), and three imaginary frequencies (-133.9, -117.2, and -117.2) respectively.

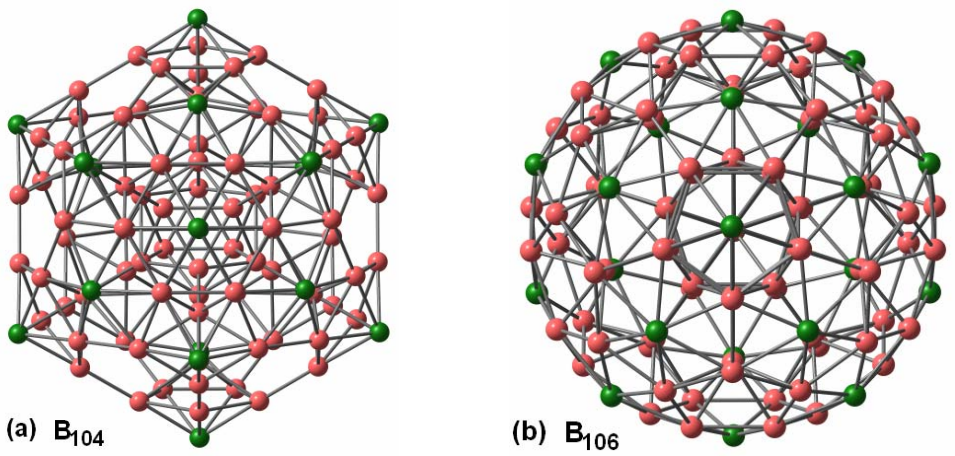

Figure 3.3.1. Stuffed fullerene-like boron clusters **(a)** B_{104} (D_{3d}) where the 12 surface pentagons of B_{84} are capped with boron atoms and another 8 boron atoms are added on the hexagonal centers. **(b)** B_{106} (D_{5d}) where 20 boron atoms are added on the hexagonal centers and the remaining two boron atoms are capped two surface pentagons of B_{84}. The added boron atoms are indicated in green colour (dark in B&W print).

Why is there a range of stable clusters (B_{98} to B_{102}) around $B_{100.66}$? We have to look at the energy of the added electrons in the molecular orbital (MO) energy spectrum. For that, the site projected density of states (PDOS) for B_{102} (high symmetry structure closest to electron sufficient $B_{100.66}$ cluster) has been generated as shown in Figure 3.3.1c. Since the required electrons are provided in terms of boron atoms one should not expect large charge variations from boron to boron. Indeed, the extra 18 boron PDOS of B_{102} are mixing largely with the B_{84} MO electronic states in the entire energy spectra as shown in Figure 3.3.1c. In B_{102} there is a large energy gap (1.348 eV) between HOMO (nearly double degenerate) and HOMO-2 (see Figure 3.3.1c, MO energy bar code), which essentially indicates stability of the $B_{100.66}$ cluster. The geometry of the spherical cluster did not change much with the excess of electrons as in Li_xC_{60} ($6 \leq x \leq 24$) fullerides.[87]

The central hexagonal boron atoms on the surface of the clusters larger than B_{102} are in fact above the surface. The highest unoccupied energy levels are determined by their geometries. If the addition of the required boron atoms retains nearly the same shape of the parent cluster, the added electrons will occupy the energy levels which are largely localized on the parent cluster as in $B_{98} - B_{102}$. The HOMO-2, HOMO, and LUMO of B_{102} cluster are shown in Figure 3.3.1d-f where these frontier orbitals mainly corresponding to the extra added boron atoms.

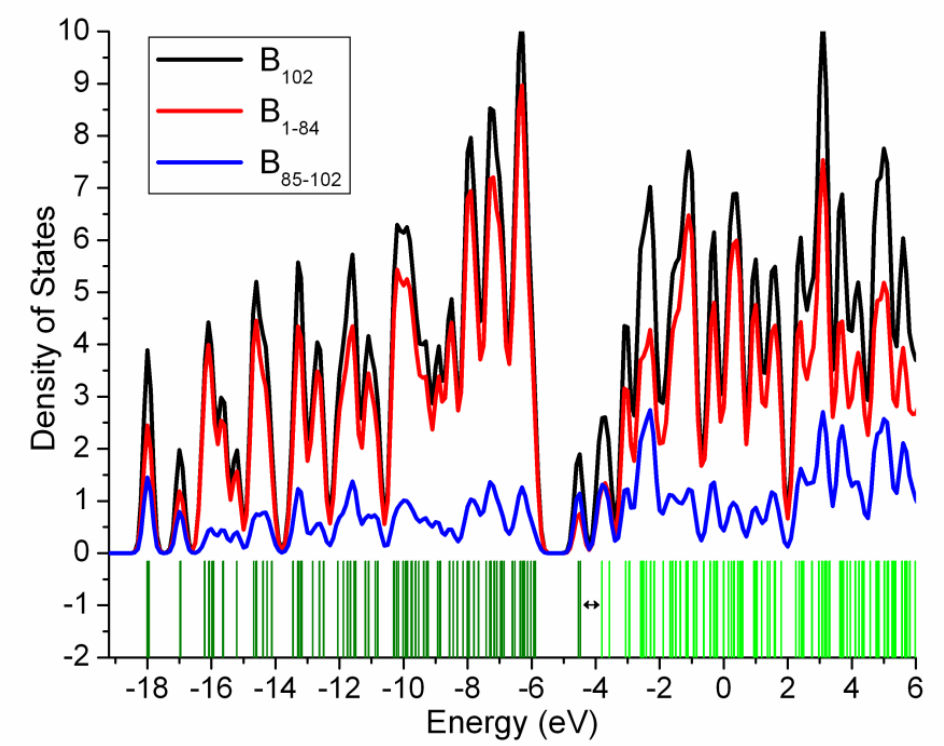

Figure 3.3.1. (c). PDOS of B_{102} stuffed fullerene-like boron cluster. The ↔ between the MO energy bar code indicates the gap between HOMO and LUMO. The energy gap (1.348 eV) between HOMO (nearly double degenerate) and HOMO-2 can be seen here.

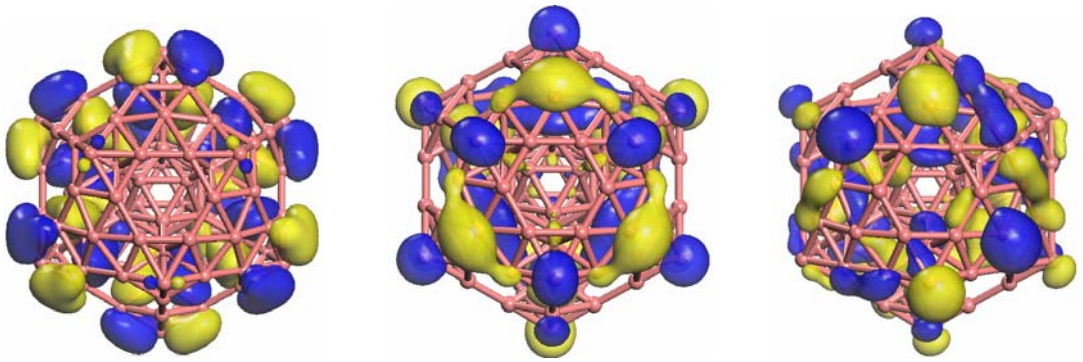

Figure 3.3.1. (left) **(d)** HOMO-2, (middle) **(e)** HOMO, and (right) **(f)** LUMO of B_{102} stuffed fullerene-like boron cluster. HOMO-2 shows the π interaction between the tangential p orbital of the pyramidal boron atoms and perpendicular p orbitals of the surface pentagon of B_6 fragment. HOMO and LUMO are non-bonding orbitals localized on extra added boron atoms.

In order to have a complete energy profile of this B_{84} cluster with respect to the electron count, the B_{108} (D_{2h}), B_{110} (D_{3d}), and B_{116} (I_h) have been generated (Figure 3.3.1g-i). The cohesive energy profile of these clusters shows lowering of energy while reaching the required electron count and rising with excess electrons (Figure 3.3.1j). This strongly suggests that the key to stability of a given cluster is the ability to provide the required number electrons as closely as possible. However, this is not the complete picture. Since several possible isomers can be generated for a given cluster size, the cohesive energy may vary depending on the effectiveness of filling the unoccupied bonding orbitals of B_{84} cluster (Figure 3.3.1c). We have calculated two isomers $\underline{B_{102}}$ (D_{3d}) and $\underline{B_{104}}$ (I_h) (Figure 3.3.1k,l) where the extra boron atoms are added only on the hexagonal centers of B_{84} cluster.

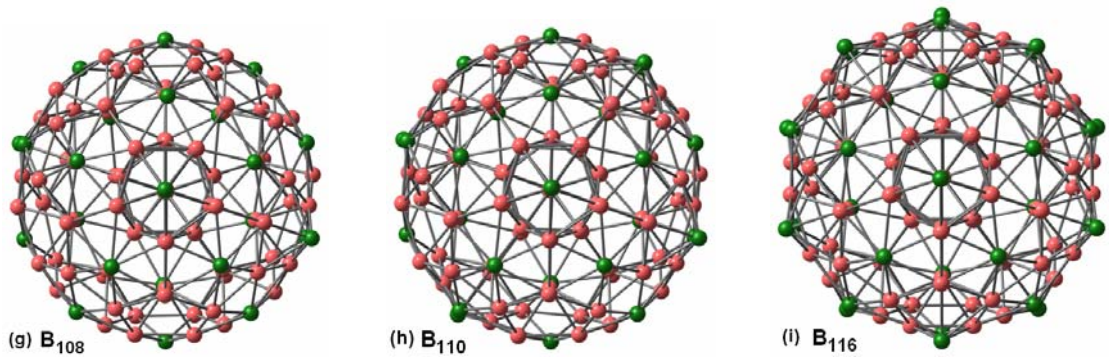

Figure 3.3.1. Stuffed fullerene-like boron clusters **(g)** B_{108} (D_{2h}), **(h)** B_{110} (D_{3d}), and **(i)** B_{116} (I_h) where 20 boron atoms are added on the hexagonal centers of all the three clusters and the rest of the boron atoms are added as caps to the surface pentagons of B_{84} respectively. The added boron atoms are indicated in green colour (dark in B&W print).

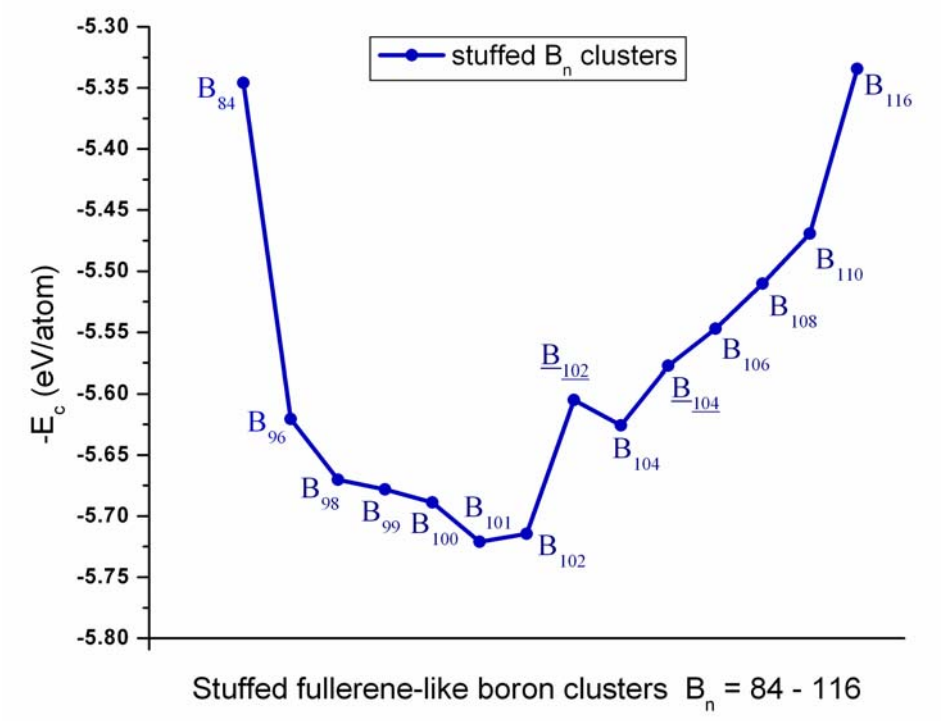

Figure 3.3.1j. Cohesive energy verses number of atoms for the optimized stuffed fullerene-like boron clusters (B_n = 84 – 116). The x-axis indicates the number of atoms not the scale.

These two isomers $\underline{B_{102}}$ (D_{3d}) and $\underline{B_{104}}$ (I_h) where only the hexagonal centers are occupied by the extra boron atoms (Figure 3.3.1k,l) are higher in energy (clusters shown with underline in Figure 3.3.1j) compared to B_{102} (D_{3d}) (Figure 3.1g), and B_{104} (D_{3d}) (Figure 3.3.1a) which were given preference to occupy all the 12 pentagonal caps and then the hexagonal centers of B_{84} cluster. This suggest that adding extra boron atoms as caps to the surface pentagons is preferable than adding on the hexagonal centers of B_{84}. It is because boron as a cap prefers pentagon (B_5 ring) rather than hexagon (B_6 ring) to have better overlap between the ring and the cap according to the ring-cap overlap compatibility.[75,76] Though, the ring-cap compatibility suggests the ring exohedral bonds (or the ring terminal bonds) should be in plane of the ring, here the fullerene-like curvature demands the exohedral bonds should bend out of the ring plane. This is also one of the reasons why icosahedral boron is ubiquitous in the allotropes of boron. Thus the curvature of the fullerene also plays an important role for stuffed fullerene-like boron clusters stability. The effect of the curvature on the stability of the fullerene-like clusters will be quantitatively discussed in the section of stuffed fullerene-like boron carbide clusters.

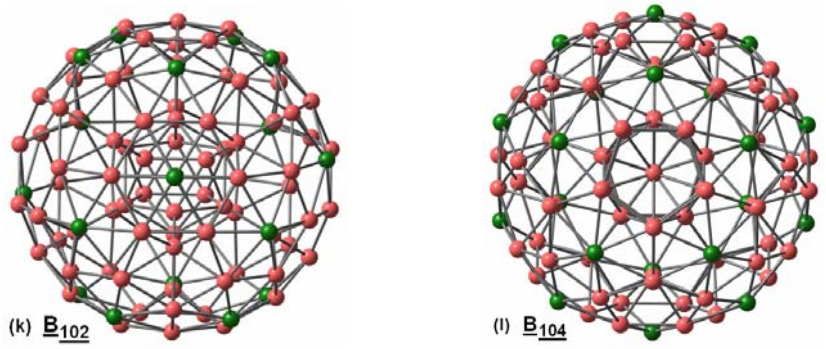

Figure 3.3.1. Stuffed fullerene-like boron clusters **(k)** $\underline{B_{102}}$ (D_{3d}) and **(l)** $\underline{B_{104}}$ (I_h) where the extra boron atoms are added only on the hexagonal centers of B_{84} cluster.

3.3.2 Stuffed Fullerene-like Boron Carbide Clusters

The hydrogenated cluster fragments 1,2-, 1,7-, and 1,12-*closo*-$C_2B_{10}H_{12}$ (**1A**, **1B**, **1C** respectively) and 1,2,5,6-, 1,3,4,6-, and 2,3,4,5-*nido*-$C_4B_2H_6$ (**2A**, **2B**, **2C** respectively) (Figure 3.1h-m) that were generated to compare the energetics of stuffed fullerene-like boron carbide clusters are optimized at GGA/PBE/DNP level of theory using DMOL3 program.[79,81] The relative energies of these positional isomers follow the valence rules of carboranes.[66-77] Among the isomers of *closo*-$C_2B_{10}H_{12}$ and *nido*-$C_4B_2H_6$, the 1,12-*closo*-$C_2B_{10}H_{12}$ (**1C** in Figure 3.1j) and 2,3,4,5-*nido*-$C_4B_2H_6$ (**2C** in Figure 3.1m) are low energy isomers (Table 3.3.2a). Therefore, the constructed fullerene-like boron carbide cluster, $C_{50}B_{34}$ (**3C** in Figure 3.1n) based on the above low energy isomers would be expected to be stable. The optimized $C_{50}B_{34}$ **(3C)** is found to be minima on the potential energy surface with relatively high HOMO-LUMO gap, 2.04 eV and with significant lowest frequencies (Table 3.3.2a). The hydrogenated cluster fragments and $C_{50}B_{34}$ **(3C)** cluster have been re-optimized at B3LYP/6-31g(d) using Gaussian 03 program.[80,82] This method also reproduces the relative stability of the positional isomers of *closo*-$C_2B_{10}H_{12}$ and *nido*-$C_4B_2H_6$ and suggests $C_{50}B_{34}$ **(3C)** is a stable species (Table 3.3.2b).

The average surface bond distances (*l*), B-B (1.802 Å), B-C (1.653 Å), and C-C (1.596 Å) of $C_{50}B_{34}$ **(3C)** are appreciable when compared to the B_{84} in β-rhombohedral boron (1.795 Å) and C_{60} (1.425 Å). The diameter, *d* (average distance between two opposite surface pentagons) is 7.574 Å which is lower than B_{84} (8.979 Å) due to the shorter C-C and B-C bond lengths (Table 3.3.2c). The curvature, θ (180° - average angle

between the center of the surface pentagon to its vertex and *exo*-bond, see Figure 3.3.2a) of $C_{50}B_{34}$ **(3C)** is 31.7° which is similar to C_{60} curvature, 31.7° and B_{102} curvature 32.1° but far from that of 2,3,4,5-*nido*-$C_4B_2H_6$ **(2C)**, 11.3° (Table 3.3.2a). This is understandable as the bond distances in C_{60} or stuffed fullerene-like boron and boron carbide clusters did not allow the surface to be flat; instead they tend to be more spherical to bind the pentagons. On the other hand the curvature in $C_4B_2H_6$ isomers is more flexible and is decided by the ring-cap orbital overlap compatibility rules.[75,76] This perception takes us to look at other possibilities where the curvature can be optimized by comparing with the remaining two *nido*-$C_4B_2H_6$ isomers (**2A** and **2B** in Figure 3.1k,l).

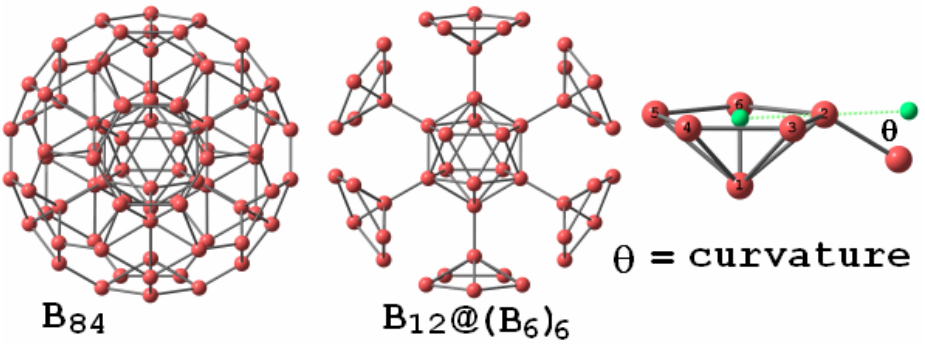

Figure 3.3.2a. Measuring the curvature of B_{84} cluster is depicted here. Icosahedral B_{84}, $B_{12}@(B_6)_6$ (for clarity 6 B_6 units are omitted) and the pentagonal pyramid of B_{84} where angle (θ) between the center of the surface pentagon to its vertex and *exo*-bond indicates the curvature.

Here onwards we use bold letters to represent the hydrogenated positional isomers of *closo*-$C_2B_{10}H_{12}$, *nido*-$C_4B_2H_6$, and the stuffed fullerene-like boron clusters as described in Figure 3.1h-m, and Figure 3.1n.

Table 3.3.2a. Total energy (TE), total energy corrected for zero point energy (TE + ZPE), relative energy, and the HOMO-LUMO (H-L) gaps are in eV, curvature (θ°), and number of imaginary frequencies (NImag) with smallest frequencies (cm^{-1}) in parenthesis of all the calculated clusters at GGA/PBE/DNP using DMOL3 program. Note: The curvature (θ) of B_{84} in β-rhombohedral boron is 32.3°.

Clusters	Pg	TE (eV)	TE+ZPE (eV)	RE (eV)	H-L (eV)	θ°	NImag (cm^{-1})
$B_{12}H_{12}^{-2}$	I_h	-8307.359	-8302.815	-	6.840	26.6	0[519.0]
1,2-$C_2B_{10}H_{12}$ (**1A**)	C_{2v}	-9025.826	-9021.070	0.675	6.599	28.8	0[438.7]
1,7-$C_2B_{10}H_{12}$ (**1B**)	C_{2v}	-9026.507	-9021.703	0.042	6.827	27.4	0[458.4]
1,12-$C_2B_{10}H_{12}$ (**1C**)	D_{5d}	-9026.642	-9021.745	0.000	6.951	28.8	0[485.3]
1,2,5,6-$C_4B_2H_6$ (**2A**)	C_s	-5589.563	-5587.133	2.479	5.023	18.8	0[410.2]
1,3,4,6-$C_4B_2H_6$ (**2B**)	C_s	-5590.450	-5588.006	1.606	6.320	18.1	0[416.1]
2,3,4,5-$C_4B_2H_6$ (**2C**)	C_s	-5592.102	-5589.612	0.000	5.748	11.3	0[499.2]
1C + **2C** = $C_{50}B_{34}$ (**3C**)	C_{2h}	-74722.286	-74710.009	14.502	2.041	31.7	0[229.6]
1C + **2B** = $C_{50}B_{34}$ (**3B**)	C_{2h}	-74736.588	-74724.511	0.000	2.852	31.7	0[286.5]
1C + **2A** = $C_{50}B_{34}$ (**3A**)	C_{2h}	-74726.114	-74714.328	10.183	1.604	31.7	0[270.6]
1A + **2B** = $C_{50}B_{34}$ (**3B'**)	C_1	-74735.547	-74723.483	1.028	2.733	31.7	0[286.7]
1B + **2B** = $C_{50}B_{34}$ (**3B″**)	C_1	-74736.296	-74724.212	0.299	2.824	31.7	0[287.0]
B_{12}^{-2} + **2C** = $C_{48}B_{36}^{-2}$ (**3′C**)	D_{3d}	-74001.769	-73989.881	19.520	1.302	31.7	0[203.6]
B_{12}^{-2} + **2B** = $C_{48}B_{36}^{-2}$ (**3′B**)	D_{3d}	-74021.487	-74009.401	0.000	2.736	31.7	0[285.6]
B_{12}^{-2} + **2A** = $C_{48}B_{36}^{-2}$ (**3′A**)	D_{3d}	-74011.768	-73999.861	9.540	1.633	31.7	0[274.4]
B_{102}	D_{3d}	-68894.571	-68882.004	-	0.632	32.1	0[207.9]
C_{60}	I_h	-62158.515	-62148.499	-	1.668	31.7	0[252.1]

Table 3.3.2b. Total energy (TE), total energy corrected for zero point energy (TE + ZPE), relative energy, and the HOMO-LUMO (H-L) gaps are in eV, curvature (θ°), nucleus independent chemical shifts (NICS in ppm), and number of imaginary frequencies (NImag) with smallest frequencies (cm^{-1}) in parenthesis of all the calculated clusters at B3LYP/6-31G(d) using Gaussian 03 program.

Clusters	Pg	TE (eV)	TE+ZPE (eV)	RE (eV)	H-L (eV)	θ°	NICS	NImag (cm^{-1})
$B_{12}H_{12}^{-2}$	I_h	-8318.319	-8313.771	-	8.996	26.6	-34.383	0[520.3]
1,2-$C_2B_{10}H_{12}$ (**1A**)	C_{2v}	-9037.095	-9032.265	0.810	8.344	27.9	-34.151	0[454.8]
1,7-$C_2B_{10}H_{12}$ (**1B**)	C_{2v}	-9037.803	-9032.953	0.122	8.524	26.3	-34.156	0[478.7]
1,12-$C_2B_{10}H_{12}$ (**1C**)	D_{5d}	-9037.920	-9033.075	0.000	8.598	28.9	-35.337	0[463.1]
1,2,5,6-$C_4B_2H_6$ (**2A**)	C_s	-5595.561	-5593.063	2.492	6.937	18.9	-24.454	0[382.8]
1,3,4,6-$C_4B_2H_6$ (**2B**)	C_s	-5596.511	-5594.000	1.555	8.148	17.9	-23.314	0[405.7]
2,3,4,5-$C_4B_2H_6$ (**2C**)	C_s	-5598.106	-5595.555	0.000	7.493	10.9	-24.162	0[496.6]
1C + **2C** = $C_{50}B_{34}$ (**3C**)	C_{2h}	-74788.164	-74775.823	16.842	3.533	31.7	-25.730	0[205.1]
1C + **2B** = $C_{50}B_{34}$ (**3B**)	C_{2h}	-74804.965	-74792.665	0.000	4.438	31.7	-34.197	0[290.6]
1C + **2A** = $C_{50}B_{34}$ (**3A**)	C_{2h}	-74793.460	-74781.424	11.241	2.939	31.7	-35.449	0[281.2]
1A + **2B** = $C_{50}B_{34}$ (**3B'**)	C_1	-74803.852	-74791.592	1.073	4.323	31.7	-32.545	0[289.6]
1B + **2B** = $C_{50}B_{34}$ (**3B″**)	C_1	-74804.661	-74792.378	0.287	4.416	31.7	-33.051	0[290.1]
B_{12}^{-2} + **2C** = $C_{48}B_{36}^{-2}$ (**3′C**)	D_{3d}	-74066.368	-74054.290	22.448	2.812	31.7	-21.067	0[162.3]
B_{12}^{-2} + **2B** = $C_{48}B_{36}^{-2}$ (**3′B**)	D_{3d}	-74088.958	-74076.738	0.000	4.293	31.7	-33.333	0[286.8]
B_{12}^{-2} + **2A** = $C_{48}B_{36}^{-2}$ (**3′A**)	D_{3d}	-74078.189	-74066.207	10.531	2.972	31.7	-34.444	0[277.7]
B_{102}	D_{3d}	-68962.016	-68949.833	-	1.299	31.7	-39.831	0[208.8]
C_{60}	I_h	-62210.450	-62200.244	-	2.760	31.7	-9.402	0[265.5]

Table 3.3.2c. Various bond distances, ring cap distance (R), diameter of B_{12} (d_{B12}) and B_{84} skeleton (d_{B84}), and number of bonds of all the calculated clusters at GGA/PBE/DNP using DMOL3 program. For completeness the curvature (θ) also added here.

Clusters	PBE/DNP of DMOL3															
	B_c-B_c	B_c-C_c	C_c-C_c	B_m-B_m	B_m-C_m	C_m-C_m	B_s-B_s	B_s-C_s	C_s-C_s	R	θ	d_{B12}	d_{B84}	# B-B	# B-C	# C-C
$B_{12}H_{12}^{-2}$	1.787	-	-	-	-	-	-	-	-	0.940	26.565	3.400	-	30	0	0
1,2-$C_2B_{10}H_{12}$ (**1A**)	1.778	1.709	1.627	-	-	-	-	-	-	0.902	28.835	3.327	-	21	8	1
1,7-$C_2B_{10}H_{12}$ (**1B**)	1.778	1.703	-	-	-	-	-	-	-	0.894	27.386	3.318	-	20	10	0
1,12-$C_2B_{10}H_{12}$ (**1C**)	1.775	1.706	-	-	-	-	-	-	-	0.865	28.833	3.222	-	20	10	0
1,2,5,6-$C_4B_2H_6$ (**2A**)	-	-	-	-	-	-	1.653	1.546	1.449	1.078	18.784	-	-	1	4	5
1,3,4,6-$C_4B_2H_6$ (**2B**)	-	-	-	-	-	-	-	1.540	1.474	1.065	18.052	-	-	0	6	4
2,3,4,5-$C_4B_2H_6$ (**2C**)	-	-	-	-	-	-	-	1.534	1.436	1.199	11.269	-	-	1	6	3
1C + **2C** = $C_{50}B_{34}$ (**3C**)	1.574	1.539	-	1.453	1.415	-	1.802	1.653	1.596	0.859	31.698	2.963	7.574	48	84	60
1C + **2B** = $C_{50}B_{34}$ (**3B**)	1.628	1.588	-	-	1.428	1.377	1.739	1.642	1.592	0.849	31.688	3.061	7.610	26	104	62
1C + **2A** = $C_{50}B_{34}$ (**3A**)	1.629	1.605	-	-	1.431	1.381	1.783	1.632	1.573	0.850	31.693	3.071	7.615	38	80	74
1A + **2B** = $C_{50}B_{34}$ (**3B'**)	1.627	1.599	1.602	-	1.426	1.386	1.735	1.646	1.593	0.851	31.691	3.072	7.611	27	102	63
1B + **2B** = $C_{50}B_{34}$ (**3B″**)	1.627	1.597	-	-	1.427	1.393	1.733	1.646	1.589	0.851	31.691	3.062	7.610	26	104	62
B_{12}^{-2} + **2C** = $C_{48}B_{36}^{-2}$ (**3′C**)	1.576	-	-	1.453	-	-	1.821	1.655	1.618	0.857	31.706	2.999	7.617	60	72	60
B_{12}^{-2} + **2B** = $C_{48}B_{36}^{-2}$ (**3′B**)	1.623	-	-	-	1.431	-	1.742	1.646	1.594	0.845	31.699	3.085	7.637	36	96	60
B_{12}^{-2} + **2A** = $C_{48}B_{36}^{-2}$ (**3′A**)	1.628	-	-	-	1.436	-	1.793	1.632	1.578	0.842	31.697	3.093	7.643	48	72	72
B_{84} in β-boron	1.839	-	-	1.772	-	-	1.795	-	-	0.985	32.315	3.535	8.979	192	0	0
B_{102}	1.680	-	-	1.579	-	-	1.760	-	-	0.955	32.067	3.196	8.187	288	0	0
C_{60}	-	-	-	-	-	-	-	-	1.425	-	31.717	-	6.654	0	0	90

B_c-B_c = central icosahedral B-B distance
B_c-C_c = central icosahedral B-C distance
C_c-C_c = central icosahedral C-C distance
B_m-B_m = central icosahedral vertex B to the middle layer B distance
B_m-C_m = central icosahedral vertex B/C to the middle layer B/C distance
C_m-C_m = central icosahedral vertex C to the middle layer C distance
B_s-B_s = Surface B-B distance
B_s-C_s = Surface B-C distance
C_s-C_s = Surface C-C distance

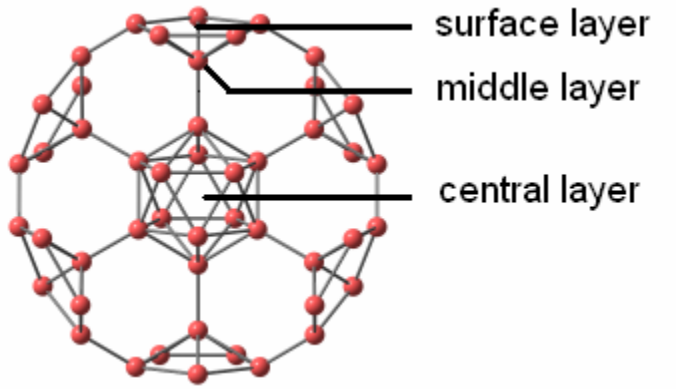

The curvature of 1,3,4,6-*nido*-$C_4B_2H_6$ (**2B**) (18.1°) and 1,2,5,6-*nido*-$C_4B_2H_6$ (**2A**) (18.8°) are found to be closer to **3C** (31.7°) than the curvature of **2C** (11.3°) vs **3C** (31.7°). Indeed, the fullerene-like boron carbide clusters based on the combinations of **1C** and **2B** [$C_{50}B_{34}$ (**3B**) = **1C** + **2B**], and **1C** and **2A** [$C_{50}B_{34}$ (**3A**) = **1C** + **2A**] are lower in energy and minima (Table 3.3.2a). The clusters **3B** and **3C** are shown in Figure 3.3.2b and 3.3.2c respectively. They are 14.50 and 4.32 eV lower than **3C**. The structure **3B** is 10.18 eV more stable than **3A** as the **2B** is 0.87 eV more stable than **2A**. In fact 12 × 0.87 is not far from 10.18 eV. The HOMO-LUMO gap of **3B** and **3C** are 2.85 and 1.60 eV and the former is larger than C_{60} gap, 1.67 eV (Table 3.3.2a). The relative stability of all the cluster isomers and corresponding HOMO-LUMO gaps are in good agreement with the results obtained from B3LYP/6-31G(d) level.

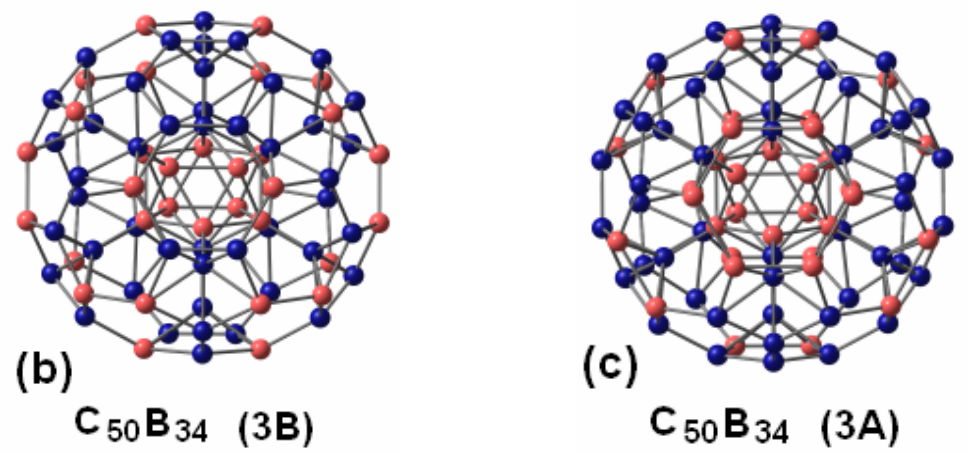

Figure 3.3.2. Stuffed fullerene-like boron carbide clusters **(b)** $C_{50}B_{34}$ (**3B**) and **(c)** $C_{50}B_{34}$ (**3C**) generated out of the combinations of [1,12-*closo*-C_2B_{10} (**1C**) and 12 (1,3,4,6-*nido*-C_4B_2) (**2B**)] and [1,12-*closo*-C_2B_{10} (**1C**) and 12 (1,2,5,6-*nido*-C_4B_2) (**2A**)] fragments respectively. The substituted carbon atoms are shown in thick blue colour (dark in B&W print).

The average bond lengths, and diameter of **3B** and **3A** are nearly similar to **3C**; particularly the curvature (θ) and the ring-cap distances (R) did not vary (Table 3.3.2c). The 2c-2e σ bonds between the C_2B_{10} and C_4B_2 fragments are shorter within the diameter ~7.6 Å of these clusters. Since majority of the bonds are B-C bonds the diameter of the series **3** clusters are lowered. The stability of **3C** is also supported by the presence of more number of strong B-C bonds over its other isomers (Table 3.3.2c).

The stability of **3B** is also examined over the combinations of **1A** (1,2-*closo*-C_2B_{10}) and **2B** [$C_{50}B_{34}$ (**3B′**)] and **1B** (1,7-*closo*-C_2B_{10}) and **2B** [$C_{50}B_{34}$ (**3B″**)]. The **3B′** and **3B″** are lower in energy than **3A** and **3C**. However, the **3B** is the most stable among all the fullerene-like boron carbide clusters (Table 3.3.2a,b). This clearly emphasizes that the bond bending (θ) energy penalties are the key in stabilizing the clusters. The $C_{50}B_{34}$ electron sufficient dianionic analogues, $C_{48}B_{36}^{-2}$ [*closo*-B_{12}^{-2} + 12 (*nido*-C_4B_2)] isomers, also follow parallel stability trends (Table 3.3.2a,b).

In order to understand the contribution of boron and carbon in $C_{50}B_{34}$ (**3B**) cluster, the PDOS has been generated as shown in Figure 3.3.2d. The PDOS of 50 carbon atoms and the PDOS of 34 boron atoms are mostly mixed near the frontier regions of HOMO and LUMO. In the far frontier regions of the occupied MOs the contribution from carbon is more than boron whereas it is reverse in the unoccupied MOs (-1 to -3 eV and 2 to 5 eV). The occupied bonding contribution largely comes from the surface pentagons and the unoccupied non-bonding and antibonding contributions are from the hexagons. The HOMO is a σ bonding that holds the pentagons and hexagons together as shown in Figure 3.3.2e. LUMO is a π antibonding localized between the five and six membered

rings (Figure 3.3.2f). The large HOMO - LUMO gap of 2.85 eV can be seen in the MO energy diagram indicated by an arrow (Figure 3.3.2d).

Aromaticity, an indicator of delocalization, has been estimated by computing the nucleus-independent chemical shifts (NICS) for the ghost atoms at the center of the clusters using GIAO-HF/6-31G(d)//B3LYP/6-31G(d).[84,84] The negative NICS values as large as $B_{12}H_{12}^{-2}$ and $C_2B_{10}H_{12}$ reveal that the B_{102}, $C_{50}B_{34}$ and $C_{48}B_{36}^{-2}$ classes of clusters are three-dimensional aromatics (Table 3.3.2b). In order to aid possible experiments the electron detachment energies and Raman-active bands are calculated.

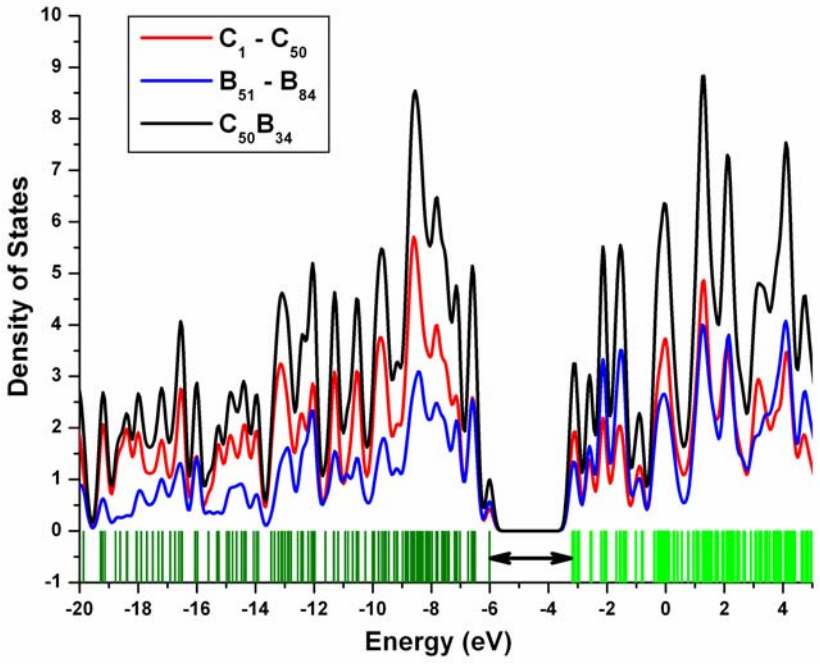

Figure 3.3.2. (d). PDOS of $C_{50}B_{34}$ (**3B**) stuffed fullerene-like boron carbide cluster. The ↔ between the MO energy bar code indicates the gap (2.85 eV) between HOMO and LUMO.

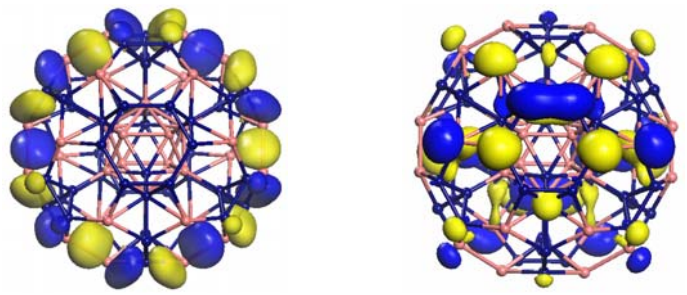

Figure 3.3.2. (left) **(e)** HOMO and (right) **(f)** LUMO of $C_{50}B_{34}$ (**3B**) stuffed fullerene-like boron carbide cluster.

The electron detachment energies of the stable stuffed fullerene-like boron and boron carbide clusters are calculated at GGA/PBE/DNP level of theory. The vertical detachment energy (VDE) is calculated as energy difference between neutral of anion optimized geometry and optimized anion geometry whereas the adiabatic detachment energy (ADE) is the energy difference between optimized neutral and optimized anion geometry. The VDE and ADE of B_{102} and $C_{50}B_{34}$ (**3B)** are 2.88 and 2.84, 2.29 and 2.25 eV respectively. They are comparable to C_{60} fullerene VDE (2.93 eV) and ADE (2.91 eV).[88,89] The negligible difference between ADE and VDE of B_{102} and $C_{50}B_{34}$ (**3B**) is 0.04 eV which is close to C_{60} (0.02 eV), suggest that there will not be any major structural changes during the relaxation. The prominent breathing modes A_g with high Raman-activity of the stable B_{102} are found at 599.8 (radial) and 1088.7, 1392.5 cm^{-1} (tangential). In $C_{50}B_{34}$ (**3B)** the A_g modes are found at 416.2 (radial) and 1146.5, 1151.1 cm^{-1} (tangential) while in C_{60} the A_g modes are at 497.1 (radial) and 1503.8 cm^{-1} (tangential).[5,90] There are several infrared- and Raman-active modes in B_{102} and $C_{50}B_{34}$ (**3B)** compared to C_{60} due to the reduction in symmetry and greater degrees of freedom (see Appendix for all the infrared- and Raman-active frequencies). The displacement vectors corresponding to these modes are shown in Figure 3.3.2g-n respectively.

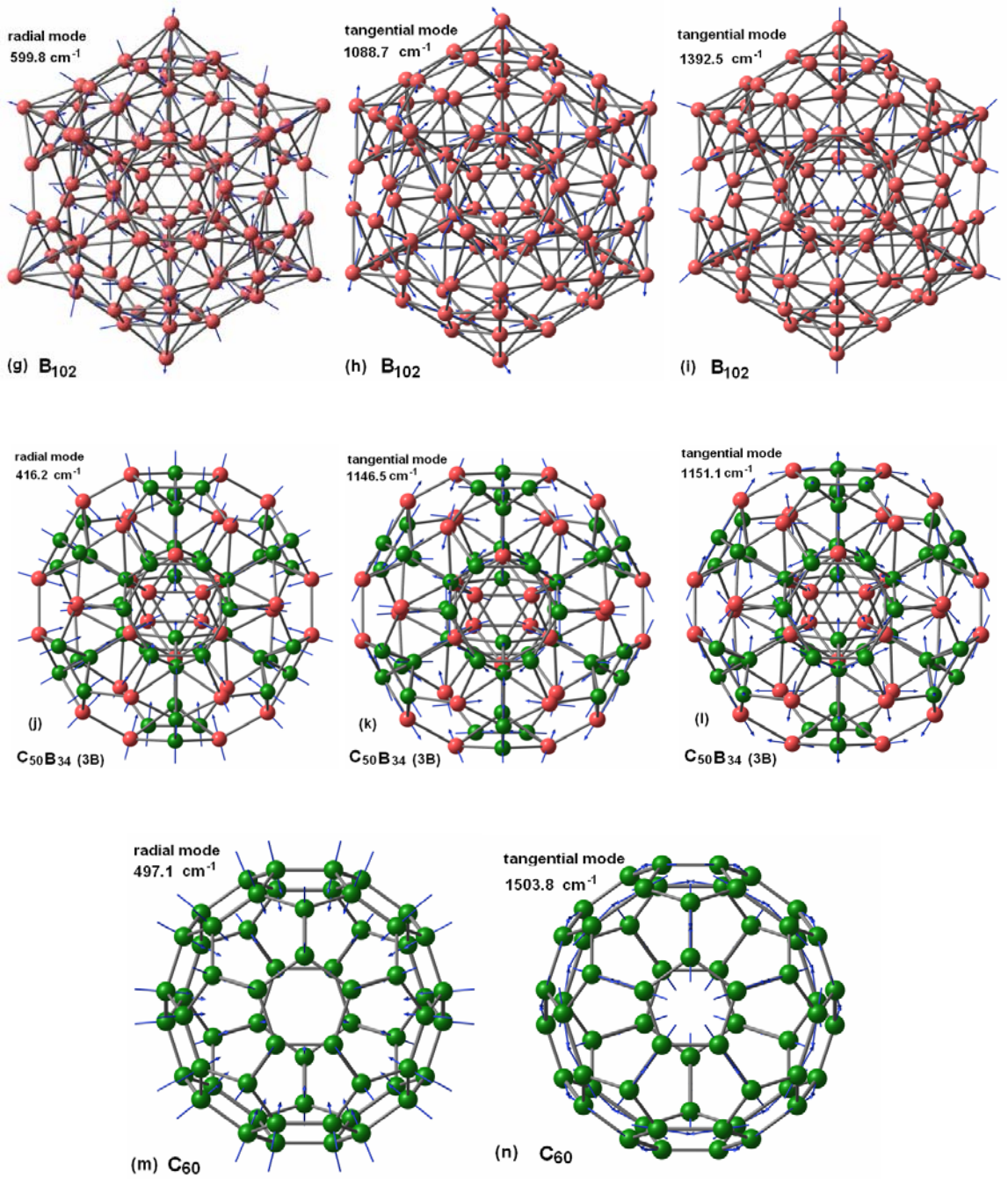

Figure 3.3.2. The displacement vectors corresponding to the radial (r) and tangential (t) A_g breathing modes of **(g)** B_{102} (599.8 cm^{-1}, r), **(h)** B_{102} (1088.7 cm^{-1}, t), **(i)** B_{102} (1392.5 cm^{-1}, t), **(j)** $C_{50}B_{34}$ (**3B**) (416.2 cm^{-1}, r), **(k)** $C_{50}B_{34}$ (**3B**) (1146.5 cm^{-1}, t), **(l)** $C_{50}B_{34}$ (**3B**) (1151.1 cm^{-1}, t), **(m)** C_{60} (497.1 cm^{-1}, r), and **(n)** C_{60} (1503.8 cm^{-1}, t).

3.4 Conclusion

Electron sufficient stuffed fullerene-like boron clusters are constructed using an icosahedral electron deficient B_{84} fragment of β-rhombohedral boron. The electron deficiency of B_{84} cluster was calculated by applying the Wade's *closo- n*+1 and *nido- n*+2 skeletal electron counting rules on the fragments of B_{84} cluster. According to these rules B_{84} was found to be 50 electron deficient and hence the B_{84}^{-50} can not be a stable species. In order to stabilize the B_{84} by providing the 50 electrons we have adopted similar bonding criteria of β-rhombohedral boron, where the required number of 50 electrons was compensated by different condensations and extra occupancies. Here, the condensation was terminating the open surface of B_{84} by capping the pentagons with boron and placing the extra boron atoms at the center of hexagons systematically. Since we can not provide 50 electrons (or 16.66 boron atoms) by integer number of boron atoms, near electron sufficient clusters were modeled that is clusters close to electron precise $B_{100.66}$. The clusters with near electron sufficient $B_{98} – B_{102}$ are indeed found to be stable and the other far from $B_{100.66}$ are destabilized. Therefore the stuffed fullerene-like boron clusters are preferentially stabilized with the stipulated electronic requirements.

On the other hand the well understood structure and stability connection between boranes and carboranes prompted us to propose a carboranes route to stabilize the B_{84}^{-50}. This gave $C_{50}B_{34}$ an isoelectronic equivalent of B_{84}^{-50}. Here we applied cluster fragment approach to evaluate the best possible position for carbon in $C_{50}B_{34}$ cluster. We found

that the stability over the $C_{50}B_{34}$ isomers is controlled by the curvature of the fullerene beside the general notion of the carboranes stability rules.

The large HOMO-LUMO gaps, three dimensional aromaticity, and the detachment energies of these stuffed fullerene-like boron and boron carbide clusters unambiguously indicate their high stability. Existence of B_{84} clusters in the β-rhombohedral boron and boron-rich icosahedral cluster solids (BRICS) prompts us towards a search for B_{12} stuffed boron fullerenes. There could be a possibility to trace the B_{84} clusters in the melt of β-rhombohedral boron or BRICS.[91,92] The recent experimental realization of boron carbide spherical nanoparticles of the order of 50-100 nm in size by laser irradiation of boron powder dispersed in ethyl acetate suggest the starting directions in bringing up these promising clusters.[93,94] These are expected to be useful in boron neutron capture therapy of cancer,[78,95-97] as incompressible materials,[98,99] and their hydrogenated analogues would be promising candidates for hydrogen storage.[100]

References

[1] H. W. Kroto, J. R. Heath, S. C. O'Brien, R. F. Curl Jr., and R. E. Smalley, Nature (London) **318**, 162 (1985).

[2] H. W. Kroto, A. W. Allaf, and S. P. Blam, Chem. Rev. (Washington, D. C.) **91**, 1213 (1989).

[3] H. W. Kroto, Comput. Math. Appl. **17**, 417 (1989).

[4] L.A. Paquette, Chem. Rev. (Washington, D. C.) **89**, 1051 (1989).

[5] M. S. Dresselhaus, G. Dresselhaus, and P.C. Eklund, *Science of Fullerenes and Carbon Nanotubes* (Academic, New York), 1996.

[6] *Perspectives of Fullerene Nanotechnology*, edited by E. Osawa (Kluwer, New York), 2002.

[7] H. A. Williams, *The Most Beautiful Molecule: The Discovery of the Buckyball* (John Wiley & Sons Inc), 1995.

[8] P. W. Fowler and D. E. Manolopoulos, *An Atlas of Fullerenes* (Dover), 2007.

[9] A. F. Hebard, M. J. Rosseinsky, R. C. Haddon, D. W. Murphy, S. H. Glarum, T. T. M. Palstra, A. P. Ramirez, and A. R. Kortan, Nature (London) **350**, 600 (1991).

[10] H. Karoly, K. Olivier, H. S. Mei, K. Richard B, F. K. Jian, W. Robert L, D. Francois, Science (Washington, DC) **252**, 5009 (1991).

[11] M. J. Rosseinsky, A. P. Ramirez, S. H. Glarum, D. W. Murphy, R. C. Haddon, A. F. Hebard, T. T. M. Palstra, A. R. Kortan, S. M. Zahurak, and A. V. Makhija, Phys. Rev. Lett. **66**, 2830 (1991).

[12] K. Tanigaki, T. W. Ebbesen, S. Saito, J. Mizuki, J. S. Tsai, Y. Kubo, and S. Kuroshima, Nature (London) **352**, 222 (1991).

[13] S. Margadonnan and K. Prassides, Journal of Solid State Chemistry **168**, 639 (2002).

[14] V. D. Blank, S. G. Buga, N. R. Serebryanaya, V. N. Denisov, G. A. Dubitsky, A. N. Ivlev, B. N. Mavrin, and M. Y. Popov, Phys. Lett. A **205**, 208 (1995).

[15] M. E. Kozlov, M. Hirabayashi, K. Nozaki, M. Tokumoto, and H. Ihara, Appl. Phys. Lett. **66**, 1199 (1995).

[16] V.D. Blank S.G. Buga G.A. Dubitsky K.V. Gogolinsky V.M. Prokhorov N.R. Serebryanaya V.A. Popov, in *Molecular Building Blocks for Nanotechnology: From Diamondoids to Nanoscale Materials and Applications*, Edited by G. Ali Mansoori, Thomas F. George, Lahsen Assoufid, (Springer) ,2007, pp. 393.

[17] Th. Braun, M. Wohlers, T. Belz, G. Nowitzke, G. Wortmann,Y. Uchida, N. Pfänder, and R. Schlögl, Catalysis Letters **43**, 167 (1997).

[18] R. Malhotra, D. F. McMillen, D. S. Tse, D. C. Lorents, R. S. Ruoff, and D. M. Keegan, Energy & Fuels, **7**, 685 (1993).

[19] J. M. Ashcroft, D. A. Tsyboulski, K. B. Hartman, T. Y. Zakharian, J. W. Marks, R. B. Weisman, M. G. Rosenblum, and Lon J. Wilson, Chem. Commun. 3004 (2006).

[20] S. Iwamatsu, T. Uozaki, K. Kobayashi, S. Re, S. Nagase, and S. Murata, J. Am. Chem. Soc. **126**, 2668 (2004).

[21] Z. Xiao, J. Yao, D. Yang, F. Wang, S. Huang, L. Gan, Z. Jia, Z. Jiang, X. Yang, B. Zheng, G. Yuan, S. Zhang, and Z. Wang, J. Am. Chem. Soc. **129**, 16149 (2007).

[22] Y. Zhao, Y-H. Kim, A. C. Dillon, M. J. Heben, and S. B. Zhang, Phys. Rev. Lett. **94**, 155504 (2005).

[23] Y. V. Vasil'ev, A. Hirsch, R. Taylor, and T. Drewello, Chem. Commun. 1752 (2004).

[24] K. R. S. Chandrakumar and S. K. Ghosh, Nano Lett. **8**, 13 (2008).

[25] Y. Chai, T. Guo, C. Jin, R. E. Hatlfler, L. P. F. Chibante, J. Fure, L. Wang, J. M. Alford and R.E. Smalley, J. Phys. Chem. **95**, 7564 (1991).

[26] T. Pradeep, V. Vijayakrishnan, A.K. Santra and C.N.R. Rao, J. Phys. Chem. **95**, 10564 (1991).

[27] N. Kurita, K. Kobayashi, H. Kumahora, K. Tago, and K. Ozawa, Chem. Phys. Lett. **95**,198 (1992).

[28] J.C. Hummelen, B. Knight, J. Pavlovich, R. Gonzalez, and F. Wudl, Science (Washington, DC) **269**, 1554 (1995).

[29] H.-J. Muhr, R. Nesper, B. Schnyder, and R. Kotz, Chem. Phys. Lett. **249**, 399 (1996).

[30] C.M. Brown, E. Beer, C. Bellavia, L. Cristofolini, R. Gonzalez, M. Hanfland, D. Hausermann, M. Keshavarz, K. K. Kordatos, K. Prassides, and F. Wudl, J. Am. Chem. Soc. **118**. 8715 (1996).

[31] Z. Chen, K. Ma, Y. Pan, X. Zhao, A. Tangb, and J. Fengb, J. Chem. Soc., Faraday Trans. **94**, 2269, (1998).

[32] Z. Chen, X. Zhao, and A. Tang, J. Phys. Chem. A **103**, 10961 (1999).

[33] S. Stafstrom, L. Hultman, N. Hellgren, Chem. Phys. Lett. **340**, 227 (2001).

[34] M. R. Manaa, D. W. Sprehn, H. A. Chords, J. Am. Chem. Soc. **124**. 13990 (2002).

[35] M. R. Manaa, D. W. Sprehn, and H. A. Ichord, Chem. Phys. Lett. **374**, 405 (2003).

[36] R-H. Xie, G. W. Bryant, J. Zhao, V. H. Smith, Jr., A. D. Carlo, and A. Pecchia, Phys. Rev. Lett. **90**, 206602 (2003).

[37] K. Balasubramanian, Chem. Phys. Lett. **391**, 64 (2004).

[38] J-G Han, and J. A. Morales, Chem. Phys. Lett. **396**, 27 (2004).

[39] Z. Chen, H. Jiao, D. Moran, A. Hirsch, W. Thiel and P. v. R. Schleyer, J. Phys. Org. Chem. **16**, 726 (2003).

[40] R. Tenne, Adv. Mater. **7**, 965 (1995).

[41] O. Vostrowsky and A. Hirsch, Chem. Rev. **106**, 5191, (2006).

[42] F-L. Liu and A. F. Jalbout, Journal of Molecular Graphics and Modelling **26**, 1327 (2008).

[43] R. Tenne, L. Margulis, M. Genut, and G. Hodes, Nature (London) **360**, 444 (1992).

[44] R. Tenne and C. N. R. Rao, Phil. Trans. R. Soc. A **362**, 2099 (2004).

[45] M. Nath, C. N. R. Rao, R. Popovitz-Biro, A. Albu-Yaron, and R. Tenne, Chem. Mater. **16**, 2238 (2004).

[46] A. Margolin, R. Popovitz-Biro, A. Albu-Yaron, L. Rapoport, R. Tenne, Chem. Phys. Lett. **411**, 162 (2005).

[47] F. Banhart, M. Zwanger, and H.-J. Muhr, Chem. Phys. Lett. **231**, 98 (1994).

[48] M. Terrones, W.K. Hsu, H. Terrones, J.P. Zhang , S. Ramos, J. P. Hare, R. Castillo, K. Prassides, A.K. Cheetham, H.W. Kroto, and D.R.M. Walton, Chem. Phys. Lett. **259**, 568 (1996).

[49] D. Golberg, Y. Bando, O. Stephan, and K. Kurashima, Appl. Phys. Lett. **73**, 2441 (1998).

[50] T. Oku, T. Hirano, M. Kuno, T. Kusunose, K. Niihara, Materials Science and Engineering B **74**, 206 (2000).

[51] W. H. Moon, M. S. Son, H. J. Hwang, Applied Surface Science **253**, 7078 (2007).

[52] M. R. Manaa, Chem. Phys. Lett. **382**, 194 (2003).

[53] K. Kobayashi and N. Kurita, Phys. Rev. Lett. **70**, 3542 (1993).

[54] S. C. Sevov and J. D. Corbett, J. Solid State. Chem. **123**, 344 (1996).

[55] M. J. Moses, J. C. Fettinger, and B. W. Eichhorn, Science (Washington, D.C.) **300**, 778 (2003).

[56] J. Bai, A. V. Virovets, and M. Scheer, Science (Washington, D.C.) **300**, 781 (2003).

[57] A. Müller, Science (Washington, D.C.) **300**, 749 (2003).

[58] S. Alvarez, Dalton Trans. 2209 (2005).

[59] E. D. Jemmis and B. Kiran, Curr. Sci. **66**, 766 (1994).

[60] E.D. Jemmis, and B. Kiran, in *Computational Chemistry: Reviews of Current Trends*, Ed., J. Leszczynski, World Scientific, Singapore, **1**, 175 (1996).

[61] E. D. Jemmis, The Relation Between Polymorphs of Elements and Their Compounds: The Story of Boron, in "*New Millennium Lectures: Celebration of Science*", Indian Science Congress 2000 Pune; Published by CSIR New Delhi.

[62] E. D. Jemmis and M. M. Balakrishnarajan, J. Am. Chem.Soc. **123**, 4324 (2001).

[63] E.D. Jemmis, M.M. Balakrishnarajan and P.D. Pancharatna, Chem. Rev. (Washington, D.C.) **102**, 93 (2002).

[64] E. D. Jemmis and E. G. Jayasree, Acc. Chem. Res. **36**, 816 (2003).

[65] K. Wade, J. Chem. Soc. D **15**, 792 (1971).

[66] R. Hoffmann, W. N. Lipscomb, J. Chem. Phys. **36**, 3489 (1962).

[67] R. N. Grimes, *Carboranes*, (Academic Press, New York), 1970.

[68] E. L. Mutterties, *Boron Hydride Chemistry*, (Academic Press, New York), 1975.

[69] The *Borane, Carborane, Carbocation Continuum*, Ed: J. Casanova, (Wiley: New York), 1998.

[70] R. E. Williams, Chem. Rev. (Washington, D.C.) **92**, 177 (1992).

[71] B. M. Gimarc, J. Am. Chem. Soc. **105**, 1979 (1983).

[72] P. v. R. Schleyer, K. Najafian, Inorg. Chem. **37**, 3454 (1998).

[73] E. D. Jemmis, P. N. V. Pavan Kumar, Proc. Indian Acad. Sci. (Chem. Sci.) **93**, 479 (1984).

[74] M. Hofmann, M. A. Fox, R. Greatrex, P. v. R. Schleyer, R. E. Williams, Inorg. Chem. **40**, 1790 (2001).

[75] E. D. Jemmis, J. Am. Chem. Soc. **104**, 7017 (1982).

[76] E. D. Jemmis and P. V. R. Schleyer, J. Am. Chem. Soc. **104**, 4781 (1982).

[77] M. Elian, M. M. L. Chen, D. M. P. Mingos, R. Hoffmann, Inorg. Chem. **15**, 1148 (1976).

[78] M. F. Hawthorne, Pure Appl. Chem. **75**, 1157 (2003).

[79] B. Delley, J. Chem. Phys. **113**, 7756 (2000).

[80] M. J. Frisch et al., computer code GAUSSIAN 03, revision B.03, Gaussian, Inc., Wallingford, CT, 2004).

[81] J. P. Perdew, K. Burke, and M. Ernzerhof, Phys. Rev. Lett. 77, 3865 (1996).

[82] A. D. Becke, J. Chem. Phys. **98**, 5648 (1993).

[83] P. v. R. Schleyer, C. Maerker, A. Dransfeld, H. Jiao, and N. v. E. Hommes, J. Am. Chem. Soc. **118**, 6317 (1996).

[84] P. v. R. Schleyer, K. Najafian, and A. M. Mebel, Inorg. Chem. **37**, 6765 (1998).

[85] G. A. Slack, C. I. Hejna, M. F. Garbauskas, and J. S. Kasper, J. Solid State Chem. **76**, 52 (1988).

[86] H. Cundy and A. Rollett, *Mathematical Models*, 3rd ed. Stradbroke, England, Tarquin Pub, 1989.

[87] M. Tomaselli, B. H. Meier, M. Riccò, T. Shiroka, and A. Sartori, Phys. Rev. B **63**, 113405 (2001).

[88] C. Lifshitz, Mass Spectrometry Reviews, **12**, 261 (1993).

[89] B. Palpant, A. Otake, F. Hayakawa, Y. Negishi, G. H. Lee, A. Nakajima and K. Kaya, Phys. Rev. B **60**, 4509 (1999).

[90] H. Kuzmany, M. Matus, B. Burger, and J. Winter, Adv. Mater. **6**, 731 (1994).

[91] S. Krishnan, S. Ansell, J. J. Felten, K. J. Volin, and D. L. Price, Phys. Rev. Lett. **81**, 586 (1998).

[92] H. Hubert, B. Devouard, L. A. J. Garvie, M. O'Keeffe, P. R. Buseck, W. T. Petuskey, and P. F. McMillan, Nature (London) **391**, 376 (1998).

[93] Y. Ishikawa, Y. Shimizu, T. Sasaki, and N. Koshizaki, Appl. Phys. Lett. **91**, 161110 (2007).

[94] B. Todorović-Marković, I. Draganić, D. Vasiljević-Radović, N. Romčević, M. Romčević, M. Dramićanin, and Z. Marković, App. Sur. Sci. **253**, 4029 (2007).

[95] M. W. Mortensen, P. G. Sørensen, O. Björkdahl, M. R. Jensen, H. J. G. Gundersen, and T. Bjørnholm, Appl. Radiat. Isot. **64**, 315 (2006).

[96] M. W. Mortensen, O. Björkdahl, P. G. Sørensen, T. Hansen, M. R. Jensen, H. J. G. Gundersen, and T. Bjørnholm, Bioconjugate Chem. **17**, 284 (2006).

[97] Z. Yinghuai, K. C. Yan, J. A. Maguire. And N. S. Hosmane, Curr. Chem. Biol. **1**, 141 (2007).

[98] B. Wei, R. Vajtai, Y. J. Jung, F. Banhart, G. Ramanath, and P. M. Ajayan, J. Phys. Chem. B **106**, 5807 (2002).

[99] L. Rapoport, N. Fleischer, and R. Tenne, J. Mater. Chem. **15**, 1782 (2005).

[100] Y. Zhao, M. T. Lusk, A. C. Dillon, M. J. Heben, and S. B. Zhang, Nano Lett, **8**, 157. (2008).

Chapter 4

Boron and Boride Sheets, Tubes, and Hollow Fullerenes

4.1 Introduction

Elemental boron is considered as one of the most complex crystal structure in the periodic table.[1] It has many allotropes whose structural chemistry is mostly dominated by the three dimensional (3D) icosahedral B_{12} units with electron deficient multi center two electron (mc-2e) bonding network.[1-3] Its next neighbor carbon has allotropes with variety of electron precise 2c-2e bonding networks namely 3D tetrahedral diamond and hexagonal graphite, 2D graphene sheet, 1D nanotubes, and 0D spherical fullerenes. Dimensionality is considered as one of the significant parameter in defining materials characteristics. The diverse chemical and physical properties of carbon: 0D fullerenes, 1D nanotubes, and 2D sheets (graphene) are the best examples.[4-6] But boron in general is not known to form allotropes with such varied dimensions like carbon. In chapter 3, we have showed one way to achieve stable 0D stuffed fullerene-like boron clusters from an

electron deficient B_{84} fragment of 3D dimensional β-rhombohedral boron. On the other hand, recently there are theoretical reports on 2D finite boron clusters,[7-9] 2D boron sheets,[10] 1D boron nanotubes,[11,12] and 0D boron fullerenes[13,14] analogous to benzenoid hydrocarbons, carbon sheets, nanotubes, and fullerenes respectively. Subsequently, the finite boron clusters,[15] nanowires[16] and nanotubes[17] are observed in experiments. This show the low-dimensional allotropes of boron are just beginning.

The finite boron clusters are 2D structures up to n≈16 (n = number of atoms) and above sixteen they are found to be double ring and tubular structures which are equipped with mainly triangular motifs.[18,19] These triangular finite 2D boron clusters are heuristically considered as precursors for the boron sheets, nanotubes, and fullerenes as the hexagonal benzenoid hydrocarbons are considered as precursors for carbon sheets, nanotubes, and fullerenes.[10] The theoretically predicted boron sheets (BSs) and boron nanotubes (BNTs) based on these triangular motifs are found to be buckled or wrinkled unlike the carbon sheets and nanotubes which are planar and tubular respectively.[11] However the recent calculations by Tang *et al* on BSs[10] and by Yang *et al* on BNTs[12] show that structures having 2/3 hexagonal voids in the triangular network are planar and tubular without buckling and also found to be more stable than the buckled sheets and tubes. The stable BS and BNT containing 2/3 hexagonal voids are named as α-sheet and α-tube respectively. Incidentally, before the prediction of stable α-sheet and α-tube, a stable hollow boron fullerene, B_{80} analogous to C_{60} was proposed by Szwacki *et al* using theoretical calculations.[13] The structure of B_{80} is similar to C_{60}, but it has an additional atom in the center of each hexagon. These allotropes of boron, analogous to carbon, appear as promising materials for all the characteristics of low-dimensional properties.

But, what made these low-dimensional allotropes of boron analogous to carbon as a stable species despite boron strongly prefers icosahedral B_{12} based allotropes is not clear. In the case of carbon the structural connections between the benzenoid hydrocarbons and the low-dimensional allotropes of carbon is understandable. The sp^2 hybridization of carbon ($1s^2,2s^1,2p_x^1,2p_y^1,2p_z^1$) flexibly transforms from 2D carbon sheets to 1D nanotubes to 0D fullerenes. While in boron, the connection between the finite boron clusters and the low-dimensional allotropes of boron is unclear. It is due to the fact that there is no boron structural precursor with the sp^2 hybridization like in benzenoid hydrocarbons. If boron were to adopt sp^2 hybridization ($1s^2,2s^1,2p_x^1,2p_y^1,2p_z^0$) it must leave the $2p_z$ orbital as empty which will make boron electron deficient. Therefore, it selects instead multi-center based electron deficient polyhedral structures. Therefore, it appears that the formation of carbon sheet, nanotube, and fullerene analogues of boron allotropes is quite an arduous task.

However, boron being next to carbon with one electron deficiency, it is known to form carbon analogues when stabilized by different elements which fulfill the electronic requirement of carbon (B^-~C). The graphene analogue of hexagonal magnesium diboride $[Mg^{+2}(B^{-1})_2$~$C_2]$[20] and polycarbyne analogue of lithium boride chain (Li^+B^-~C)[21,22] are notable experimental examples. This view suggests that if boron were to adopt the carbon skeleton it would need an extra electron for the stability. If the extra electrons are provided by the additional boron atoms without much disturbing the atomic arrangement of the carbon skeleton then we would see boron allotropes analogous to carbon. As a generalization, carbon analogue of boron requires n extra electrons or $n/3$ extra boron

atoms (where n is the number of atoms in carbon skeleton). These carbon analogue of boron allotropes contain a $4n/3$ total number of boron atoms would be stable. In that prospect here we show systematically the adaptation of carbon sheets, nanotubes, and fullerenes by boron with respect to the electron count (or number of boron atoms) using first principles density functional and semi-empirical tight-binding calculations. In order to understand the structure and stability of BSs, BNTs, and boron fullerenes with respect to the electron count we analyze projected density of states (PDOS), crystal orbital overlap populations (COOP), electron density isosurfaces (EDI), and cohesive energy per atom (E_c). Similarly, we also study the electronic structure and stability of MgB_2 sheets, nanotubes, and fullerenes which are isostructural and isoelectronic to graphene, carbon nanotube, and C_{60} fullerene respectively. We further intuitively assess the scope of viability of BSs and BNTs by comparing with the graphene and MgB_2 structures. We also discuss the carbon analogues of boron allotropes structural preference over the icosahedral B_{12} based boron allotropes.

The chapter is organized in the following way: The construction of graphene and carbon nanotube analogues of boron viz BSs and BNTs are illustrated in Sec. 4.2. Computational details are described in Sec. 4.3. The results and discussion of the structure and stability with respect to the electron count and electrical properties of the BSs, BNTs, and B_{80} fullerenes are presented in Sec. 4.4.1, 4.4.2, and 4.4.3 of Sec 4.4 respectively. Subsequently, MgB_2 based sheets, nanotubes, and fullerenes are given in Sec 4.5. Finally in Sec. 4.6 the conclusions are given.

4.2 Construction of BSs and BNTs

The BSs are constructed by taking the hexagonal graphene sheet as a beginning lattice with space group *P6/mm* where all the carbon atoms are substituted by boron. Such hexagonal BS contains two boron atoms (B_2) per primitive unit cell is shown in Figure 4.2a. The lattice vectors are denoted by a_1 and a_2, where $a_1 = a\,(\frac{1}{2}\,x + \frac{\sqrt{3}}{6}\,y)$ and $a_2 = a\,(\frac{2\sqrt{3}}{6})\,y$; $\|a_1\| = \|a_2\| = \frac{a}{\sqrt{3}}$. The B_2 unit-cell is two electron deficient when compare to graphene (C_2). According to $4n/3$ rule a graphene analogue of boron should have 2.67 boron atoms per primitive unit cell. The 0.67 fractional boron atoms do not allow us to keep in the calculatable plane lattice without disturbing the symmetry. However, this can be overcome by considering a super-cell contain six carbon atoms per graphene unit cell (C_6) to construct an electron sufficient BS. The C_6 graphene unit cell effectively contains three hexagonal voids. Substituting C_6 by B_6 we get a B_6-sheet with deficiency of six electrons (Figure 4.2a). Placing the required six electrons by two boron atoms (each boron atom provides three valence electrons) at the center of the two hexagonal voids out of the three within *P6/mm* space group generates an electron sufficient B_8-sheet as shown in Figure 4.2b. The lattice vectors for B_8-sheet are denoted by b_1 and b_2, where $b_1 = ax$ and $b_2 = a\,(\frac{-1}{2}\,x + \frac{\sqrt{3}}{2}\,y)$; $\|b_1\| = \|b_2\| = a = 3l_{B\text{-}B}$. Filling the vacant hexagonal void in the B_8-sheet gives a fully triangular sheet (B_9) which is a three electron excess sheet (Figure 4.2c). The BNTs are constructed from the B_6 unit cell (Figure 4.2a) much similar to the construction of carbon nanotubes (CNTs) from graphene[4] as shown in Fig. 4.2d-f. The BNTs satisfy the chiral vector or circumferential vector $C_h = nb_1 + mb_2 = (n, m)$, where n,

m are integers, $n \geq m \geq 0$. The diameter of the tube can be given as $d = \frac{\sqrt{3}}{\pi} l_{B\text{-}B} \sqrt{n_1^2 + n_1 n_2 + n_2^2}$. The BSs are wrapped up into BNTs in such a way that the vector b_2 will be the translational vector for the BNTs. As an example here we constructed a zigzag (6,0) (following the CNTs terminology) BNTs with different electron counts similar to the above BSs. The (6,0) CNT contains 24 atoms per unit cell (C_{24}). Substituting 24 carbon atoms by boron we get a B_{24} tube (Figure 4.2d) which is 24 electrons deficient when compared to C_{24}. Applying the $4n/3$ rule on B_{24} we get electron sufficient B_{32} tube that is filling 2/3 of hexagonal holes (8 out of 12 in B_{24} tube) (Figure 4.2e). Occupying the remaining hexagonal holes of B_{32} by boron gives a 12 electron rich B_{36} tube (Figure 4.2f). Thus the constructed BSs and BNTs with different electron counts will be exploited in assessing their structure, stability and electrical conductivity.

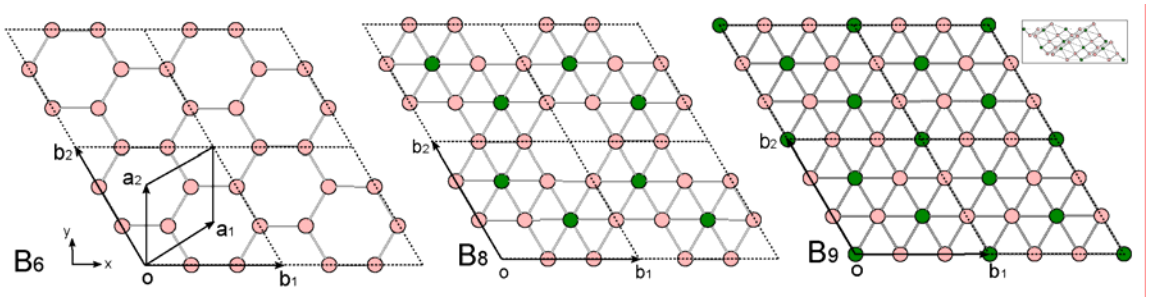

Figure 4.2. (left) **(a)** Electron deficient hexagonal boron sheet (equivalent to graphene), where the primitive unit-cell (B_2) is represented by two lattice vectors a_1 and a_2. It also represents the lattice vectors b_1 and b_2 for the super-cell B_6-sheet or C_6-graphene. (middle) **(b)** Electron sufficient B_8-sheet which primitive unit-cell is represented by b_1 and b_2 lattice vectors as in B_6-sheet. (right) **(c)** Electron rich B_9-sheet which super-cell is represented by b_1 and b_2 lattice vectors as in B_6-sheet and B_8-sheet. The extra added boron atoms at the center of the hexagons of B_8-sheet and B_9-sheet are indicated in green colour (dark in B&W print). The unit-cells of B_6-sheet, B_8-sheet, and B_9-sheet are considered in such a way that the shift in the electronic energy levels can be directly compared. The inset in **(c)** is the side view of the optimized B_9-sheet structure.

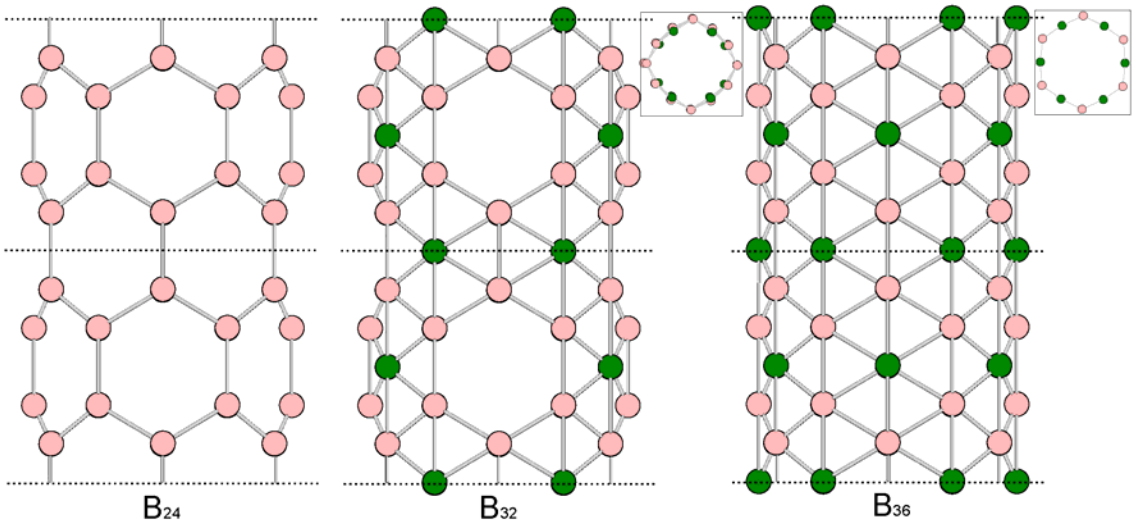

Figure 4.2. (left) **(d)** Electron deficient (6,0) boron or B_{24}-tube. (middle) **(e)** Electron sufficient B_{32}-tube. (right) **(f)** Electron rich B_{36}-tube. The unit-cells of the tubules considered here are shown with the dotted lines. The extra added boron atoms at the center of the hexagons of B_{32}-tube and B_{36}-tube are indicated in green colour (dark in B&W print). The inset in **(e)** and **(f)** are optimized structures of B_{32}-tube and B_{36}-tube shown along the tube axis respectively.

4.3 Computational Methods

The calculations are performed for sheets and nanotubes using density functional theory (DFT) implemented in CASTEP code which uses a plane-wave basis set approach to expand the electronic wavefunctions.[23,24] Exchange and correlation of electrons are treated within the local density approximation (LDA) of Ceperley and Alder–Perdew and Zunger (CA-PZ) functional.[25,26] Vanderbilt ultrasoft pseudopotentials for B($2s$,$2p$), C($2s^2$,$2p^2$), Mg($2p^6$,$3s^2$) are used to describe the interaction between electrons and ions with cutoff energy of 240, 310, and 340 eV for the plane-wave basis set respectively.[27]

Integration of the wavefunctions is sampled over the first Brillouin zone with 6×6×4 (for sheets), 2×2×6 (for tubes), and 6×6×6 (for α-boron) *k*-point mesh generated by Monkhorst-Pack scheme.[28] Pulay's density mixing method is employed in the self-consistent filed (SCF) electronic minimization procedure with charge mixing amplitude 0.5 and SCF cutoff 5×10^{-7} eV/atom.[29] Geometry optimizations are performed using Broyden-Fletcher-Goldfarb-Shanno[30] method with convergence tolerances of energy 5×10^{-6} eV/atom, force 0.01 eV/Å, stress 0.02 GPa, and displacement 5×10^{-4} Å. A super cell approach has been used (8 for sheets and 10 Å for nanotubes) to avoid the interlayer and intertubular interactions. Subsequently the PDOS are calculated for the optimized sheets and tubes. The EDIs are produced to indicate the formation of bonding types.

Further extended Hückel (eH) PDOS and COOP are calculated upon the CASTEP optimized geometries using YAeHMOP program to get more insight into the bonding picture.[31-33] The parameters used for boron and carbon are B_{2s} (H_{ii} = -15.2 eV, ζ = 1.3), B_{2p} (H_{ii} = -8.5 eV, ζ = 1.3), and C_{2s} (H_{ii} = 21.4 eV, ζ = 1.625), C_{2p} (H_{ii} = -11.4 eV, ζ = 1.625), where H_{ii} and ζ are the valence ionization potentials and radial exponents of the Slater type orbitals respectively.

The finite boron and MgB_2 fullerene-like structures are calculated with DMOL3 program[34] using generalized gradient approximation (GGA) treated by Perdew-Burke-Ernzerhof (PBE) exchange-correlation potential and an all electron double numerical atomic orbital augmented by d-polarization functions (DNP) as basis set is used.[35] Geometry optimizations were performed with a convergence threshold of 0.002 a.u./Å on the gradient, 0.005 Å on displacements, and 10^{-5} a.u. on the energy.

4.4 Results and Discussion

4.4.1 BSs and BNTs

We begin with the BSs in comparison to C_6-graphene. The optimized B_6 and B_8 are retained in the C_6 graphene-like flat structure whereas the B_9 converged to a buckled structure (Figure 4.2a-c). Among them the electron sufficient B_8 is found to be the lowest energy sheet. For completeness with respect to the electron count a three electron deficient B_7-sheet (arrived by removing one central hexagonal boron atom from B_8-sheet) also has been calculated which holds the flat structure close to B_8 but higher in energy. The relative cohesive energy decreasing stability order of the BSs is B_8 (0.000) > B_9 (0.205) > B_7 (0.315) > B_6 (1.023) eV (Table 4.4.1a).

Table 4.4.1a. Cohesive energy per atom (E_c) in eV and the range of bond lengths in Å of the optimized B_6, C_6, B_7, B_8, and B_9 sheets.

	B_6	C_6	B_7	B_8	B_9
E_c (eV)	-5.893	-9.967	-6.601	-6.916	-6.711
$l_{B\text{-}B}$ (Å)	1.671 to 1.754	1.409	1.654 to 1.713	1.677 to 1.692	1.686 to 1.829

The reason behind the stability order can be appraised by the notion of "*better the occupied bonding and unoccupied antibonding bands greater the stability*" of the system. This can be interpreted distinctly by looking at the PDOS, COOP and EDI of the different electron count B_6, B_8, and B_9-sheets. The calculated DFT PDOS, eH PDOS, and eH COOP are shown in Figure 4.4.1a. The shape of the DOS curves is similar in both the methods. In general the bonding picture of C_6 graphene can be considered as each carbon

atom ($2s^1\ 2p_x^1\ 2p_y^1\ 2p_z^1$) sharing an electron with each of its three in-plane nearest neighbors forming three localized sp^2 σ-bonds and the fourth electron forms out-of-plane delocalized π-bond (p_z) among them. That is the valence band is occupied by the σ and π bonding and the conduction band σ^* and π^* antibonding bands. The PDOS of C_6 shows the above bonding scenario where the bonding and antibonding states are distinctly divided by the Fermi energy (E_f) (Figure 4.4.1a). Whereas in B_6 ($2s^1\ 2p_x^1\ 2p_y^1\ 2p_z^0$) the DOS above the E_f and below 3.5 eV are bonding which are unoccupied (DFT DOS of B_6 in Figure 4.4.1a). These unoccupied bonding states mainly stem from the B(p_z) bonding orbitals (π) as shown in the eH PDOS of B_6 in Figure 4.4.1a. The COOP of B_6 clearly shows the bonding character of the empty orbitals above the E_f (eH COOP of B_6 in Figure 4.4.1a). In the electron sufficient B_8 the E_f is shifted above by occupying the unoccupied B_6 bonding states and separates the bonding and antibonding states as in C_6. Moving to the electron rich buckled B_9 the E_f is shifted up compared to B_8 but above the E_f hardly any antibonding character is found. It is due the fact that the sheet is buckled and there is a mixing of the σ and π orbitals. This brings up a dominant PDOS of hexagonal central 3B of buckled B_9 near the E_f when compared 2B PDOS of B_8 (DFT PDOS of B_8 and B_9 sheets in Figure 4.4.1a). The E_f in the flat B_9 is about 1.0 eV shifted up compared with buckled B_9 as shown in B_9 COOP plot in Figure 4.4.1a. The COOP of flat B_9 shows antibonding states below E_f (between 7.5 to 6.3 eV) as expected which is 0.068 eV/atom higher than the buckled B_9. The PDOS of hexagonal central boron atoms in B_8 and B_9 coincide with the rest of six boron atoms (6B) as they do not disturb the local symmetry as a whole. The DOS at E_f indicates that all the BSs are metallic and C_6 is a semi-metallic.

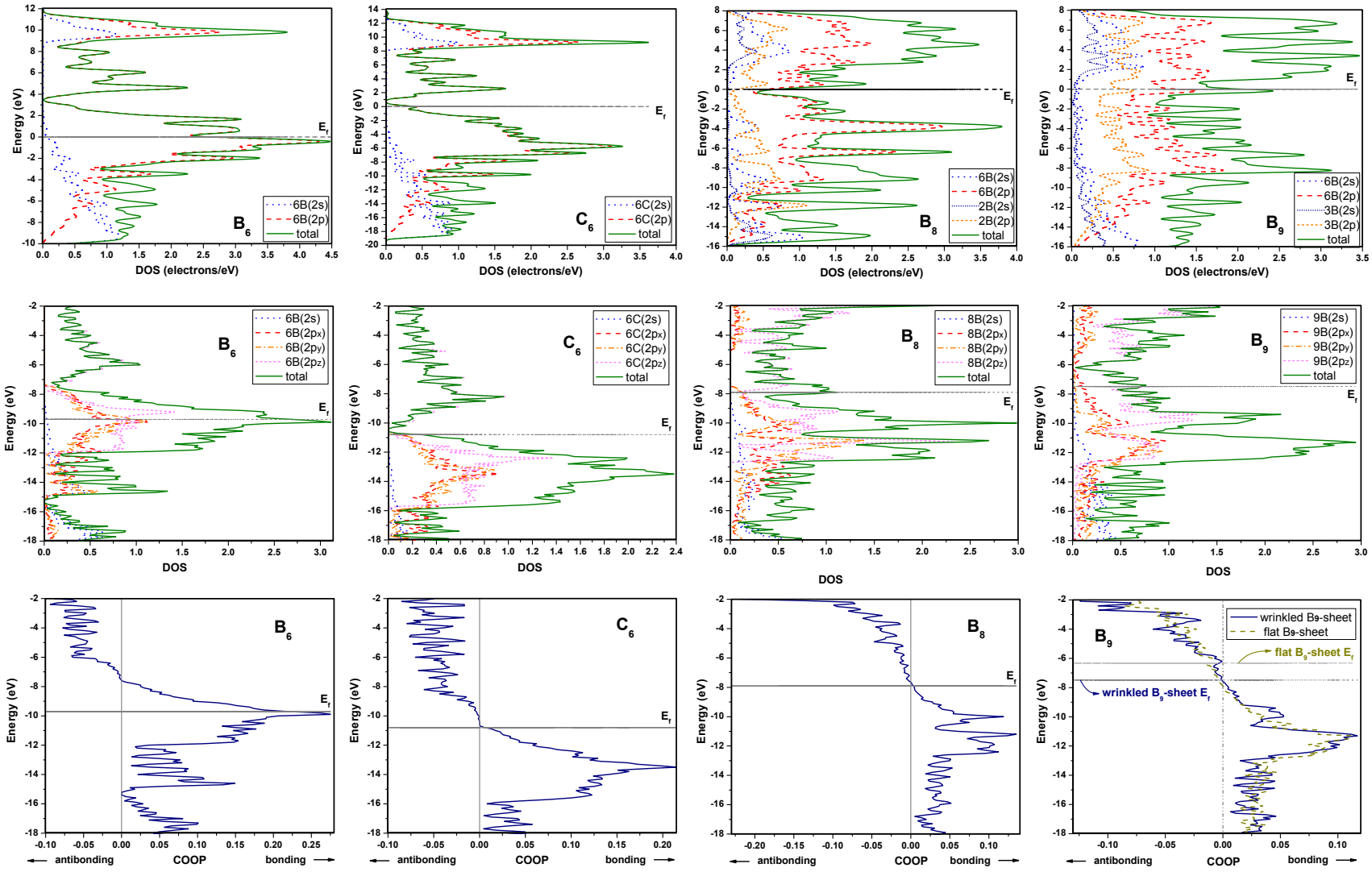

Figure 4.4.1a. Total density of states (DOS), atom and orbital projected DOS, and crystal orbital overlap populations (COOP) of B_6, C_6, B_8, and B_9 sheets are depicted here. The top row results are obtained from DFT calculations. The middle and bottom row results are obtained from eH calculations. Fermi energy level (E_f) is indicated by a dotted line.

The B-B bond distances in the optimized BSs are in the range of 1.671 to 1.829 Å (Table 4.4.1a). The six-electron-deficient B_6 and the three-electron-rich B_9 have two distinguishable hexagonal B-B bond lengths (1.671, 1.754 and 1.686, 1.829 Å) due to the unoccupied bonding and occupied antibonding states which breaks the degeneracy of the valence bands. The electron sufficient B_8 also has unequal bond lengths but with small differences (1.677 – 1.692 Å) which contrast to the C_6 graphene where it has resonating C-C bonds (1.410 Å). It is because the hexagonal central B atoms induce a delocalized mc-2e bonding and other hexagonal holes are vacant which is indicated by the EDIs of B_8-sheet shown in Figure 4.4.1b.

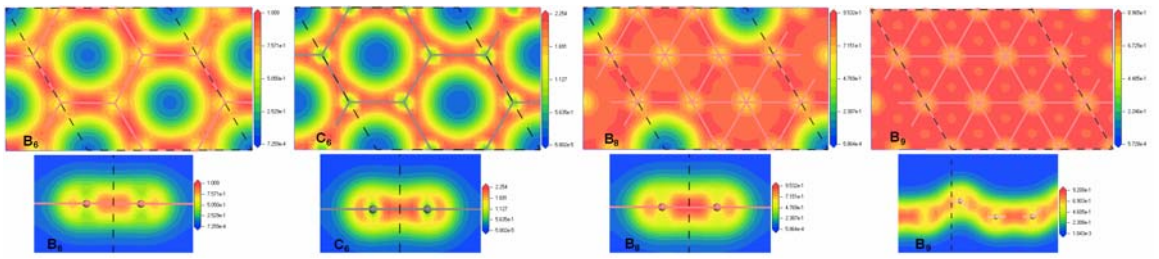

Figure 4.4.1b. Electron density isosurfaces along the σ (in-plane) and π (out-of-plane) bonds of B_6, C_6, B_8, and B_9 sheets are shown in the top and bottom row respectively. The close to red colour regions indicates accumulation of electron density and close to blue colour regions indicates depletion of electron density.

Compared to C_6 the electron density is depleted in B_6 along the σ and π-frame. The σ-frame shows a 2-long and 4-short B-B bonds much similar to a cationic C_6H_6 molecule. The depletion of electron density in B_6 is restored back into B_8 by fulfilling the electronic requirement of C_6. However, the EDI of B_8 suggests that the in-pane has a combination of localized 2c-2e (along the hexagonal B-B bond) and mc-2e bonding

(along the hexagonal B and to its central B). On the other hand in B_9 the electrons are much delocalized over the sheet indicates its electron richness. Thus the bonding and antibonding analysis with respect to the electron count supports the stability order of the B_6, B_8 and B_9 sheets and in turn the applicability of $4n/3$ rule holds good.

The constructed BNTs B_{24}, B_{32} and B_{36} from the three BSs B_6, B_8, and B_9 are converged to tubular structures with little local distortions within the symmetry constraints as shown in the Figure 4.2d-f. Among them the B_{32} is found to be lower in energy as it is the isoelectronic and isostructural equivalent of C_{24}. The relative cohesive energy decreasing stability order of these three BNTs is B_{32} (0.000) > 0.230 (B_{36}) > 0.548 (B_{24}) eV (Table 4.4.1b).

Table 4.4.1b. Cohesive energy per atom (E_c) in eV, the range of bond lengths in Å, and diameter in Å of the optimized B_{24}, B_{32}, and B_{36} tubules.

	B_{24}	C_{24}	B_{32}	B_{36}
E_c (eV)	-6.237	-9.611	-6.785	-6.555
l_{B-B} (Å)	1.464 to 1.533	1.406 to 1.431	1.732 to 1.647,	1.720 to 1.779
d (Å)	4.065	4.771	5.014	5.632

In order to have a complete stability order of the BNTs with respect to the electron count we have filled the 12 hexagonal gaps of B_{24} systematically which gives B_{24+x} (where x = 1-7, 9-11) tubes. We have chosen several different hexagonal positions of which the lowest energy tubules are considered here. Thus generated BNTs cohesive

energies are calculated without atomic relaxations including B_{24}, B_{32}, and B_{36} as shown in Figure 4.4.1c. This shows that B_{32} is the most stable in the (6,0) zig-zag BNTs series.

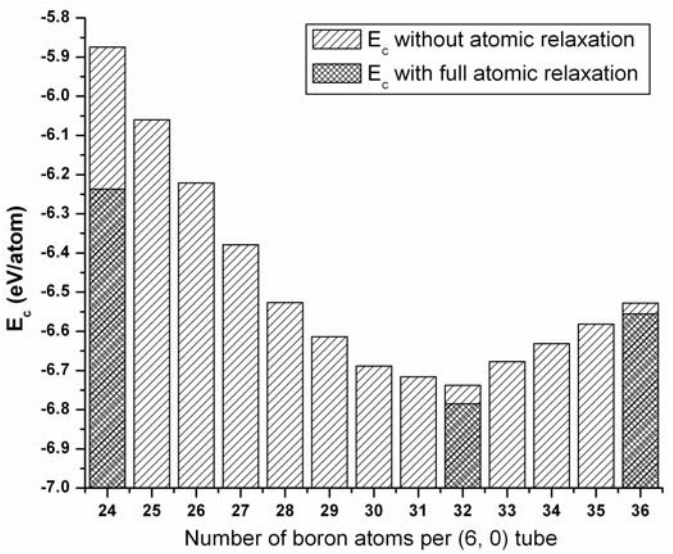

Figure 4.4.1c. Cohesive energy of all the boron nanotubes in (6,0) zig-zag series. The BNTs without atomic relaxation are shown with light crossed gray bars and the BNTs with full atomic relaxation are shown with thick crossed gray bars. The B-B distance =1.720 Å is considered in all the unrelaxed tubules cohesive energy calculations.

The reasons for the stability of BNTs with respect to the electron count are similar as explained for BSs. The calculated DFT PDOS, eH PDOS, and eH COOP are shown in Figure 4.4.1d. The shape of the eH PDOS near E_f is qualitatively same as DFT DOS. It is known that the dominant hybridization effects in the small diameter nanotubes play a key role in shifting the bands.[4,36] However, the general trend of shifting E_f in connection with the electron count of BNTs is apparent in all the methods. COOP of B_{24} and B_{36} shows the bonding and antibonding nature of the states above and below the E_f respectively, whereas in B_{32} the bonding states are fully occupied as in C_{24}. This helps to B_{32} lowering energy over the other electron deficient and electron rich BNTs.

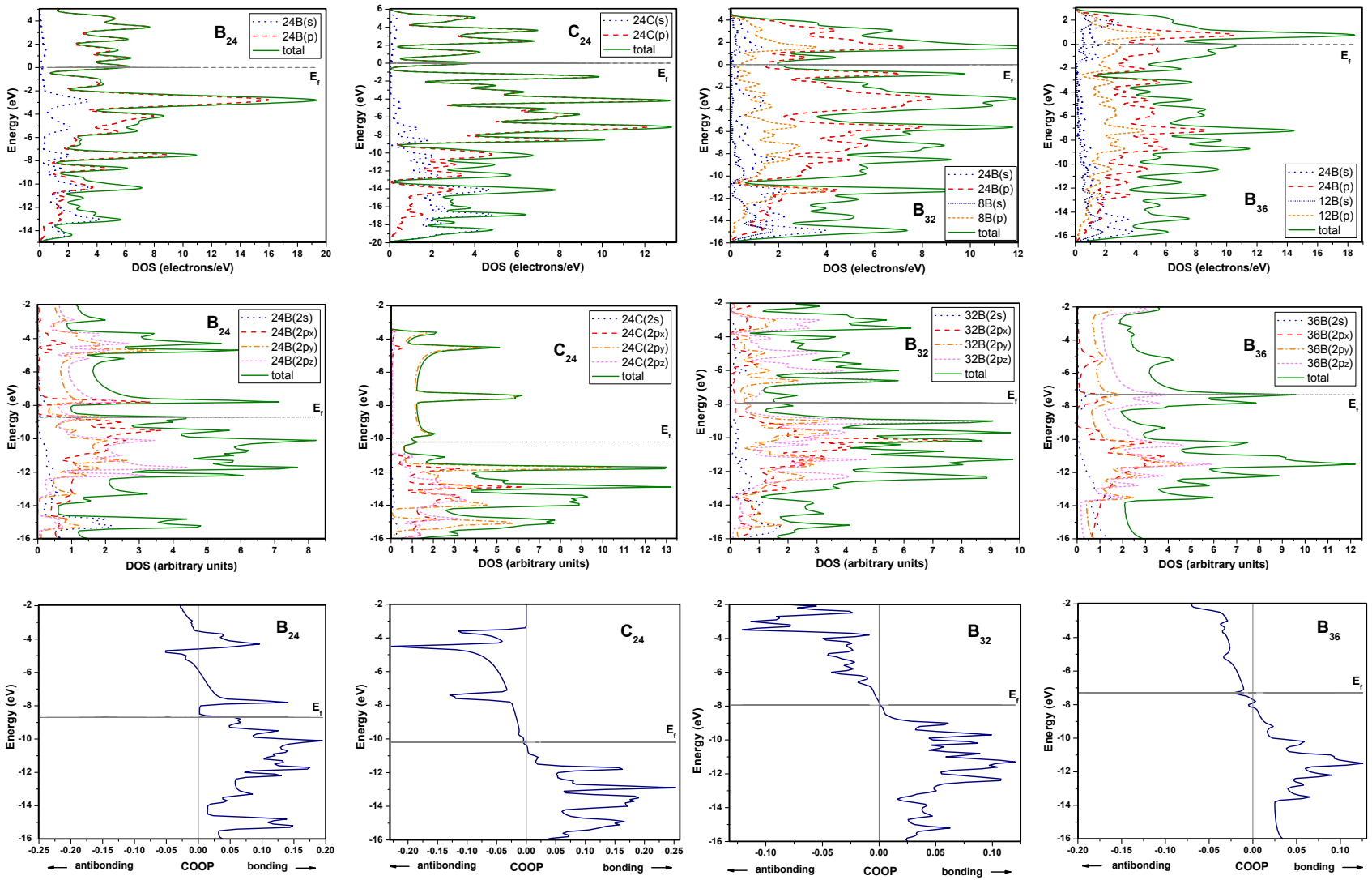

Figure 4.4.1d. Total density of states (DOS), atom and orbital projected DOS, and crystal orbital overlap populations (COOP) of B_{24}, C_{24}, B_{32}, and B_{36} tubules are depicted here. The top row results are obtained from DFT calculations. The middle and bottom row results are obtained from eH calculations. Fermi energy level (E_f) is indicated by a dotted line.

The EDIs of BNTs shown in Figure 4.4.1e suggest the similar bonding patterns as in BSs other than bringing the curvature effects and hence the σ and π hybridization. The B-B bond lengths are increased from B_{24} to B_{36} as the diameter increases (Table 4.4.1b). There are two different B-B and C-C bonds in B_{24} (1.464, 1.533), B_{36} (1.720, 1.779) and C_{24} (1.406, 1.431 Å). This is the result of broken symmetry (sheets rolled into tubes) of C_6 graphene for C_{24} and in addition to this the unoccupied bonding and occupied antibonding states for B_{24} and B_{36}. The B_{32} has several different B-B bonds with average distance of 1.710 Å (Table 4.4.1b only shows the highest and lowest bond distances). The change in the bond distances in tubes can be seen from Figure 4.4.1e where the shorter bonds are accumulated with electron density and the longer ones are depleted. The depletion of electron density is slowly vanished from B_{24} to B_{36}. The electron density distribution perpendicular to the tube surface is similar to the BSs (Figure 4.4.1b).

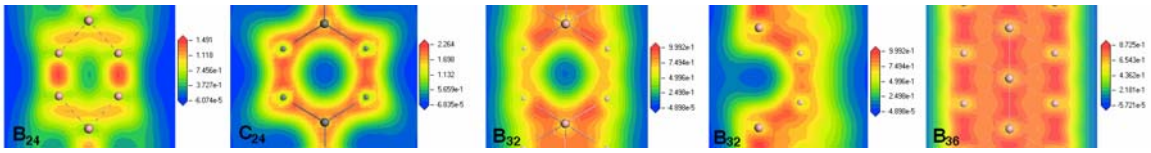

Figure 4.4.1e. Electron density isosurfaces along the σ bonds of B_{24}, C_{24}, B_{32}, and B_{36} are shown in here. The close to red colour regions indicates accumulation of electron density and close to blue colour regions indicates depletion of electron density.

The eH DOS presented in Figure 4.4.1d shows the metallic nature of BNTs and CNT. However, we have noticed a small gap of 0.05 eV in the DFT calculated B_{24} tube at G point which is not observed in eH (see appendix for eH and DFT band structures of B_{32} tube). It shows that the rehybridization effects play a significant role in calculating the band gaps of nanotubes with small diameter.[12,37] The effect of rehybridization on electrical conduction in different BNTs is yet to be understood in detail.

4.4.2 Hollow Boron Fullerenes

Let us now look at the fullerene-like boron clusters. The fullerene-like boron clusters are arrived by choosing the C_{60} fullerene as a basic skeleton where all the carbon atoms are substituted by boron. This gives a B_{60} fullerene which is 60 electrons deficient when compared to C_{60}. The 60 electron deficient icosahedral B_{60} structure would certainly an unstable species due to its high electron deficiency which is similar to the 50 electron deficient stuffed fullerene-like B_{84} structure that we have discussed in Chapter 3. However, in Chapter 3, the unstable 50 electron deficient B_{84} stuffed fullerene-like boron cluster was stabilized by compensating the required 50 electrons by placing the extra boron atoms on the surface of the B_{84} cluster. Here, we have adopted similar route to stabilize the 60 electron deficient B_{60} fullerene by adding 20 boron atoms (each boron provides three valence electrons) in the centers of 12 pentagons and 20 hexagons of B_{60}. This process generates several fullerene-like boron clusters with 80 boron atoms which are isoelectronic equivalent of C_{60} fullerene.

However, placing 20 boron atoms in the centers of 20 hexagons of B_{60} generates an icosahedral B_{80} (B_{80}-I_h) cluster which is symmetrically identical to C_{60} fullerene as shown in Figure 4.4.2a. According to $4n/3$ rule the C_{60} fullerene analogue (isoelectronic and isostructural) of boron, B_{80}-I_h would be expected as a stable species. We also have generated structures that are close to $4n/3$ number of boron atoms and few high symmetric structures to understand the structure and stability with respect to the electron count.

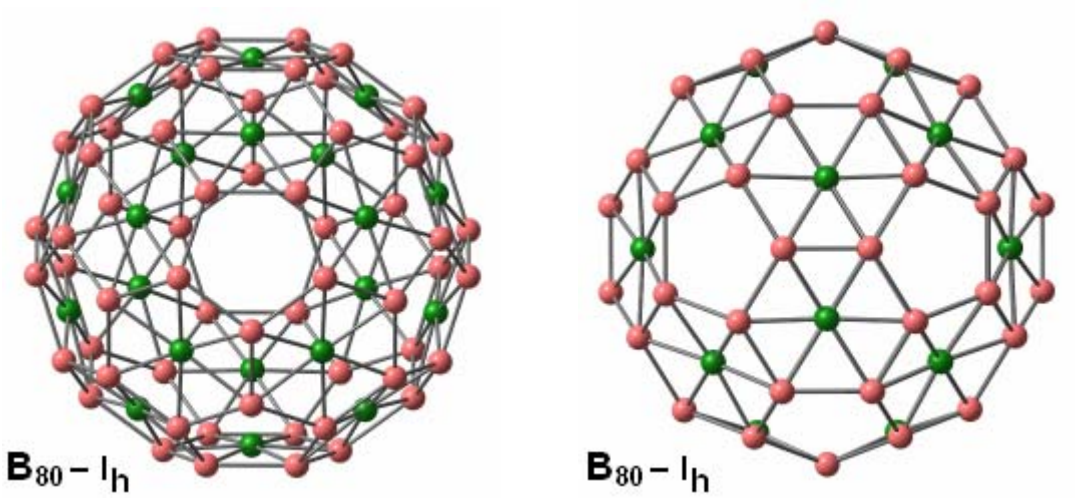

Figure 4.4.2a. Icosahedral structure of B_{80} fullerene is shown along the C_5 axis (left) and C_2 axis (right) which is arrived by substitution of each carbon of C_{60} fullerene by boron and placing a boron atom in the center of each hexagon. The extra boron atoms (20 B) in the center of each hexagon of B_{60} are shown in green colour (dark in B&W print).

The optimized B_{80}-I_h retains in the same icosahedral symmetry. The central hexagonal boron atoms also retain in the plane of hexagons without much distortions. There are three distinguishable B-B bond length groups in B_{80}: 30 short (1.687 Å) and 60 long (1.732 Å) similar to C-C bond lengths in C_{60}, 30 short (1.398 Å) and 60 long (1.451 Å). The third group belongs to 120 medium B-B bonds (1.711 Å) that correspond to the B-B bonds between each central hexagonal boron to its six nearest neighbors. The diameter (distance between two opposite pentagons) of B_{80} (7.97 Å) is larger than the C_{60} diameter (6.65 Å).

Further, the harmonic vibrational frequencies of the optimized B_{80} structure are calculated. It is found that B_{80} has 7 low imaginary frequencies. These low imaginary frequencies correspond to small up and down displacements of central hexagonal boron

atoms. Therefore, the B_{80}-I_h structure is not local minimum on the potential energy surface.[38] However, by following-up of these frequencies the B_{80} structure is found to be minimum on the potential energy surface with T_h symmetry. A systematic structural relaxation by following the 7 imaginary frequencies of icosahedral B_{80} structure produced another isomer of B_{80} which is also a minimum within T_h symmetry as shown in Figure 4.4.2b. The difference between the two isomers of B_{80}-T_h (1) and B_{80}-T_h (2) is the slight change in the positions of the central hexagonal boron atoms. The B_{80}-I_h is found to be higher in energy when compare to B_{80}-T_h (1) and B_{80}-T_h (2) isomers (Table 4.4.2a). But after including the zero-point energy, the energy order is reversed. The isomer stabilization energy has been verified with other DFT method (PBEPBE/6-31g(d, p)) as well. This also shows the similar trends (Table 4.4.2a). The highest occupied and lowest unoccupied (HOMO – LUMO) gap is almost similar (~1.0 eV) in all the isomers of B_{80}.

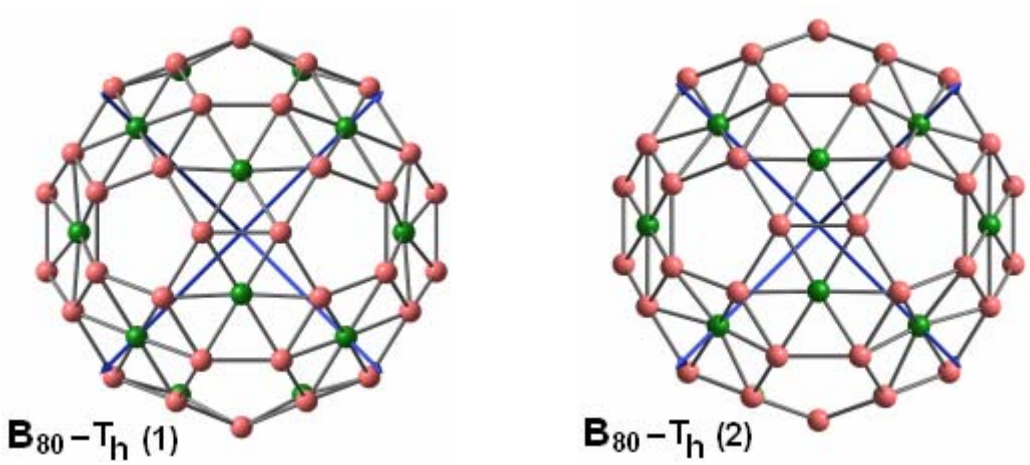

Figure 4.4.2b. The two structures of B_{80} isomers [T_h (1) and T_h (2)] are shown along the C_2 axis. The difference between the two isomers is the floppy displacement of the central hexagonal boron atoms. In B_{80}-T_h (1) structure, the central hexagonal boron atoms are shifting slightly away from the center along the T_h symmetry directions (indicated by arrows) whereas in B_{80} T_h (2) it is reversed. See appendix for list of B_{80}-I_h frequencies.

Table 4.4.2a. Total electron energies (T.E), zero-point energies (Z.P.E.), T.E + Z.P.E., cohesive energy per atom (E_c) HOMO – LUMO (H – L) gaps of B_{80} isomers in eV.

Results from DMOL3 calculated at GGA/PBE with all electron DNP level of theory					
B_{80} isomers	T.E (eV)	Z.P.E (eV)	T.E + ZPE (eV)	E_c (eV) [with ZPE]	H – L (eV)
B_{80}-I_h	-54028.9908	9.5711	-54019.4197	-5.5203	0.987
B_{80}-T_h (1)	-54028.9414	9.6302	-54019.3112	-5.5189	0.911
B_{80}-T_h (2)	-54027.9852	9.6388	-54018.3464	-5.5069	1.076
Results from Gaussian03 calculated at PBEPBE/6-31g(d, p) level of theory					
B_{80}-I_h	-54016.0384	9.3327	-54006.7057	-5.6531	1.015
B_{80}-T_h (1)	-54016.0856	9.4427	-54006.6429	-5.6523	0.971
B_{80}-T_h (2)	-54016.0527	9.3939	-54006.6588	-5.6525	1.010

Few structures that are close to 4*n*/3 number of boron atoms, isomers of B_{80}, and high symmetric structures such as B_{72}-I_h, B_{74}-D_{3d}, B_{76}-C_{2h}, B_{78}-D_{3d}, B_{80}-D_{5d}, B_{80}-tube, B_{82}-D_{5d}, B_{82}-D_{5d} (1), B_{82}-D_{5d} (2), B_{84}-D_{2h}, B_{86}-D_{3d}, B_{88}-D_{2h}, and B_{92}-I_h are generated as shown in Figure 4.4.2c. These optimized structures retains in the spherical shape. But the central hexagonal boron atoms are much deviated from the center of the hexagons. The cohesive energy profile (Figure 4.4.2d) of the clusters shows the C_{60} fullerene analogue of B_{80}-I_h structure is the lowest energy structure. Though, the structure B_{80}-D_{5d} and B_{80}-tube are isoelectronic equivalent of C_{60}, their cohesive energies are far from B_{80}-I_h. It suggests that the carbon analogue of boron not only required sufficient electrons but also the atomic arrangement should be as close to as carbon skeleton. The PDOS of the extra added 20 boron atoms mixing largely with the PDOS of B_{60} molecular orbital energy states in the entire energy spectrum of B_{80}-I_h as shown in Figure 4.4.2e. This suggests that

there will not be any large charge variation from boron to boron. The mixing of extra added 20 boron atoms PDOS with B_{60} PDOS in B_{80} is similar to the mixing of extra added 18 boron atoms PDOS with B_{84} PDOS in B_{102} stuffed fullerene-like cluster (Figure 3.3.1c in Chapter 3). The degeneracy of HOMO (five-fold, h_u) and LUMO (three-fold, t_{1u}) in B_{80}-I_h is similar to C_{60} fullerenes. Not only are the degeneracy of the orbitals, but also the HOMO and LUMO similar to each other as show in Figure 4.4.2f.

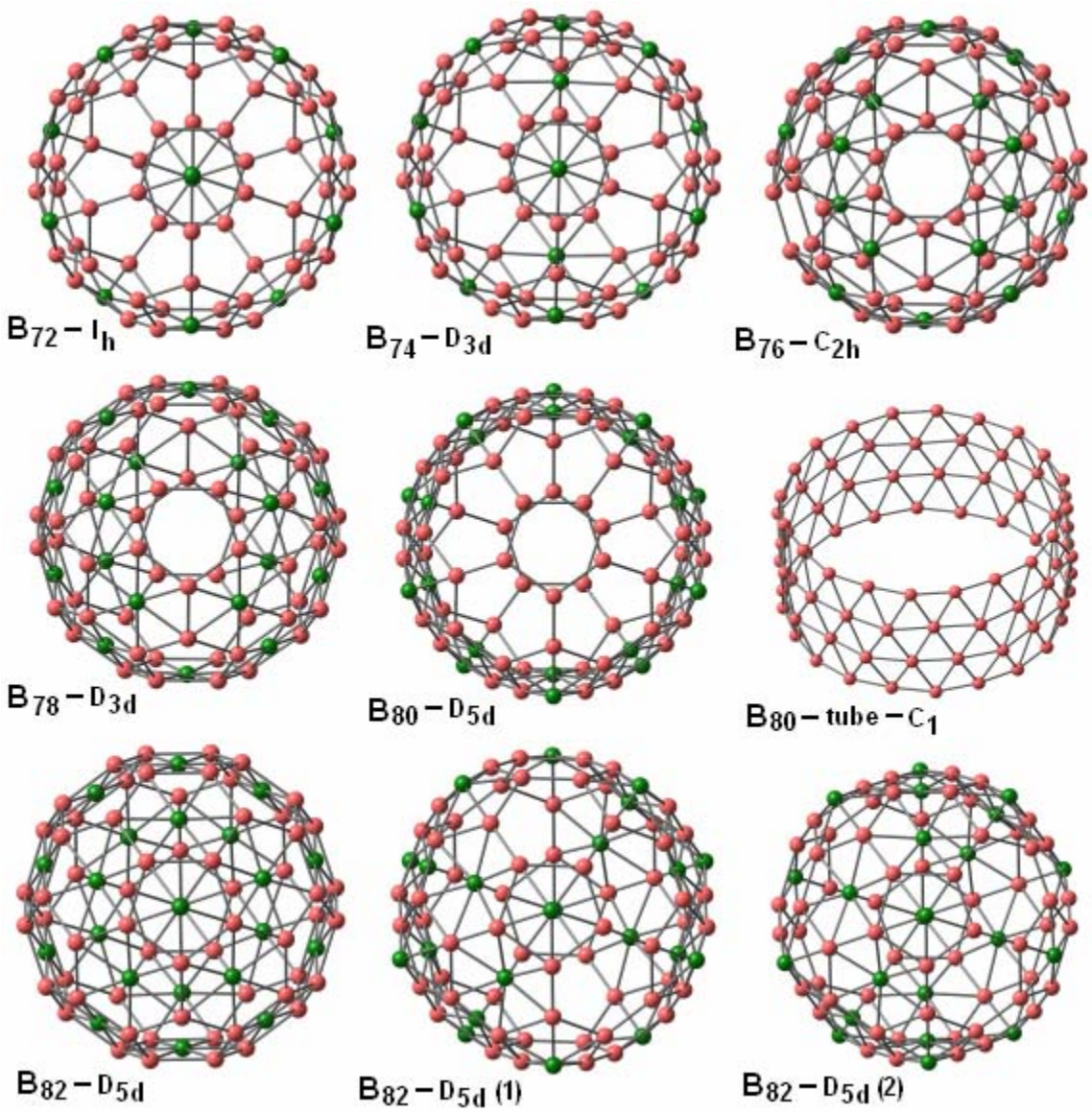

continued on the next page …..

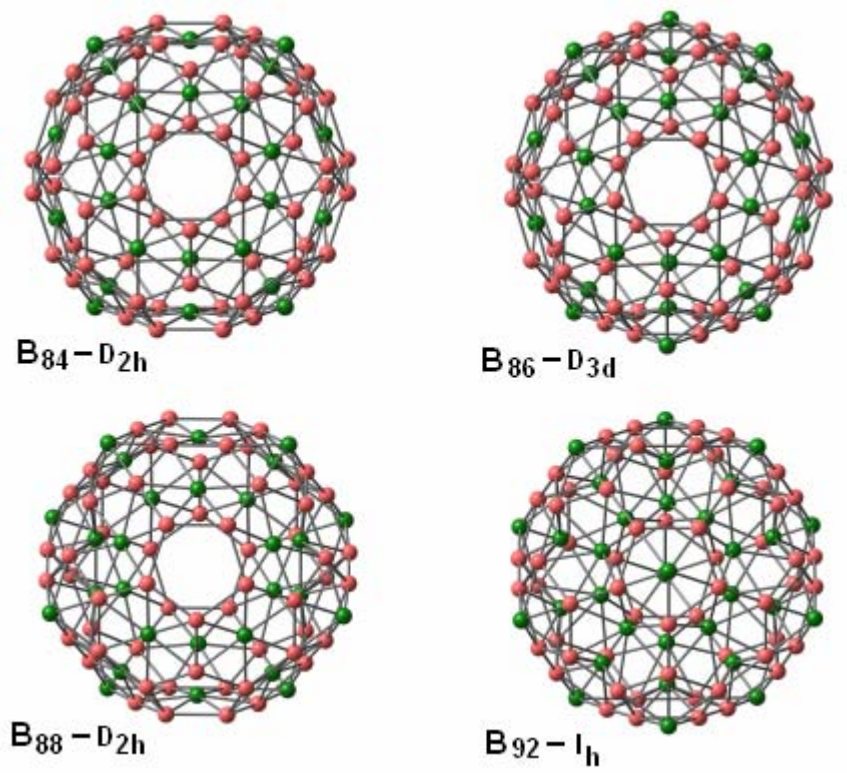

Figure 4.4.2c. Hollow fullerene-like boron clusters B_{72}-I_h, B_{74}-D_{3d}, B_{76}-C_{2h}, B_{78}-D_{3d}, B_{80}-D_{5d}, B_{80}-tube, B_{82}-D_{5d}, B_{82}-D_{5d} (1), B_{82}-D_{5d} (2), B_{84}-D_{2h}, B_{86}-D_{3d}, B_{88}-D_{2h}, and B_{92}-I_h are constructed from 60 electron deficient B_{60}. The added boron atoms at respective positions are indicated in green colour (dark in B&W print).

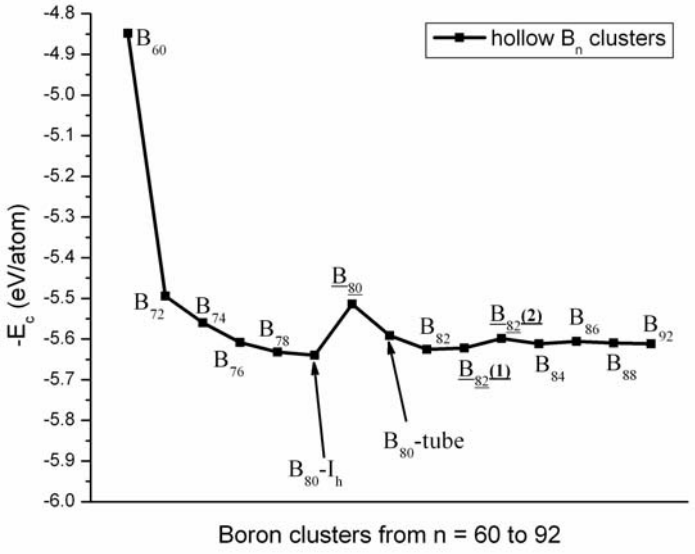

Figure 4.4.2d. Cohesive energy verses number of atoms for the optimized hollow fullerene-like boron clusters (B_n = 60 – 92). The isomers are underlined. The x-axis indicates the number of atoms not the scale.

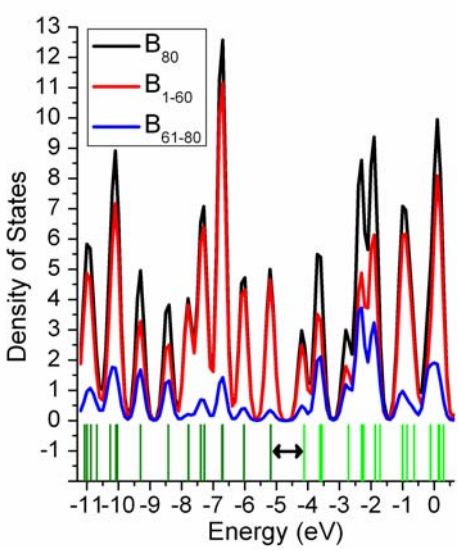

Figure 4.4.2e. PDOS of B_{80}-I_h hollow fullerene-like boron cluster. The ↔ between the MO energy bar code indicates the gap between HOMO and LUMO (~1.0 eV).

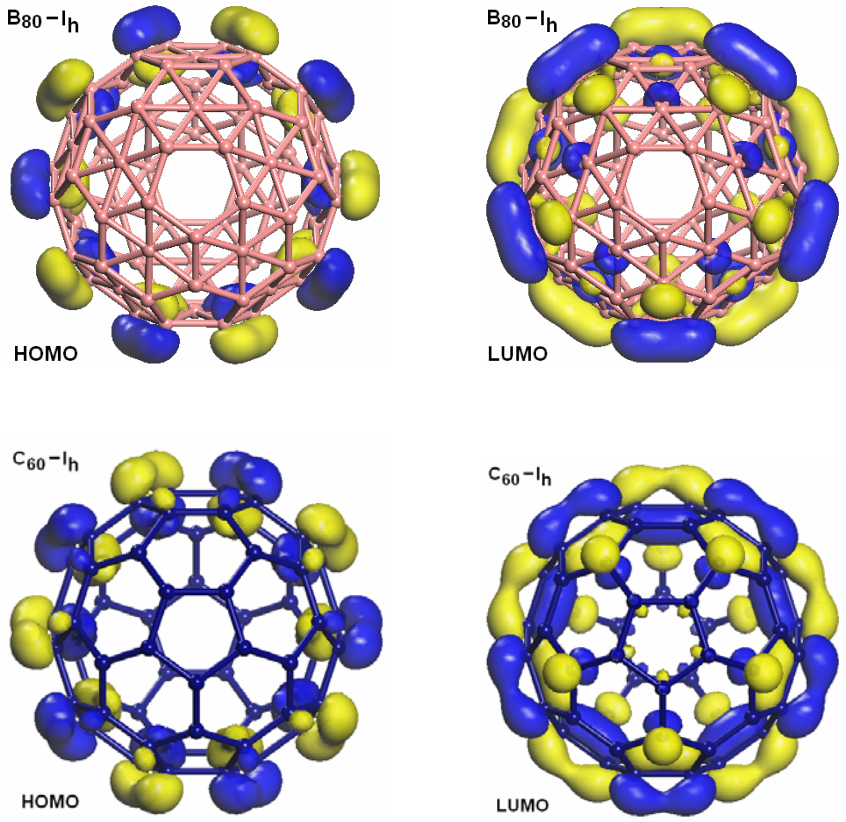

Figure 4.4.2f. (top left) B_{80}-I_h HOMO (top right) B_{80}-I_h LUMO, (bottom left) C_{60}-I_h HOMO, and (bottom right) C_{60}-I_h LUMO. HOMO and LUMO of B80-I_h and C_{60}-I_h are π bonding and largely π nonbonding.

Thus, we have shown that the boron analogues (B_8-sheet, B_{32}-tube, and B_{80}-I_h fullerene) of C_6-sheet, C_{24}-tube, and C_{60} fullerene which follow the $4n/3$ rule are low energy structures among their low-dimensional alternatives. But, the allotropes of boron based on icosahedral B_{12} skeleton are found to be lower in energy than the low-dimensional allotropes of carbon analogues of boron. The B_8-sheet and B_{32}-tube are 0.472 eV and 0.604 eV higher in energy than the three dimensional α-rhombohedral boron (α-B_{12}) allotrope. The B_{80}-I_h fullerene is also 0.075 eV (including Z.P.E. it is 0.071 eV) higher in energy when compared to B_{102} stuffed fullerene-like boron cluster (Chapter 3). The stability of the icosahedral based allotropes over the low-dimensional allotropes of carbon analogues of boron is due to the intrinsic stability of icosahedral B_{12} skeleton which was discussed in Chapter 2 and 3.

Though, the low-dimensional allotropes of carbon analogues of boron are higher in energy when compared to icosahedral B_{12} based allotropes, the energy barriers can be overcome if one would begin with a graphene/graphite analogue of boron. This process can be thought of similar to the experiments where carbon fullerenes and nanotubes are observed by ablating the carbonaceous feed stocks such as graphite.[39,40] The attempts made for pure boron produced clusters up to n = 55 (n = number of atoms).[41] The structural aspects of clusters were characterized by photoelectron spectroscopy, collision cross section measurements in combination with quantum mechanical calculations show that clusters up to n≈25 have planar and ring structures.[18,19] Alternatively, the laser vaporization of YB_{66} produced multiple B_{12} icosahedra, the kind of $[B_{13}^{-}@(B_{12})_{n=0,2,3}]$ clusters which would likely a seeding point for super-icosahedral $[B_{12}@(B_{12})_{12}]$ structure

assembly.[42,43] But the hollow fullerene-like boron clusters have not been observed so far. Is it that the experiments were not carried out with graphite-like boron? If so, how about materials based on hexagonal metal diborides where we have graphene-like boron sheets capped with metals. Here, we chose an intuitive scheme considering hexagonal MgB_2 (Figure 4.4.2g) as a feed stock to calculate the energetics that will enlighten our understanding towards the novel low dimensional boron allotropes.

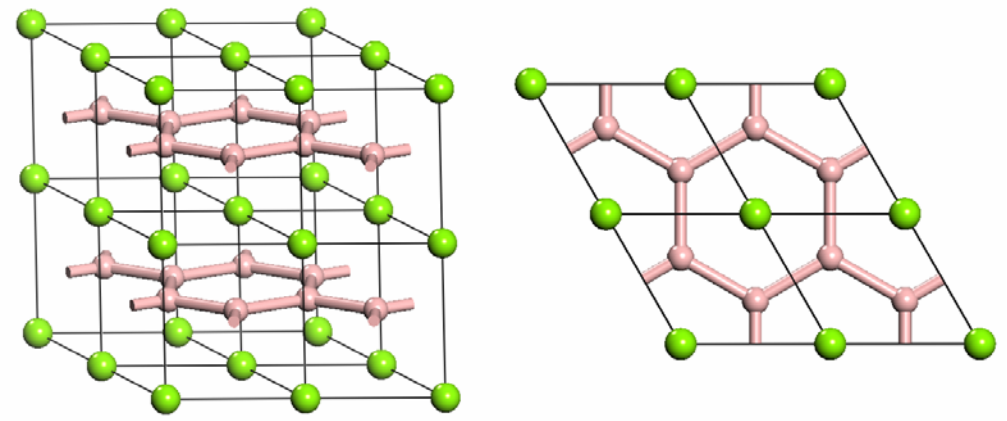

Figure 4.4.2g. The crystal structure of MgB_2 (space group: *P6/mmm*) shown in 2×2 super cell along the side view (left) and top view (right) of the hexagonal boron sheet. The magnesium atoms are located above the centers of the boron hexagons.

$Mg_3B_6 \longrightarrow Mg_3 + B_6 \quad \Delta H = 12.1$ eV (1)

$4(B_6) \longrightarrow 3(B_8) \quad \Delta H = -24.5$ eV (2)

$4(B_6) \longrightarrow 2(\alpha\text{-}B_{12}) \quad \Delta H = -35.8$ eV (3)

In the scheme we have constructed Mg_3B_6 supercell from the hexagonal MgB_2 crystal which is isoelectronic equivalent of C_6 and B_8 sheets $[(Mg^{+2}B_2^{-2})_3 \sim C_6 \sim B_8]$. Equation (1) suggests that exfoliation of Mg_3-sheet from Mg_3B_6 requires 12.1 eV. It

supports the instability of B_6-sheet. However, the conversion of the unstable B_6-sheet into B_8–sheet and α-B_{12} is 24.5 and 35.8 eV favorable (equation 2 and 3) respectively. Though the formation of α-B_{12} is favorable than B_8-sheet, the B_6 to B_8 heat of formation still encourages to search for graphene analogue of boron. Eventually, the graphene analogue of boron (or bundles of boron sheets) would act as a feed-stock for the boron nanotubes and fullerenes. A detailed thermodynamic and kinetics study based on first principles molecular dynamic simulations would answer the possible path ways to achieve these novel low dimensional boron allotropes.

4.4.3 Boride Sheets, Tubes, and Hollow Fullerenes

Based on the isoelectronic and isostructural similarities between MgB_2 and graphene [$Mg^{+2}(B^{-1})_2 \sim C_2$], we have constructed Mg_3B_6 sheet, $Mg_{12}B_{24}$ nanotube, and $Mg_{30}B_{60}$ fullerene similar to B_8-sheet, B_{32}-tube, and B_{80}-I_h fullerene as shown in Figure 4.4.3. The magnesium atoms are kept above the center of hexagons in Mg_3B_6 sheet and $Mg_{12}B_{24}$ nanotube as in the bulk MgB_2 crystal (Figure 4.4.2g). In the case of $Mg_{30}B_{60}$, the B_{60} fullerene has 20 hexagons and 12 pentagons (total 32 rings). But we need only 30 rings to add 30 Mg atoms to be isoelectronic equivalent to C_{60} [$(Mg_{30})^{+60}$ $B_{60}^{-60} \sim C_{60}$]. Therefore we have chosen two high symmetric configurations D_{5d} and D_{3d} where two opposite pentagons and hexagons are left vacant as shown in Figure 4.4.3c,d. We also have considered the icosahedral symmetric $Mg_{32}B_{60}$ where all the rings of B_{60} are capped with Mg atoms which is four electrons in excess when compared to C_{60} or B_{80}.

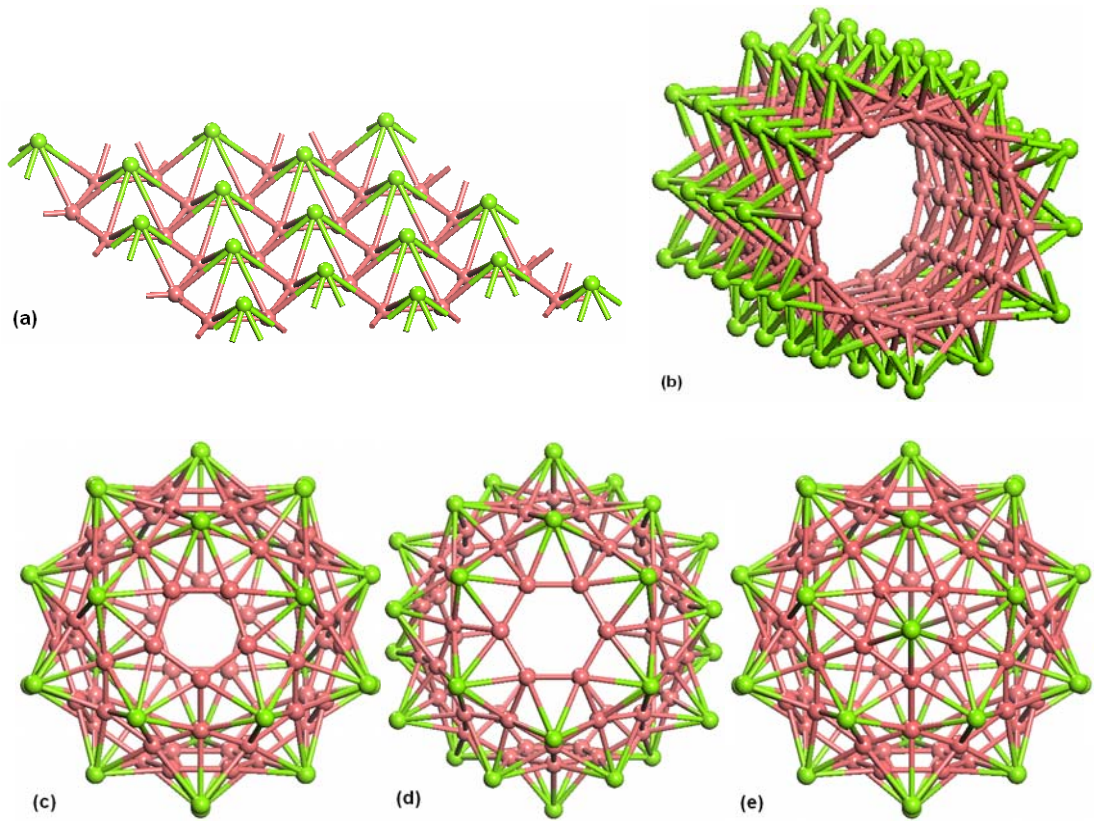

Figure 4.4.3. Structures of **(a)** Mg_3B_6-sheet, **(b)** $Mg_{12}B_{24}$-tube, **(c)** $Mg_{30}B_{60}$-D_{5d}, **(d)** $Mg_{30}B_{60}$-D_{3d}, and **(e)** $Mg_{32}B_{60}$-I_h.

The optimized Mg_3B_6 sheet retains the hexagonal sheet structure for boron and the magnesium atoms located above the center of hexagons at Mg-B distance of 2.374 Å which is 0.1 Å shorter than the Mg-B distance in bulk Mg_3B_6 (Table 4.4.3a). The hexagonal B_6 ring of the Mg_3B_6 sheet has two types of B-B distances 1.731 and 1.733 Å whereas the bulk Mg_3B_6 has resonating B-B bonds (1.748 Å). But the difference in the B-B bond lengths of Mg_3B_6-sheet is very small similar to the B_8-sheet. The optimized $Mg_{12}B_{24}$ nanotube, $Mg_{30}B_{60}$ (D_{5d} and D_{3d}), and $Mg_{32}B_{60}$ fullerenes also holds the tubular and spherical structures respectively (Figure 4.4.3b-e). The B-B and Mg-B bond

distances of $Mg_{12}B_{24}$ tube, $Mg_{30}B_{60}$ (D_{5d} and D_{3d}), and $Mg_{32}B_{60}$ fullerenes are within the bonding range (Table 4.42a). The diameters of the boron tube of $Mg_{12}B_{24}$ and $Mg_{30}B_{60}$ (D_{5d} and D_{3d}), $Mg_{32}B_{60}$ (I_h) fullerenes are close to B_{80}-I_h diameter (~8.0 Å).

Table 4.4.3a. Average bond distances and diameters in Å, band or HOMO – LUMO gaps (H – L) in eV of Mg_3B_6-bulk, Mg_3B_6-sheet, $Mg_{12}B_{24}$-tube, and $Mg_{30}B_{60}$-D_{5d}, $Mg_{30}B_{60}$-D_{3d}, $Mg_{30}B_{60}$-I_h fullerenes.

System	B-B	Mg-B	Mg-Mg	Diameter	H – L
Mg_3B_6-bulk	1.748	2.476	3.028	0	0
Mg_3B_6-sheet	1.732	2.374	3.005	0	0
$Mg_{12}B_{24}$-tube	1.661	2.3075	3.332	5.334	0
$Mg_{30}B_{60}$- (D_{5d})	1.758	2.305	3.768	8.151	0.097
$Mg_{30}B_{60}$- (D_{3d})	1.749	2.304	3.721	8.167	0.077
$Mg_{32}B_{60}$- (I_h)	1.755	2.306	3.732	8.162	0.278

The $Mg_{30}B_{60}$-D_{5d}, $Mg_{30}B_{60}$-D_{3d}, and $Mg_{32}B_{60}$-I_h fullerenes are calculated for their harmonic vibrational frequencies. All the three are found to be minima on the potential energy surface. Among the $Mg_{30}B_{60}$-D_{5d} and $Mg_{30}B_{60}$-D_{3d} isomers, the $Mg_{30}B_{60}$-D_{5d} fullerene is found to be 1.5 eV lower in energy. The stability of $Mg_{30}B_{60}$-D_{5d} over the $Mg_{30}B_{60}$-D_{3d} could be due to not using the two pentagons which are in general strained than the hexagons for Mg cap. However, they have very low HOMO-LUMO gaps compared to B_{80}-I_h fullerene. This is because the molecular orbital electronic states belonging to Mg atoms are falling in the gaps of boron states. The site projected density of states are plotted for Mg_3B_6-bulk, Mg_3B_6-sheet, $Mg_{12}B_{24}$-tube, and $Mg_{30}B_{60}$-D_{5d} fullerene (Figure 4.4.3f-i). The PDOS profile of all these systems clearly shows that Mg and B having their own manifold of states unlike in the boron sheets, tubes, and

fullerenes. It is understandable that the high electropositive Mg atoms can easily donate electrons to the unoccupied boron molecular orbitals. Comparing the PDOS of Mg_3B_6-bulk with Mg_3B_6-sheet, the Mg states are relatively more dominant near E_f in sheet than in the bulk (Figure 4.4.3f,g) due to the shorter Mg-B bonds (Table 4.4.3a). The boron states are similar in both bulk and sheet structures.

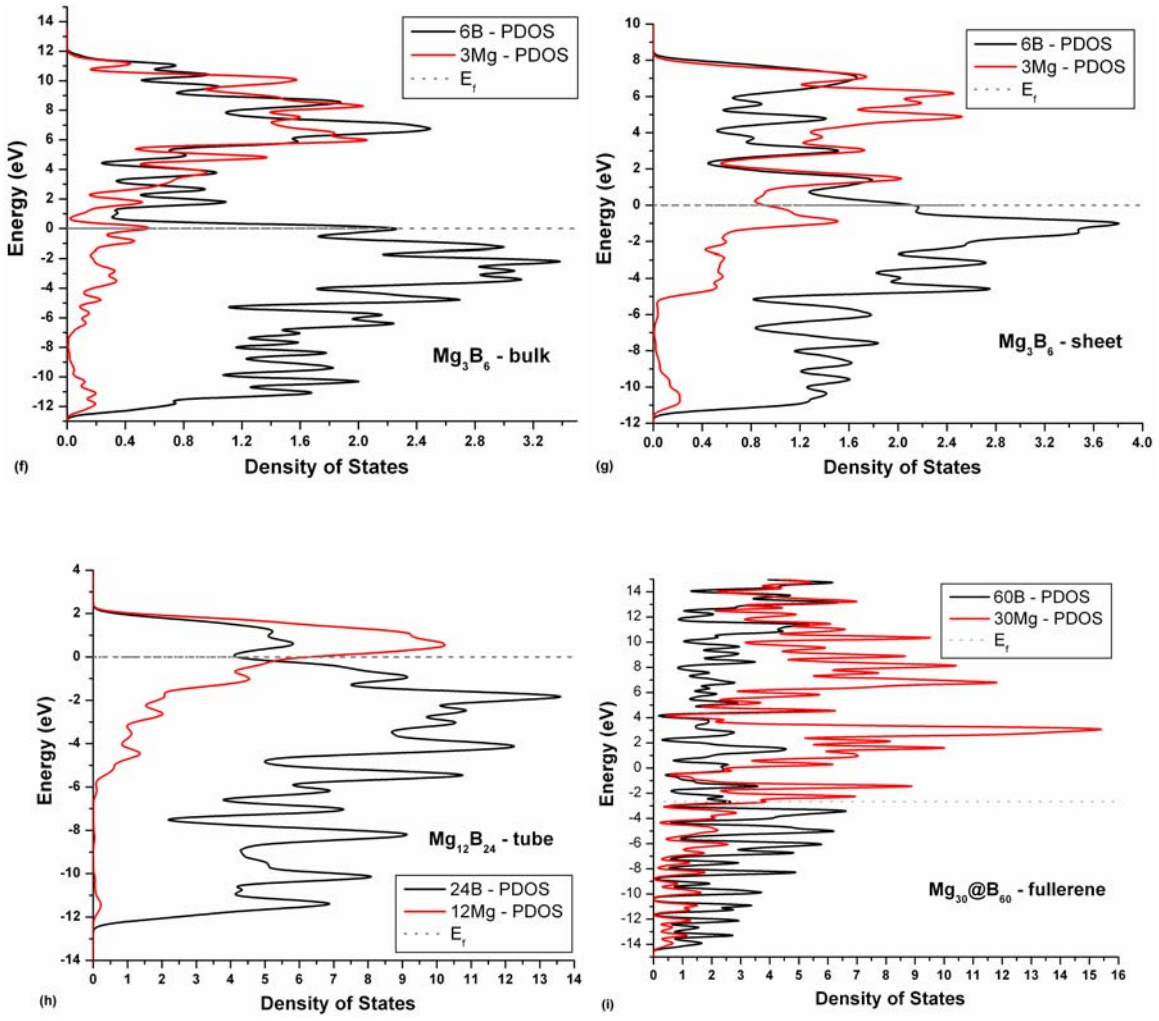

Figure 4.4.3. Site projected density of states of **(f)** Mg_3B_6-bulk, **(g)** Mg_3B_6-sheet, **(h)** $Mg_{12}B_{24}$-tube, and **(i)** $Mg_{30}B_{60}$-D_{5d} fullerene. The Fermi energy level (E_f) or HOMO is indicated by dotted line.

The high DOS near the E_f of Mg_3B_6-bulk and Mg_3B_6-sheet indicates their metallic character.[44,45] In the case of $Mg_{12}B_{24}$ tube the PDOS profile is much broaden due to curvature of the tube and its high DOS at E_f depicts metallic nature (Figure 4.4.3h). The PDOS of $Mg_{30}B_{60}$ is also similar to the sheets and tubes where the gap between occupied and unoccupied states is very small (0.1 eV) despite its molecular nature (Figure 4.4.3f,i).

Analysis of the well converged structures of MgB_2 based sheets, tubes, fullerenes suggests that the $4n/3$ rule holds good similar to the boron sheets, tubes, and fullerenes. A more rigorous study on the electronic and vibrational stability of these structures would improve our understanding of qualitative aspects of chemical bonding ideas. However, the structure and stability trends of these novel low dimensional boron and boride structures with respect to the electron count that we have adopted from the carbon skeletons suggest new ways of looking at the materials that were not conceived.

4.5 Conclusion

We have showed that despite boron prefers three dimensional icosahedral B_{12} based allotropes due to its intrinsic electron deficiency, it is possible for boron to form low dimensional allotropes analogous to carbon sheets, nanotubes and fullerenes provided an extra electron per boron atom. That is when boron has similar electronic configuration that carbon has (B^-~C) boron can adopt structures of carbon. We have considered the hexagonal graphene sheet (C_6), (6, 0) nanotube (C_{24}), and C_{60} fullerene to

construct analogous boron allotropes by substituting all the carbon atoms by boron and then compensated the electron deficiency by adding sufficient number of boron atoms systematically. This generated B_8-sheet, B_{24}-tubule, and B_{80} fullerene which are isoelectronic and symmetrical equivalents of C_6-sheet, C_{24}-tubule, and C_{60} fullerene. We also generated sheet-like B_6, B_7, B_9, tube-like B_{24} to B_{36}, and fullerene-like B_{60} to B_{90} structures which are either electron deficient or electron rich. Among all these structures, we found based on the cohesive energies that structures having $4n/3$ (where n is the number of atoms in carbon analogous skeleton) numbers of boron atoms with carbon allotrope equivalent symmetry, B_8-sheet, B_{24}-tubule, and B_{80}-I_h fullerene are in low energy. The bonding analysis based on PDOS and COOP suggested that the reason for the better stability of the low energy structures is the presence of better occupied bonding and unoccupied antibonding orbitals. Similarly we also studied Mg_3B_6-sheet, $Mg_{12}B_{24}$-tubule, and $Mg_{30}B_{60}$ fullerene structures and found to be viable. The DOS indicate boron and boride sheets are metallic. The novel low-dimensional boron and boride structures with their high metallic conducting nature expected to be useful in the nano-electronic regime. Despite of all these we also found that the graphene analogue of boron, B_8-sheet and C_{60} analogue of B_{80} fullerene are higher in energy when compare to icosahedral B_{12} based allotropes α-B_{12} and stuffed fullerene-like B_{102} by 0.472 and 0.075 eV respectively. However, our intuitive scheme based on Mg_3B_6 sheet suggests that crossing the barrier of (12.1 eV) exfoliation of Mg atoms from Mg_3B_6 sheet would form graphene like boron and it would act as feed-stock for other low dimensional boron allotropes.

References

[1] J. Donohue, *The Structure of the Elements*, (Wiley: New York), 1974.

[2] A. F. Wells, *Structural Inorganic Chemistry*, (5th ed., Oxford), 1984.

[3] *Boron-Rich Solids*, edited by D. Emin, T. L. Aselage, A. C. Switendick, B. Morosin, and C. L. Beckel, AIP Conf. Proc. No. 231 (AIP, New York), 1991.

[4] M. S. Dresselhaus, G. Dresselhaus, and P.C. Eklund, *Science of Fullerenes and Carbon Nanotubes* (Academic, New York), 1996.

[5] *Perspectives of Fullerene Nanotechnology*, edited by E. Osawa (Kluwer, New York), 2002.

[6] A. K. Geim and K. S. Novoselov, Nat. Mater. **6**, 183 (2007).

[7] I. Boustani, I. Phys. Rev. B **55**, 16426 (1997).

[8] A. Quandt and I. Boustani, Chem. Phys. Chem. **6**, 2001 (2005).

[9] S. Chacko, D. G. Kanhere, and I. Boustani, Phys. Rev. B **68**, 035414 (2003).

[10] H. Tang and S. Ismail-Beigi, Phys. Rev. Lett. **99**, 115501 (2007).

[11] J. Kunstmann and A. Quandt, Phys. Rev. B **74**, 035413 (2006).

[12] X. Yang, Y. Ding, and J. Ni, Phys. Rev. B **77**, 041402(R) (2008).

[13] N. G. Szwacki, A. S. and B. Yakobson, Phys. Rev. Lett. **98**, 166804 (2007).

[14] N. G. Szwacki, Nanoscale Research Letters **3**, 49 (2008).

[15] H. J. Zhai, B. Kiran, J. Li, and L. S. Wang, Nat. Mater. **2**, 827 (2003).

[16] C. J. Otten, O. R. Lourie, M.-F. Yu, J. M. Cowley, M. J. Dyer, R. S. Ruoff, and W. E. Buhro, J. Am. Chem. Soc. **124**, 4564 (2002).

[17] D. Ciuparu, R. F. Klie, Y. Zhu, and L. Pfefferle, J. Phys. Chem. B **108**, 3967 (2004).

[18] B. Kiran, S. Bulusu, H-J. Zhai, S. Yoo, X. C. Zeng, and L-S. Wang, Proc. Natl. Acad. Sci. U.S.A. **102**, 961 (2005).

[19] E. Oger, N. R. M. Crawford, R. Kelting, P. Weis, M. M. Kappes, and R. Ahlrichs, Angew. Chem. Int. Ed. **46**, 8503 (2007).

[20] J. Nagamatsu, N. Nakagawa, T. Muramaka, Y. Zenitani, and J. Akimitsu, Nature (London) **410**, 63 (2001).

[21] M. Worle and R. Nesper, Angew. Chem., Int. Ed. **39**, 2349 (2000).

[22] E. D. Jemmis and E. G. Jayasree, Acc. Chem. Res. **36**, 816 (2003).

[23] M. D Segall, P. J. D. Lindan, M. J. Probert, C. J. Pickard, P. J. Hasnip, S. J. Clark, and M. C. Payne, J. Phys.: Condens. Matter **14**, 2717 (2002).

[24] Accelrys Inc., Materials Studio CASTEP, San Diego, *Accelrys Inc*, 2001.

[25] D. M. Ceperley, B. J. Alder, Phys. Rev. Lett. **45**, 566 (1980).

[26] J. P. Perdew and A. Zunger, Phys. Rev. B **23**, 5048 (1981).

[27] D. Vanderbilt, Phys. Rev. B **41**, 7892 (1990).

[28] H. J. Monkhorst and J. D. Pack, Phys. Rev. B **13**, 5188 (1976).

[29] P. Pulay, J. Comput. Chem. **3**, 556 (1982).

[30] T. H. Fischer and J. Almlof, J. Phys. Chem. **96**, 9768 (1992).

[31] R. Hoffmann, J. Chem. Phys, **39**, 1397 (1963).

[32] G. A. Landrum and W. V. Glassy, YAeHMOP (http://yaehmop.sourceforge.net).

[33] R. Hughbanks and R. Hoffmann, J. Am. Chem. Soc., **105**, 3528 (1983).

[34] B. Delley, J. Chem. Phys. **113**, 7756 (2000).

[35] J. P. Perdew, K. Burke, and M. Ernzerhof, Phys. Rev. Lett. **77**, 3865 (1996).

[36] P. N. D'yachkov and D. V. Makaev, Phys. Rev. B **76**, 195411 (2007), and references there in.

[37] A. K. Singh, A. Sadrzadeh, and B. I. Yakobson, Nano Lett. **8**, 1314, 2008.

[38] G. Gopakumar, M. T. Nguyen, and A. Ceulemans, Chem. Phys. Lett. **450**, 175 (2008).

[39] H. W. Kroto, J. R. Heath, S. C. O'Brien, R. F. Curl Jr., and R. E. Smalley, Nature (London) **318**, 162 (1985).

[40] H. W. Kroto, A. W. Allaf, and S. P. Blam, Chem. Rev. (Washington, D. C.) **91**, 1213 (1989).

[41] S. J. L. Placa, P. A. Roland, and J. J. Wynne, Chem. Phys. Lett, **190**, 163 (1992).

[42] S.-J. Xu, J.M. Nilles, D. Radisic, W.-J. Zheng, S. Stokes, K.H. Bowen, R. C. Becker, and I. Boustani, Chem. Phys. Lett. **379**, 282 (2003).

[43] C. L. Perkins, M. Trenary, and T. Tanaka, Phys. Rev. Lett. **77**, 4772 (1996).

[44] L.A. Chernozatonskii, JETP. Lett. **74**, 335 (2001).

[45] V. V. Ivanovskaya, A. N. Enyashin, and A. L. Ivanovskii, Inorg. Mater. **40**, 134 (2004).

[46] A. Quandt, A.Y. Liu, and I. Boustani, Phys. Rev. B **64** 125422 (2001).

Chapter 5

Mechanical Properties of Boron and Boron-Rich Solids

5.1 Introduction

Allotropes of boron and boron rich icosahedral cluster solids (BRICS) are known for their robust mechanical properties and greater hardness.[1-4] Boron and BRICS such as boron carbide ($B_{12}C_3$), boron suboxide ($B_{12}O_2$) are the hardest known materials after boron nitride and diamond.[5-7] Boron is ranked at 9.3 on the Mohs hardness scale where diamond is 10 and on the extended Mohs hardness scale $B_{12}C_3$ and $B_{12}O_2$ are ranked at 14 and >14 where diamond is 15.[8-10] The excellent mechanical properties of boron and its related materials allow withstanding to hostile conditions. Recently high pressure experiments using diamond anvil cell showed that the elemental β-rhombohedral boron as a superconductor with transition temperature of 11.2 K at a record pressure of 250 GPa.[11] Despite these promising applications the complete list of elastic stiffness constants of β-rhombohedral boron and relative mechanical stability of α-rhombohedral boron and

β-rhombohedral boron are not known either from experiments or from theory. There are few theoretical calculations on elastic stiffness constants of α-rhombohedral boron.[12,13] There exists no experimental data for elastic stiffness constants of α- rhombohedral boron and there is an incomplete experimental data for β-rhombohedral boron hitherto.[14,15] This is mainly because of two reasons: (i) Boron has relatively small X-ray-scattering power which makes difficult to perform the diffraction experiments. Though boron has large neutron-scattering cross-section (~ 760 barns), the large pristine samples are not easily accessible due to their high melting point (~2300 °C) where almost every element in the periodic table can mix with boron.[16-18] It is also the problem of irreversible phase transformation of α-rhombohedral boron to β-rhombohedral boron at around 1200 °C.[17-20] (ii) The overwhelming preference of B_{12} icosahedron in β-rhombohedral boron and its borides create complex crystal structures of large lattice constants with intrinsic defects such as partially occupied lattice and interstitial sites (Table 2.3.2a, 2c, and 2.3.3a in Chapter 2). Therefore it is difficult to compute such complex structures along with intrinsic defects for any desired information from first-principles calculations.[21,22] On the other hand, the role of the intrinsic defects or electron deficiency in mechanical stability of β-rhombohedral boron and BRICS is also not understood so far.

If the complete list of elastic stiffness constants for both the phases, α- and β-rhombohedral boron were known, it would be possible to propose their relative mechanical stability and mechanical properties. Therefore, in this Chapter, we present a complete list of elastic stiffness constants and their derived mechanical properties such as

bulk modulus, shear modulus, and Young's modulus of α-rhombohedral boron (α-B_{12}) and β-rhombohedral boron (β-$B_{106.83}$) using first principles DFT calculations.

Unfortunately, the β-$B_{106.83}$ is not calculable due to intrinsic defects. Therefore, we use the modeled solids $Li_8Be_3B_{102}$ and $Li_{10}CB_{102}$ based on *mno* electron counting rule that were discussed in Chapter 2 which closely represents the electronic structure of β-$B_{106.83}$. In order to understand the role of intrinsic defects in mechanical stability of β-$B_{106.83}$, the ideal β-rhombohedral boron (β-B_{105}) also calculated for elastic stiffness constants and their derived properties. We further attempted to understand the role of electron sufficient chemical bonds in improving the hardness of α-B_{12} and β-$B_{106.83}$ and compared with the known superhard $B_{12}C_3$ and $B_{12}O_2$ materials. Before discussing the results let us briefly outline the computational methods that are used to calculate the elastic stiffness constants and their derived properties.

5.2 Computational Methods

The structures are initially optimized using CASTEP code based on DFT.[23,24] The plane-wave basis set approach has been used to expand the electronic wavefunctions. Interaction between the ions and the electrons were described using the Vanderbilt ultrasoft pseudopotentials.[25] Exchange and correlation of electrons is treated within the Generalized Gradient Approximation (GGA) of Perdew-Burke-Ernzerhof (PBE) functional.[26] Over the converged geometries the zero pressure 6×6 linear elastic stiffness

constants matrix $[C_{ij}]_{6\times6}$ is calculated with finite strain technique (applying a given homogeneous strain and calculating the resulting stress while optimizing the geometry with fixed lattice parameters).[23] Since all the crystal structures under study belong to $R\bar{3}m$ space group, the matrix $[C_{ij}]_{6\times6}$ contains six independent elastic stiffness constants ($C_{11,}$ C_{33}, C_{44}, C_{12}, C_{13}, and C_{14} (here we followed Voigt notation).[27,28] The arrival of six independent elastic stiffness constants is briefly shown in the following equations.

Within the elastic limit (small deformations) the stress (σ_{ij}) is directly proportional to the strain (ε_{kl}) (Hooke's law), so that the stress components are linear functions of the strain components. This can be written as

$$\sigma_{ij} = \sum_{kl} C_{ijkl}\ \varepsilon_{kl} \qquad \text{---- (1)}$$

where σ_{ij} and ε_{kl} are second order stress and strain tensor matrices. The C_{ijkl} are fourth order tensors which are the elastic stiffness constants of the crystal. Similarly, the strain can be expressed in terms of stress

$$\varepsilon_{ij} = \sum_{kl} S_{ijkl}\ \sigma_{kl} \qquad \text{---- (2)}$$

where S_{ijkl} are the elastic compliances of the crystal. The C_{ijkl} and S_{ijkl} in equation (1) & (2) stands for 9×9 square matrices respectively. Here, we chose equation (1) to represent the elastic stiffness constants using symmetry equality conditions (the compliances are similar to this). The equation (1) can be represented in matrix form

$$\left|\begin{array}{l}\sigma_{11} = C_{1111}\ \varepsilon_{11} + C_{1112}\ \varepsilon_{12} + C_{1113}\ \varepsilon_{13} + C_{1121}\ \varepsilon_{21} \ldots\ldots\ldots + C_{1133}\ \varepsilon_{33} \\ \sigma_{12} = C_{1211}\ \varepsilon_{11} + C_{1212}\ \varepsilon_{12} + C_{1213}\ \varepsilon_{13} + C_{1221}\ \varepsilon_{21} \ldots\ldots\ldots + C_{1233}\ \varepsilon_{33} \\ . \\ . \\ . \\ \sigma_{33} = C_{3311}\ \varepsilon_{11} + C_{3312}\ \varepsilon_{12} + C_{3313}\ \varepsilon_{13} + C_{321}\ \varepsilon_{21} \ldots\ldots\ldots + C_{3333}\ \varepsilon_{33}\end{array}\right|_{9\times 9} \quad \text{---- (3)}$$

The 9×9 elastic stiffness constants matrix can be reduced to a 6×6 matrix by applying the symmetric conditions of both the stress ($\sigma_{ij} = \sigma_{ji}$) and strain ($\varepsilon_{ij} = \varepsilon_{ji}$) tensors. Before writing the reduced 6×6 elastic stiffness constant matrix, let us simplify the four-index C_{ijkl} notation by Voigt simplified vector notation which is as follows.

$$xx = 11 = 1, \quad yy = 22 = 2, \quad zz = 33 = 3$$
$$yz = 23 = zy = 32 = 4, \quad zx = 31 = xz = 13 = 5, \quad xy = 12 = yx = 21 = 6$$

According to this notation the stress matrix is represented as

$$\left|\begin{array}{ccc}\sigma_{11} & \sigma_{12} & \sigma_{13} \\ \sigma_{21} & \sigma_{22} & \sigma_{23} \\ \sigma_{31} & \sigma_{32} & \sigma_{33}\end{array}\right| \rightarrow \left|\begin{array}{ccc}\sigma_1 & \sigma_6 & \sigma_5 \\ \sigma_6 & \sigma_2 & \sigma_4 \\ \sigma_5 & \sigma_4 & \sigma_3\end{array}\right| \quad \text{---- (4)}$$

Therefore, the reduced 6×6 elastic stiffness constant matrix can be written as

$$\left|\begin{array}{l}\sigma_1 = C_{11}\ \varepsilon_1 + C_{12}\ \varepsilon_2 + C_{13}\ \varepsilon_3 + C_{14}\ \varepsilon_4 + C_{15}\ \varepsilon_5 + C_{16}\ \varepsilon_6 \\ \sigma_2 = C_{21}\ \varepsilon_1 + C_{22}\ \varepsilon_2 + C_{23}\ \varepsilon_3 + C_{24}\ \varepsilon_4 + C_{25}\ \varepsilon_5 + C_{26}\ \varepsilon_6 \\ \sigma_3 = C_{31}\ \varepsilon_1 + C_{32}\ \varepsilon_2 + C_{33}\ \varepsilon_3 + C_{34}\ \varepsilon_4 + C_{35}\ \varepsilon_5 + C_{36}\ \varepsilon_6 \\ .\sigma_4 = C_{41}\ \varepsilon_1 + C_{42}\ \varepsilon_2 + C_{43}\ \varepsilon_3 + C_{44}\ \varepsilon_4 + C_{45}\ \varepsilon_5 + C_{46}\ \varepsilon_6 \\ \sigma_5 = C_{51}\ \varepsilon_1 + C_{52}\ \varepsilon_2 + C_{53}\ \varepsilon_3 + C_{54}\ \varepsilon_4 + C_{55}\ \varepsilon_5 + C_{56}\ \varepsilon_6 \\ \sigma_6 = C_{61}\ \varepsilon_1 + C_{62}\ \varepsilon_2 + C_{63}\ \varepsilon_3 + C_{64}\ \varepsilon_4 + C_{65}\ \varepsilon_5 + C_{66}\ \varepsilon_6\end{array}\right|_{6\times 6} \quad \text{---- (5)}$$

Now the Hooke's law takes the form

$$\sigma_i = \sum_j C_{ij}\ \varepsilon_j \qquad \text{---- (6)}$$

The 6×6 elastic stiffness constant matrix in equation (5) by definition is also symmetric ($C_{ij} = C_{ji}$), therefore the 6×6 or 36 independent elastic stiffness constants reduced to 21 (as shown in equation (7)).

$$\begin{vmatrix} C_{11} & & & & & \\ C_{21} & C_{22} & & & & \\ C_{31} & C_{32} & C_{33} & & & \\ C_{41} & C_{42} & C_{43} & C_{44} & & \\ C_{51} & C_{51} & C_{51} & C_{51} & C_{51} & \\ C_{61} & C_{62} & C_{63} & C_{64} & C_{65} & C_{66} \end{vmatrix} \qquad \text{---- (7)}$$

Using these 21 independent elastic stiffness constants one can study mechanical deformations of any arbitrary crystal structure completely. However, by virtue of crystal structure symmetry, the 21 independent elastic stiffness constants can be further reduced. The high symmetric cubic crystals only need three independent elastic stiffness constants, C_{11}, C_{12}, and C_{44} to study complete mechanical deformations. In our case, the rhombohedral $R\bar{3}m$ space group crystal structures only need 6 independent elastic stiffness constants [$C_{11,}$ C_{33}, C_{44}, C_{12}, C_{13}, and C_{14}] to study complete mechanical deformations.[27,28] Once we have the C_{ij} matrix elements the bulk modulus, shear modulus, Young's modulus, etc are possible to be calculated using the stress-strain relations and different average schemes [Voigt–Reuss–Hill (VRH)].[29-31]

5.3 Results and Discussion

The calculated elastic stiffness constants and their derived properties, bulk modulus (*B*), shear modulus (*G*), and young's modulus (*E*) of α-B_{12}, β-B_{105}, $Li_8Be_3B_{102}$, and $L_{10}CB_{102}$ are tabulated in Table 5.3a. The calculated volume and density are also added to this Table and compared with the available experimental results. The calculated volume and density of α-B_{12} and β-B_{105} are in agreement with the experimental data. But the calculated volume of β-B_{105} is relatively increased and hence decrease in the density when compare to β-$B_{106.83}$. This could be due to the fact that the β-B_{105} does not represent the real experimental structure (β-$B_{106.83}$). While the calculated volumes of $Li_8Be_3B_{102}$ and $L_{10}CB_{102}$ are lowered when compare to β-$B_{106.83}$ which is similar to the α-B_{12}.

The calculated zero pressure six independent elastic stiffness constants [C_{11}, C_{33}, C_{44}, C_{12}, C_{13}, and C_{14}] stability can be checked using the Born-Huang criterion.[32,33] According to Born-Huang criterion for stability of a crystal the elastic stiffness constants matrix [C_{ij}] must be positive definite. For rhombohedral structure with six independent C_{ij}, the conditions for the stability are that C_{11}, $C_{11} - C_{12}$, $[(C_{11} + C_{12})C_{33} - 2(C_{12})^2]$, $[(C_{11} - C_{12})C_{44} - 2(C_{14})^2]$ are must be greater than zero. The C_{ij} of all the crystal structures listed in Table 5.3a (the figures of α-B_{12}, β-B_{105}, and $Li_8Be_3B_{102}$ are shown in Chapter 2, Figure 2.3.1a-d, 2.3.2a-d, and 2.3.3c respectively) satisfies the above stability conditions other than the α-B_{12}. This indicates that the α-B_{12} is mechanically a metastable species which is consistent with experimental results that α-B_{12} irreversibly transforms into β-

rhombohedral boron at around 1200 °C. The previous elastic constants calculations based on force constants and lattice vibrations also supports the metastable nature of α-B_{12}.[13]

Table 5.3a. The six independent elastic stiffness constants (C_{ij}) with diagonal component [$C_d = (2C_{11}+C_{33})/3$] and their derived properties, bulk modulus (B), shear modulus (G), and young's modulus (E) in GPa, and volume (Å^3), density (D in gm/cm^3) of α-B_{12}, α-B_{12}(exp), β-B_{105}, β-$B_{106.83}$ (exp) $Li_8Be_3B_{102}$, and $L_{10}CB_{102}$.

C_{ij}	α-B_{12}	α-B_{12} (exp)[a]	β-B_{105}	β-$B_{106.83}$ (exp)[b,c]	$Li_8Be_3B_{102}$	$L_{10}CB_{102}$
11	508.8		316.2	467.0	503.3	488.2
33	598.1		213.1	473.0	488.4	486.7
44	265.1		58.4	198.0	226.2	214.1
12	74.5		52.6	241.0	47.7	47.3
13	53.0		91.7		53.4	63.5
14	-17.2		42.1	15.1	0.0	0.0
C_d	538.6		281.9	469.0	498.3	487.7
B	218.9	224.0[d]	144.3	185.0[d]	200.4	201.3
G	249.1		82.9	203.0[e]	226.7	216.2
E_x	492.9		238.7		493.9	476.8
E_y	492.9		238.7		493.9	476.8
E_z	588.4		167.4		478.0	471.7
V	83.3	87.3	823.4	820.3	815.3	807.9
D	2.58	2.46	2.29	2.33	2.41	2.43

[a]Ref[34], [b]Ref[35], [c]Ref[14], [d]Ref[16], [e]Ref[15]

Among the six C_{ij}'s of α-B_{12}, C_{33} has largest value (598.1 GPa), that is the bonds oriented along the z direction (aligned with crystallographic c-axis) of the rhombohedral unit cell should be stiffer. Indeed the bonds aligned along the z direction are the 2c-2e B-B covalent bonds (polar bonds shown in Chapter 2, Figure 2.3.1a-d) which are shorter (1.652 Å) than the equatorial 3c-2e B-B bonds (1.987 Å) lying approximately in the x-y plane. The other two longitudinal elastic stiffness constants $C_{11} = C_{22}$ = (508.8 GPa) < C_{33}

supports the above argument. The greater Young's modulus along the E_z (588.4 GPa) compare to E_x and E_y (492.95 GPa) also in good agreement that $C_{33} > C_{11}$, C_{22} (Table 5.3a). The shear elastic stiffness constant C_{44} is found to have 265.1 GPa which is greater than the other C_{12} (74.5 GPa) and C_{13} (53.0 GPa) shear elastic stiffness constants. The calculated bulk modulus (219 GPa) is close to the experimental value ~224 GPa and other theoretical values 222, 207 GPa.[12,16,36] However, the calculated C_{ij}'s and elastic moduli of β-B_{105} are in disagreement with the experimental results (Table 5.3a). This is due to the fact that the β-B_{105} is a five electron deficient structure (as discussed in Chapter 2) and does not represent the experimental structure, $B_{106.83}$. It appears that the x-y plane condensed icosahedrons (the B_{28} fragments, Chapter 2, Figure 2.3.2i) of β-B_{105} are not much effected by the electron deficiency since the relatively close values of C_{11} = C_{22} = 316.2 GPa are comparable to experimental C_{11} = 467 GPa,. While the C_{33} (213 GPa) which is far from the experimental value (473 GPa) indicates that the B-B cluster bonds of edge aligned icosahedral B_{12} fragments (as show in Chapter 2, Figure 2.3.2c) are weaken due to the effect of electron deficiency. This is understandable as the B_{28} fragment is not electron deficient (B_{28}^{+1}) whereas the B_{12} need two electrons (B_{12}^{-2}) to form stable bonds.

At this point we make use of the modeled solids $Li_8Be_3B_{102}$ and $Li_{10}CB_{102}$ which are electron sufficient and found to show close resemblance with the electronic structure of β-$B_{106.83}$. The elastic stiffness constants, bulk modulus and shear modulus of $Li_8Be_3B_{102}$ and $Li_{10}CB_{102}$ are almost in good agreement with the experimental results of β-$B_{106.83}$ (Table 5.3a). This suggests that the missing five electrons in β-B_{105} are

essentially needed not only for the thermal stability but also for the mechanical stability. The electron sufficiency has really made significant contribution to increase the C_{33} in the model solids which was found to be weakened in the electron deficient β-B_{105}. The close values of C_{33} and C_{11} in β-$B_{106.83}$ and model solids essentially indicates that all the B-B bonds are cluster type unlike in α-B_{12} where the polar B-B bonds are 2c-2e in nature which reflected in $C_{33} > C_{11}$. The close equal values of Young's modulus in three directions (E_x, E_y, E_z) of the model solids also supports the condensed nature of the B_{12} polyhedral clusters throughout the crystal structure whereas in α-B_{12} crystal the B_{12} polyhedral network is connected by the directional 2c-2e and quasi-directional 3c-2e bonds which is clear by the inequality $C_{33} > C_{11}$. The C_{44} shear component of the model solids also found to be closer to the experimental C_{44} of β-$B_{106.83}$ but not the other shear component C_{12}. The shear component C_{44} of β-$B_{106.83}$ and model solids is lower than α-B_{12}. This reflected in lowering the average shear modulus (Table 5.3a) of β-$B_{106.83}$ and model solids than the α-B_{12}. The bulk modulus of α-B_{12} is greater than the β-$B_{106.83}$ and model solids because α-B_{12} has higher density.

The experimentally undetermined C_{13} in β-$B_{106.83}$ can be taken as the average C_{13} (58.4 GPa) of the two model solids which is close to the C_{13} of α-B_{12}. Though the Born-Huang criterion for the elastic stability holds good in the model solids, the C_{14} component is just zero whereas it is 15 GPa in β-$B_{106.83}$. However, we could see that the other C_{ij} values and the elastic moduli of the model solids are closely corroborate with the experimental results (Table 5.3a). The diagonal component $C_d = (2C_{11}+C_{33})/3$ of β-$B_{106.83}$ (469 GPa) is slightly lesser than the C_{33} (473 GPa) which indicates that the B_{10}-B-B_{10}

chain is less stiff than the icosahedral B_{12} chain running along the edges of the rhombohedral unit cell [Chapter 2, Figure 2.3.2. (g)]. Experimental compressibility data (below 10 GPa) on β-rhombohedral boron supports $C_d < C_{33}$.[18] But in model solids, it found to be reversed ($C_d > C_{33}$). This is due to the fact that the B_{10}-B-B_{10} analogous chains in model solids $Li_8Be_3B_{102}$ (BeB_9-Be-BeB_9) and $Li_{10}CB_{102}$ (LiB_9-C-LiB_9) (see Chapter 2, Figure 2.3.3c) are electron sufficient whereas the B_{10}-B-B_{10} chain in β-$B_{106.83}$ has six boron partially occupied sites (B[13] site). The partially occupied sites in β-$B_{106.83}$ appear to weaken the B_{10}-B-B_{10} chain, though the chain is 0.01 % shorter than the BeB_9-Be-BeB_9 and LiB_9-C-LiB_9 chains of the model solids. The diagonal component, C_d of α-B_{12} (538.6 GPa) is greater than β-$B_{106.83}$ and the model solids. Unlike in β-$B_{106.83}$ and model solids there is no such chain-like B_{10}-B-B_{10} cluster bonded network (average B-B cluster bond distance in B_{10}-B-B_{10} chain of β-$B_{106.83}$ is 1.805 Å) in α-B_{12} along the diagonal axis. Instead we could see the strong polar 2c-2e B-B bonds (1.652 Å) running in the rhombohedral axis around the diagonal axis as sown in Figure 5.3a. Though there are the weak equatorial 3c-2e B-B bonds (1.987 Å) approximately perpendicular to the diagonal axis of α-B_{12} (the two 2c-2e and 3c-2e networks of α-B_{12} individually depicted in Chapter 2, Figure 2.3.1c,d), the greater C_{33} elastic stiffness constant contributes in improving the C_d. If these weak 3c-2e B-B bonds were to be 2c-2e bonds, the structure would be mechanically more stable, certainly thermodynamically also. That is what happened in few of the hardest boron rich phases, $B_{12}C_3$ and $B_{12}O_2$ crystals[37] where the equatorial sites are connected via stabilizing 2c-2e B-C and B-O bonds respectively as shown in Figure 5.3b,c. It emphasizes that though α-B_{12} has grater bulk modulus and

shear modulus than β-$B_{106.83}$, the mechanically destabilizing C_{14} and the weak 3c-2e equatorial bonds makes it a metastable structure.

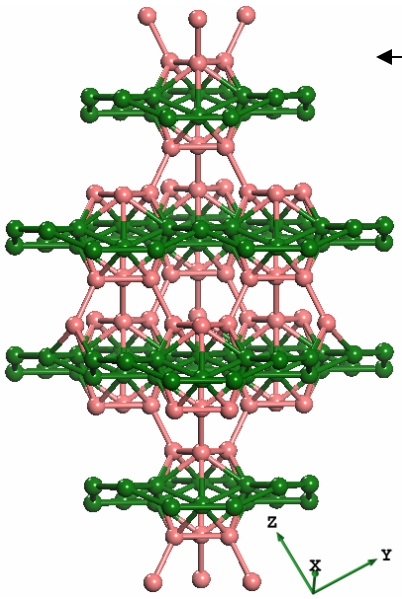

Figure 5.3a. Crystal structure of α-B_{12} perpendicular to the diagonal axis. The boron atoms shown in light-salmon colour belong to the polar sites and the green colour atoms belong to the equatorial sites. The polar B-B bonds running in the rhombohedral axis (not the Cartesian coordinate axis which is shown here) around the diagonal axis and the equatorial 3c-2e bonds perpendicular to the diagonal axis can be seen here.

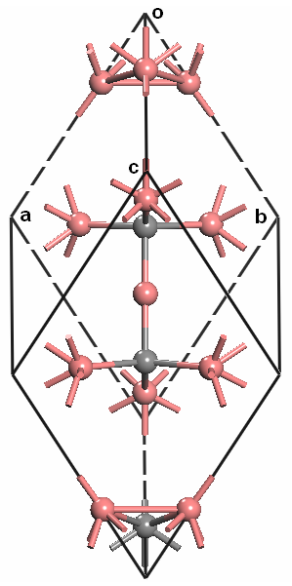

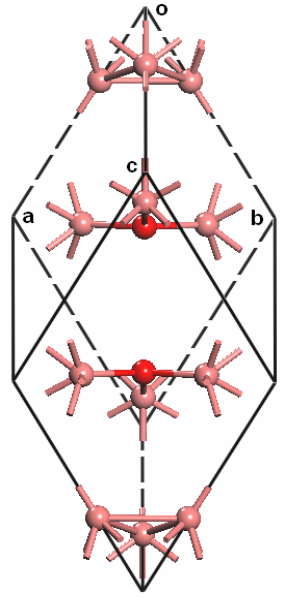

Figure 5.3. (left) **(b)** Crystal structure of $B_{12}C_3$ where the equatorial boron atoms are connected to the carbon atoms of the diagonal C-B-C chain by 2c-2e B-C bonds. (right) **(c)** The equatorial boron atoms of $B_{12}O_2$ are connected to the diagonally situated oxygen atoms by 2c-2e B-O bonds. The polar boron/carbon sites are similar to α-B_{12}.

The calculated bulk modulus of $B_{12}C_3$ (242.3 GPa) and $B_{12}O_2$ (234.4 GPa) are in good agreement with the experimental values 245 and 228 GPa respectively[4] and greater than that of α-B_{12}, β-$B_{106.83}$, and the model solids. The bulk modulus is considered as one of the parameter in correlating hardness of materials.[4,38] The hardest material diamond bulk modulus is 443 GPa which is far above from the boron and boron-rich solids.[39] Therefore, any relative improvement in the bulk modulus of boron and boron-rich solids would also improve the hardness. One way is improving the relative strength of the chemical bonds and density of the crystals under electron sufficient requirements which would expect to increase the bulk modulus.

In order to examine this we have calculated $B_{12}C_2Be$, $B_{12}N_2Be$, $B_{12}C_2$, and $B_{12}N_2$ for bulk modulus within the framework of $B_{12}C_3$ and $B_{12}O_2$ crystal structures. The C-B-C chain in $B_{12}C_3$ (Figure 5.3b) is substituted by C-Be-C and N-Be-N to get $B_{12}C_2Be$ and $B_{12}N_2Be$ respectively. Similarly the oxygen atoms in $B_{12}O_2$ (Figure 5.3c) are substituted by carbon and nitrogen to get $B_{12}C_2$ and $B_{12}N_2$. The bulk modulus of these solids $B_{12}C_2Be$, $B_{12}N_2Be$, $B_{12}C_2$, and $B_{12}N_2$ are found to be 227.6, 245.6, 217.0, and 226.7 GPa respectively. We have only noticed improvement in the bulk modulus of $B_{12}N_2Be$ which is isoelectronic to $B_{12}C_3$. In $B_{12}N_2Be$ though the chain N-Be-N length (3.079 Å) is increased, the B_{12} cluster equatorial vertex to its nearest chain atom bond distance (B-N) is shorter (1.524 Å) when compared to $B_{12}C_3$ (Table 5.3b). In addition to this the density of $B_{12}N_2Be$ is slightly increased in comparison to $B_{12}C_3$. This might have caused the bulk modulus of $B_{12}N_2Be$ to increase over that of $B_{12}C_3$.

Table 5.3b. Bulk modulus in GPa, chain length (C-B-C type in $B_{12}C_3$ and O--O type in $B_{12}O_2$), distance between B_{12} vertex (B_v) to its nearest chain atom (X_c) in Å, volume in $Å^3$, and density in gm/cm^3 of the optimized $B_{12}C_3$, $B_{12}C_2Be$, $B_{12}N_2Be$, $B_{12}O_2$, $B_{12}C_2$, and $B_{12}N_2$ crystal structures.

Crystal	Bulk modulus (GPa)	Chain length (Å)	B_v-X_c (Å)	Volume ($Å^3$)	Density (gm/cm^3)
$B_{12}C_3$	242.3	2.828	1.587	104.79	2.626
$B_{12}C_2Be$	227.6	3.308	1.545	107.90	2.505
$B_{12}N_2Be$	245.6	3.079	1.524	104.86	2.641
$B_{12}O_2$	234.4	2.979	1.481	99.39	2.702
$B_{12}C_2$	217.0	3.176	1.527	104.92	2.433
$B_{12}N_2$	226.7	3.064	1.465	100.56	2.605

In the case of $B_{12}C_2Be$ the bond length trends are similar to $B_{12}N_2Be$, but it is deficient by two electrons and also has lower density compared to $B_{12}C_3$ or $B_{12}N_2Be$ and hence found with lower bulk modulus (Table 5.3b). The other $B_{12}O_2$ framework based solids $B_{12}C_2$ and $B_{12}N_2$ also followed the similar trends of $B_{12}C_3$ framework solids. However, we have to notice that the $B_{12}O_2$ which is having shorter bonds and higher density than $B_{12}C_3$ found to have lower bulk modulus but the experimental indentation/scratch tests suggested that $B_{12}O_2$ is harder than $B_{12}C_3$.[7,40] Therefore, the bulk modulus should be considered only a relative parameter in correlating with hardness for particular type of crystals. Nevertheless, our limited examples $Li_8Be_3B_{102}$ and $Li_{10}CB_{102}$ of β-$B_{106.83}$, $B_{12}C_2Be$ and $B_{12}N_2Be$ of $B_{12}C_3$, and the $B_{12}C_2$ and $B_{12}N_2$ of $B_{12}O_2$ type of crystals suggests that the electron precise solids with high density have higher bulk modulus and expected to improve the hardness.

5.4 Conclusion

We have calculated from first principles DFT the complete list of elastic stiffness constants and their derived mechanical properties bulk modulus, shear modulus, and Young's modulus of α-B_{12}, the five electron deficient β-B_{105}, and electron sufficient model solids $Li_8Be_3B_{102}$ and $Li_{10}CB_{102}$ which resembles β-$B_{106.83}$ using finite strain technique. The elastic stiffness constants matrix of α-B_{12} was found to be less than zero $\{[C_{ij}] < 0\}$ and therefore according to Born-Huang criterion the α-B_{12} is mechanically a metastable structure. On the other hand, though, β-B_{105} is deficient by five electrons it was found to be mechanically stable. But the calculated elastic stiffness constants and their derived mechanical properties of β-B_{105} were in disagreement with the available experimental results of β-$B_{106.83}$. However these experimental results of β-$B_{106.83}$ were achieved by the electron sufficient model solids $Li_8Be_3B_{102}$ and $Li_{10}CB_{102}$. This suggests that the missing five electrons in β-B_{105} are essential for better mechanical stability. The concept of bond strength vs elastic stiffness constant was analyzed in α-B_{12}, β-B_{105}, and the models solids. The analysis suggests that the 3c-2e bonds (presented in x-y plane) in α-B_{12} are weak and the 2c-2e bonds (along the z-axis) are strong which is also reflected in the Young's modulus ($Ez > E_x = E_y$). While in the model solids the elastic stiffness constants of C_{11} and C_{33} and the Young's modulus E_x, E_y, and E_z are relatively close to each other which indicate the high cluster bonding nature of β-rhombohedral phase. The calculated bulk modulus of $B_{12}C_3$, $B_{12}O_2$ and their framework based solids $B_{12}C_2Be$, $B_{12}N_2Be$, $B_{12}C_2$, and $B_{12}N_2$ suggest that the electron sufficient nature of the chemical bond with high crystal density would improve the hardness of the materials.

References

[1] M. L. Wilkins, in *Boron and Refractory Borides,* edited by V. I. Matkovich (Springer-Verlag, Berlin) 1977, pp 633.

[2] J. H. Gieske, T. L. Aselage, and D. Emin, in *Boron-Rich Solids*, edited by D. Emin, T. L. Aselage, A. C. Switendick, B. Morosin, and C. L. Beckel, AIP Conf. Proc. No. 231 (AIP, New York) 1991, pp 376.

[3] D. Emin, Phys. Today **40**, 55 (1987).

[4] T. Lundström, J. Solid State Chem. **133**, 88, (1997).

[5] R. Riedel, Adv. Mater. **4**, 759 (1992).

[6] F. Thévenot, J. European Cermic Society **6**, 205 (1990).

[7] V. V. Brazhkin, A. G. Lyapin, and R. J. Hemley, Philos. Mag. A **82**, 231 (2002).

[8] R. Riedel, Adv. Mater. **6**, 549 (1994).

[9] S.F. Matar, E. Betranhandy, M. Nakhl, M. Zakhour-Nakhl, and N. Ouaïni, Progress in Solid State Chemistry **34**, 21 (2006).

[10] *Handbook of Chemistry and Physics,* 72nd ed., edited by David R. Lide (CRC, Boca Raton, FL), 1991.

[11] M. Eremets, V. Struzhkin, H. K. Mao, and R. Hemley, Science **293**, 272 (2001).

[12] S. Lee, D. M. Bylander and L. Kleinman, Phys. Rev. B **45**, 3245 (1992).

[13] K. Shirai, Phys. Rev. B **55**, 12235 (1997).

[14] I. M. Silvestrova, L. M. Belayev, Y. V. Pisarevski and T. Niemyski, Mater. Res. Bull. **9**, 1101 (1974).

[15] D. Gerlich and G. A. Slack, J. Mater. Sci. Lett. **4**, 639 (1985).

[16] R. J. Nelmes, J. S. Loveday, D. R. Allan, J. M. Besson, G. Hamel, P. Grima, and S. Hull, Phys. Rev. B **47**, 7668 (1993).

[17] S. O. Shalamberidze, G. I. Kalandadze, D. E. Khulelidze, and B. D. Tsurtsumia, Journal of Solid State Chemistry **154**, 199 (2000).

[18] Y. Ma, C. T. Prewitt, G. Zou, H-K. Mao, and R. J. Hemley, Phys. Rev. B **67**, 174116 (2003).

[19] P. Runow, J. Mater. Sci. **7**, 499 (1972).

[20] D. N. Sanz, P. Loubeyre, and M. Mezouar, Phys. Rev. Lett. **89**, 245501 (2002).

[21] Y. Imai, M. Mukaida, M. Ueda, and A. Watanabe, J. Alloys and Comp. **347**, 244 (2002).

[22] K. Shirai, A. Masago, and H. Katayama-Yoshida, phys. stat. sol. (b) **244**, 303 (2007).

[23] M. D Segall, P. J. D. Lindan, M. J. Probert, C. J. Pickard, P. J. Hasnip, S. J. Clark, and M. C. Payne, J. Phys. Condens. Matter **14**, 2717 (2002).

[24] Accelrys Inc., Materials Studio CASTEP, San Diego, *Accelrys Inc*, 2001.

[25] D. Vanderbilt, Phys. Rev. B **41**, 7892 (1990).

[26] J. P. Perdew, K. Burke, and M. Ernzerhof, Phys. Rev. Lett. **77**, 3865 (1996).

[27] J. F. Nye, *Physical Properties of Crystals* (Oxford University Press, Clarendon), 1957, pp 141.

[28] S. Bhagavantam, *Crystal Symmetry and Physical Properties*, (Academic Press, London) 1966, pp 135.

[29] W. Voigt, Lehrbuch der Kristallphysik (Teubner, Leipzig) 1928.

[30] A. Reuss, Z. Angew. Math. Mech. **9**, 49 (1929).

[31] R. Hill, Proc. Phys. Soc. London **65**, 349 (1952).

[32] M. Born, Proc. Camb. Phil. Soc. **36**, 160 (1940).

[33] M. Born and K. Huang, *Dynamical theory of Crystal Lattices* (Oxford University Press, Clarendon), 1956.

[34] B. F. Decker, J. S. Kasper, Acta Crystallogr.**12**, 503 (1959).

[35] G. A. Slack, C. I. Hejna, M. F. Garbauskas, and J. S. Kasper, J. Solid State Chem. **76**, 52 (1988).

[36] R. Lazzari, N. Vast, J. M. Besson, S. baroni, and A. Dal Corso, Phys. Rev. Lett. **83**, 3230 (1999).

[37] D. Emin J. Solid State Chem. **179**, 2791 (2006).

[38] M. L. Cohen, Mater. Sci. Eng. A **105/106**, 11 (1988).

[39] C. Kettel, *Introduction to Solid State Physics*, 7th ed. (John Wiley & Sons, Inc., Singapore), 2004, pp59.

[40] Z. Wanga, Y. Zhao, P. Lazor, H. Annersten, and S. K. Saxena, App. Phys. Lett. **86**, 041911 (2005).

Appendix

A.1 Infra-red and Raman active frequencies for B_{102}-D_{3d}, $C_{50}B_{34}$-C_{2h}, B_{80}-I_h, and C_{60} fullerenes

Harmonic vibrational frequencies of B_{102}-D_{3d} at B3LYP/6-31G*							
Frequencies (cm^{-1})	IR (km/mole)	Raman ($Å^4$/amu)	Mode	Frequencies (cm^{-1})	IR (km/mole)	Raman ($Å^4$/amu)	Mode
208.7952	0	0	?A	615.7802	0	0	A1U
212.1392	10.787	0	?A	620.477	0	0	A1U
212.1412	10.7896	0	?A	623.6231	7.4074	0	EU
216.8132	0.0014	0	EU	623.6293	7.413	0	EU
216.8139	0.0013	0	EU	632.6932	0	19.2126	EG
222.2418	0	74.5775	EG	632.6961	0	19.27	EG
222.2437	0	74.5901	EG	647.073	10.4603	0	A2U
225.3686	0	29.7448	A1G	647.0758	10.4626	0	A2U
229.5765	0	114.8729	EG	648.4938	0	14.2087	EU
229.579	0	114.8908	EG	648.6699	0	0.5918	EU
238.2184	0	41.8665	EG	648.6732	0	0.5837	EU
238.2232	0	41.7359	EG	648.947	0	0.0003	EU
243.8496	133.0175	0	EU	656.9702	3.7911	0	A2U
243.8562	133.0567	0	EU	660.8893	6.133	0	A2U
258.7664	0.0001	0	?A	660.8924	6.1545	0	A2U
261.8551	69.951	0	?A	665.9059	11.2525	0	A2U
261.859	69.9035	0	?A	665.9137	11.2445	0	A2U
266.2466	2.6314	0	A2U	666.1636	0	21.4189	EG
269.9737	0	11.585	?B	666.1674	0	21.4558	EG
269.9741	0	11.5876	?B	672.2805	0	3.2936	EG
274.3522	0	2.2501	A1G	672.2866	0	3.2821	EG

276.0301	0	0	?B	673.4475	97.4305	0	?C
284.5361	1.6399	0	EU	673.4597	97.3978	0	?C
284.5369	1.6412	0	EU	673.5613	0.0995	0	?C
288.2122	25.3814	0	A2U	678.3353	0	71.3567	?B
307.3659	0	21.9763	EG	678.3449	0	71.3391	?B
307.3735	0	21.9969	EG	679.2844	0.0001	0	?C
311.5552	0	0	A2G	682.5373	0.3189	0	?C
321.0571	4.1876	0	A2U	682.5394	0.3211	0	?C
322.4036	0	30.6382	A1G	685.3636	0	0	?B
328.9508	1.6599	0	EU	690.1291	0	3.0452	A1G
328.9531	1.6583	0	EU	693.0502	46.7143	0	EU
329.8608	0	35.783	?A	693.0509	46.7102	0	EU
329.8612	0	35.7071	?A	694.0525	6.9625	0	A2U
330.8415	0	91.978	?A	697.486	0	0	A1U
338.62	7.94	0	EU	697.8192	0	277.7864	EG
338.6203	7.9379	0	EU	697.8227	0	276.9632	EG
339.2512	0	0	A2G	704.7718	0	0	A2G
339.721	0.0003	0	A2U	712.4847	0	0	A1U
344.9	0	19.4271	EG	725.9897	2.3289	0	?D
344.9041	0	19.4885	EG	726.0002	2.3342	0	?D
349.7666	0	16.0305	?A	726.2971	30.5405	0	?D
349.7689	0	15.9931	?A	729.2842	0	22.49	EG
349.9564	0	98.0692	?A	729.2865	0	22.4546	EG
355.1844	0	0	A2G	729.869	8.1623	0	?D
355.3213	0	0	A1U	729.8699	8.1733	0	?D
361.7064	0	25.5922	EG	740.9242	0	64.3577	?A
361.7073	0	25.5888	EG	740.998	0	79.1397	?A
362.5859	16.9599	0	EU	741.004	0	78.9653	?A
362.5871	16.96	0	EU	744.6489	3.1546	0	A2U
371.6625	13.7922	0	EU	756.5164	0	205.1534	A1G
371.6633	13.799	0	EU	760.9287	0	14.2961	EG
372.0886	0	150.7765	A1G	760.9357	0	14.3018	EG
375.6825	0	0	A1U	763.3348	17.7041	0	EU
379.0613	7.1773	0	A2U	763.3362	17.7002	0	EU
384.4343	19.4296	0	EU	777.1348	0	39.7767	EG
384.4373	19.4259	0	EU	777.1373	0	39.7627	EG
385.3925	0	3.5772	EG	790.5344	0	223.5692	A1G
385.3932	0	3.5792	EG	799.0483	18.9936	0	EU
390.1417	0.7423	0	EU	799.0512	18.9964	0	EU
390.1434	0.7452	0	EU	808.9082	2.0056	0	A2U
393.5271	0	0	A1U	849.4526	0	47.089	EG
398.6648	0	0	A2G	849.4531	0	47.0529	EG
406.2246	16.6642	0	A2U	852.8291	0	41.5449	A1G
406.5485	0	16.4422	A1G	854.8766	0	0	A2G
408.8558	0	0.4776	EG	857.5543	0	19.1855	EG
408.8561	0	0.4757	EG	857.5556	0	19.1577	EG
421.0007	5.5309	0	EU	859.8658	11.0029	0	?A
421.0011	5.5309	0	EU	859.8675	11.0031	0	?A
426.9621	0	0	A2G	860.3161	0	0	?A
433.8646	0	6.5132	EG	860.8149	54.7533	0	A2U
433.8705	0	6.5236	EG	869.4806	0	7.9838	?A
437.5949	0	0	A1U	869.482	0	7.9903	?A
443.3236	0	32.4798	EG	869.6382	0	32.7044	?A
443.329	0	32.4212	EG	874.2409	124.7781	0	A2U
449.6183	13.8145	0	EU	877.3784	0	0.5847	EU
449.6187	13.8209	0	EU	877.3787	0	0.5852	EU

450.3425	0	9.0888	EG	877.4461	0	0.0001	EU
450.3435	0	9.0962	EG	877.9583	58.3862	0	EU
453.4343	11.4602	0	?B	877.9584	58.387	0	EU
453.6441	3.702	0	?B	880.4087	0	2.2476	EU
453.6464	3.7082	0	?B	888.3627	0	5.7271	EG
460.4346	0	2.5179	EG	888.3638	0	5.7373	EG
460.4367	0	2.5172	EG	893.0455	4.1451	0	EU
464.7717	2.9784	0	?B	893.0475	4.1501	0	EU
467.4358	2.0634	0	?B	896.4868	0	71.3069	A1G
467.4404	2.0648	0	?B	902.8233	2.1001	0	EU
470.1193	0	0	A2G	902.8236	2.0987	0	EU
476.3949	0	5.0106	?B	904.4089	11.9933	0	A2U
476.3987	0	5.0295	?B	913.0447	0	9.8169	EG
478.6414	0	0	A1U	913.0469	0	9.8275	EG
482.774	0	0	?B	914.1358	85.6983	0	?B
483.524	0	1.2687	A1G	915.6429	5.6591	0	?B
484.2358	1.3096	0	?B	915.6435	5.6552	0	?B
484.3945	32.1759	0	?B	923.988	0	0	A2G
484.3951	32.1767	0	?B	929.3799	0	0	A1U
488.8945	0	24.1972	EG	930.4533	0	0	A2G
488.8951	0	24.2087	EG	935.6949	63.5087	0	EU
493.8273	0	0.5812	A1G	935.6963	63.5076	0	EU
499.649	2.58	0	EU	941.2638	0	59.4612	EG
499.6494	2.5794	0	EU	941.264	0	59.474	EG
504.5639	0	0	A1U	944.5787	0	283.1932	A1G
505.0202	0	10.9975	EG	951.4031	10.5593	0	EU
505.0204	0	11.0092	EG	951.4041	10.5602	0	EU
508.971	0	255.5722	A1G	955.8201	0	198.6972	EG
513.8268	4.8263	0	EU	955.8209	0	199.2356	EG
513.8318	4.8267	0	EU	967.5027	0	0	A1U
516.7775	1.5816	0	A2U	971.1279	0	0	A2G
517.6762	0	0	A2G	978.2312	19.5907	0	EU
529.8195	0	218.874	EG	978.2336	19.5941	0	EU
529.82	0	218.8573	EG	989.5466	12.0254	0	A2U
530.5964	11.4332	0	EU	1002.9962	0	53.1112	EG
530.5979	11.4368	0	EU	1002.9966	0	53.0882	EG
536.0782	0	0.4643	A1G	1003.2494	0.004	0	?A
537.1376	11.6594	0	EU	1003.2505	0.004	0	?A
537.1402	11.661	0	EU	1004.2835	0	0	?A
539.1064	0	0	A1U	1010.8324	5.7015	0	EU
539.2437	0	4.4738	EG	1010.8325	5.7007	0	EU
539.2447	0	4.477	EG	1011.5965	0.0028	0	A2U
541.9499	8.7697	0	A2U	1018.0376	0	32.3046	?E
547.084	16.8984	0	EU	1018.0527	0	32.2308	?E
547.085	16.9005	0	EU	1023.006	0	15.7068	?E
549.2565	0	68.9991	EG	1023.0116	0	15.7018	?E
549.2573	0	68.985	EG	1024.3783	0	3.5149	A1G
562.1866	0.4664	0	EG	1024.8319	6.526	0	A2U
562.1877	0.4672	0	EG	1032.0615	0	38.5205	A1G
565.7352	0	73.3122	A1G	1069.2535	0	72.4852	A1G
567.5558	0	31.1203	EG	1074.4298	2.0652	0	EU
567.5603	0	31.0974	EG	1074.4299	2.065	0	EU
567.7791	0	0	EG	1074.9918	26.1674	0	A2U
569.4119	0.0338	0	EG	1077.5038	0	48.065	EG
573.6588	0	0	A2G	1077.505	0	47.9583	EG
574.87	6.1286	0	EU	1088.7202	0	224.6576	A1G

574.8739	6.1345	0	EU	1091.1121	0.1852	0	EU
580.4986	0	159.7278	EG	1091.1131	0.1853	0	EU
580.5019	0	159.7675	EG	1095.247	0	17.9858	EG
583.1643	0.0398	0	EU	1095.2474	0	18.0362	EG
583.1647	0.0399	0	EU	1097.5731	0	0	A1U
584.0215	0.4883	0	A2U	1320.7295	10.1625	0	EU
585.0643	0	58.3604	EG	1320.731	10.175	0	EU
585.0646	0	58.314	EG	1322.3249	0	116.9314	EG
591.2124	0	0	A2G	1322.3269	0	117.0085	EG
594.5289	47.9586	0	A2U	1330.4089	0	3.3009	A1G
597.7572	0	13.8197	EG	1337.0567	0.0018	0	A2U
597.7581	0	13.7849	EG	1342.102	0	64.4479	EG
599.8131	0	183.4104	A1G	1342.1027	0	64.4122	EG
600.2663	36.7358	0	EU	1353.4084	127.1052	0	A2U
600.2678	36.7342	0	EU	1368.9255	194.8152	0	EU
612.4235	0	0	A2G	1368.9374	194.8091	0	EU
615.3874	0	7.7128	A1G	1392.5362	0	65.275	A1G

Harmonic vibrational frequencies of $C_{50}B_{34}$-D_{3d} at B3LYP/6-31G*							
Frequencies (cm^{-1})	IR (km/mole)	Raman ($Å^4$/amu)	Mode	Frequencies (cm^{-1})	IR (km/mole)	Raman ($Å^4$/amu)	Mode
290.6477	0.8092	0	AU	776.1909	0.1017	0	AU
290.7533	0.4689	0	BU	777.8359	0	7.3179	BG
297.0619	0	22.3776	AG	778.1539	0	6.2836	AG
299.317	0	21.572	BG	789.9328	11.3502	0	AU
302.7268	5.4714	0	BU	790.7179	0	1.3737	AG
303.8682	2.4216	0	AU	794.3066	4.3125	0	BU
307.1072	1.6603	0	AU	794.7332	1.8105	0	AU
311.5083	20.0174	0	BU	794.8233	0	0.8394	BG
312.2357	0	18.6047	BG	798.5112	0	3.0871	AG
314.0832	14.5239	0	AU	800.8313	0	0.7713	BG
314.186	0	18.3222	AG	804.4319	0	0.0992	BG
318.463	16.4722	0	BU	804.6007	14.6062	0	BU
323.7225	0	21.1222	AG	804.9886	2.9255	0	AU
327.8343	0.7	0	AU	806.6992	0	1.6311	BG
358.125	0	0.1014	BG	807.6864	0	0.9319	AG
361.5165	0.8399	0	BU	809.3602	1.0881	0	AU
368.9133	3.4754	0	AU	810.225	3.1585	0	BU
377.8955	5.6904	0	BU	811.924	0	1.0996	AG
380.4007	0	0.1234	BG	815.904	0	2.5367	AG
384.1316	0	0.514	AG	815.9759	7.7361	0	AU
384.9137	0	0.1672	AG	820.5064	1.9678	0	BU
397.3802	0	0.0744	BG	823.1268	4.5686	0	AU
399.278	0	0.061	BG	831.3154	0.0791	0	AU
402.5659	0	0.4917	AG	837.2721	1.7419	0	BU
413.3308	0.4168	0	BU	837.2928	0	1.8261	BG
416.2638	0	129.181	AG	838.3065	0	1.0304	AG
418.018	0	0.0235	BG	848.4446	0	1.9201	BG
435.1054	0	0.0025	BG	854.7542	9.6018	0	AU
435.2002	0	0.862	AG	855.2454	6.9393	0	BU
445.4227	0	0.3755	BG	857.9566	0	10.686	AG
446.1836	0.2894	0	AU	859.8681	3.0186	0	AU

446.324	0	0.6374	AG	861.0715	0	2.3228	BG
449.1978	2.1036	0	BU	862.5174	20.4678	0	BU
455.6579	4.5829	0	AU	871.5419	0	8.5088	AG
458.6619	0.5939	0	BU	930.7353	0	4.8024	AG
462.3395	0	0.3283	AG	941.0639	0	2.3003	BG
464.8086	0.3525	0	AU	943.0507	6.8472	0	AU
470.512	1.2953	0	BU	948.172	17.4217	0	BU
477.2817	0	1.6018	AG	949.4807	0	0.4508	BG
477.3504	0	1.0815	BG	950.4473	0	2.2547	AG
478.9068	0	0.4795	BG	951.4335	0	0.3414	BG
487.7502	0	1.7811	AG	952.2207	19.3225	0	BU
487.9114	0	0.3892	BG	957.7474	0	1.1739	BG
493.3916	0.3753	0	AU	958.4139	40.9363	0	BU
499.8887	0	1.3422	AG	960.8693	0	28.5223	AG
503.6724	0.0008	0	AU	962.6023	0	0.4559	AG
508.1241	0	0.2609	BG	963.539	87.2904	0	AU
508.5999	0	0.7809	AG	968.3252	11.6064	0	AU
512.584	1.7547	0	BU	969.5424	0	2.2934	AG
513.7072	0	0.6047	AG	972.8633	102.0038	0	BU
514.2096	1.4275	0	AU	973.4593	0	2.633	BG
523.4091	4.5568	0	BU	974.5508	0	1.5845	AG
523.4415	5.6692	0	AU	981.1005	0	4.8925	AG
526.7386	0	1.9653	AG	981.2501	0	0.4935	BG
530.5844	0	2.0948	BG	984.5009	57.6672	0	BU
551.5419	0.4541	0	BU	991.7915	0	3.4214	AG
556.9232	0.134	0	AU	992.2218	11.0798	0	AU
560.684	0.6066	0	BU	1001.400	9.6976	0	BU
568.9073	24.8168	0	AU	1005.444	0	1.6445	AG
569.9918	74.1262	0	BU	1006.784	0	0.2274	BG
570.9877	22.6395	0	AU	1013.517	0	0.7803	BG
578.3811	77.7806	0	BU	1022.194	16.4414	0	BU
585.9472	0	0.276	BG	1026.886	1.9878	0	AU
588.652	0	0.4264	AG	1032.945	0	7.7903	AG
601.7709	13.5451	0	AU	1033.785	24.1988	0	AU
604.0223	0	0.0245	BG	1034.017	0	7.6451	BG
604.9738	14.1291	0	BU	1036.663	14.3111	0	BU
613.3737	0	0.1243	BG	1041.574	0	3.8643	BG
627.5774	0	15.2665	AG	1042.380	75.3012	0	AU
630.1268	0	11.9876	AG	1047.581	0	4.1242	AG
630.9639	0	1.9878	BG	1049.758	93.7901	0	BU
634.2069	2.1111	0	AU	1051.808	19.7452	0	BU
634.5869	0	1.9084	BG	1052.238	0	5.1053	AG
638.6482	2.8462	0	BU	1056.572	0.4767	0	AU
639.1516	0	0.8119	BG	1058.809	18.7969	0	BU
640.5913	8.9554	0	BU	1064.183	0	0.1245	BG
642.0655	0	0.8811	AG	1072.872	8.908	0	AU
642.2166	35.7901	0	BU	1073.276	0	1.8626	BG
648.627	3.6629	0	AU	1077.337	0	1.1149	AG
649.689	0	4.0911	AG	1085.396	0	2.0648	AG
650.7303	0	2.6846	BG	1091.259	17.4408	0	AU
652.83	3.0761	0	AU	1093.152	18.3147	0	BU
652.9729	10.386	0	BU	1098.655	0	0.4743	AG
655.728	33.0247	0	BU	1098.983	0	0.6939	BG
660.6369	0.0228	0	AU	1100.909	3.4466	0	AU
664.9901	21.4721	0	BU	1105.949	2.4516	0	BU
665.5512	0.0732	0	AU	1116.789	18.5519	0	BU

665.5903	0	5.0161	BG	1121.167	0	1.4681	AG
665.9849	0	4.1541	AG	1123.916	0.0859	0	AU
668.4388	0	2.59	AG	1124.044	0	0.7657	BG
672.3278	18.9893	0	BU	1125.881	3.0557	0	BU
673.5134	34.8671	0	AU	1128.510	1.1437	0	AU
679.0338	0	1.0512	BG	1132.060	1.1713	0	AU
680.9384	1.534	0	BU	1133.462	0	5.6831	AG
690.6379	0	1.4548	AG	1135.851	3.6991	0	BU
699.6854	0	3.8661	AG	1137.549	0	0.0209	BG
704.4779	0	0.8538	BG	1138.380	7.5977	0	AU
705.6306	5.7764	0	BU	1140.524	6.1951	0	BU
706.6064	15.9148	0	AU	1146.502	0	52.0979	AG
710.3445	9.3357	0	BU	1149.821	0	1.0397	BG
710.7912	0	2.2225	BG	1151.148	0	30.0412	AG
712.4065	0	0.2968	AG	1155.961	0.0452	0	AU
716.3711	1.8538	0	AU	1172.500	0	0.0305	BG
717.819	0	6.1126	AG	1181.795	0	1.1951	AG
718.5851	0	5.2646	BG	1186.382	18.4687	0	BU
719.7713	3.4325	0	BU	1194.961	8.8888	0	AU
721.1048	2.7472	0	AU	1195.773	0.2978	0	BU
726.7663	0.5643	0	AU	1201.430	4.846	0	BU
736.9113	0	2.5508	AG	1210.448	0	0.1961	BG
738.0218	1.0552	0	BU	1215.440	0	0.6237	AG
738.5723	0.3196	0	AU	1248.379	0	2.4599	AG
742.5483	0	2.102	BG	1624.534	11.3046	0	BU
743.204	2.058	0	BU	1627.502	0	21.8558	AG
744.322	0	0.2572	BG	1628.621	0	18.6609	BG
753.198	1.2011	0	BU	1645.016	122.0291	0	AU
756.899	2.3078	0	AU	1648.163	0	25.1984	AG
762.059	0	11.7961	AG	1650.658	160.4625	0	BU
765.1643	0	5.7909	AG	1679.639	0	27.4258	AG
766.0996	0	1.7332	BG	1682.549	31.3727	0	BU
772.1604	0.1272	0	AU	1717.156	0	11.4488	BG
773.3426	0.2309	0	BU	1730.287	101.9385	0	AU
774.0559	20.9544	0	BU	1742.443	153.3064	0	BU
775.6372	0	2.9429	BG	1753.020	0	33.5896	AG

Harmonic vibrational frequencies of B_{80}-I_h at B3LYP/6-31G*							
Frequencies (cm^{-1})	IR (km/mole)	Raman ($Å^4$/amu)	Mode	Frequencies (cm^{-1})	IR (km/mole)	Raman ($Å^4$/amu)	Mode
-141.6405	0	0	T2U	636.2709	0	0	?B
-141.6396	0	0	T2U	636.2715	0	0	?B
-141.6355	0	0	T2U	665.899	0	0	GU
-126.532	0	0	GG	665.8999	0	0	GU
-126.5308	0	0	GG	665.9012	0	0	GU
-126.5228	0	0	GG	665.9026	0	0	GU
-126.5219	0	0	GG	667.9155	0	0	T2U
176.795	0	66.7135	HG	667.9158	0	0	T2U
176.7954	0	66.7128	HG	667.916	0	0	T2U
176.7957	0	66.7119	HG	673.9838	0	0	T2G
176.7962	0	66.7156	HG	673.9843	0	0	T2G
176.7971	0	66.7179	HG	673.985	0	0	T2G

232.9207	0	0	GU	675.5829	0	0	T1G
232.9224	0	0	GU	675.583	0	0	T1G
232.9235	0	0	GU	675.5843	0	0	T1G
232.9253	0	0	GU	686.3354	0	0	GG
237.1148	0	0	T2U	686.3366	0	0	GG
237.1164	0	0	T2U	686.338	0	0	GG
237.1171	0	0	T2U	686.3385	0	0	GG
242.6701	0	0	GU	718.8595	0	2.0361	HG
242.6713	0	0	GU	718.8599	0	2.0341	HG
242.6723	0	0	GU	718.861	0	2.0361	HG
242.6728	0	0	GU	718.8614	0	2.0361	HG
264.8847	0	0	HU	718.8616	0	2.0373	HG
264.8848	0	0	HU	722.6764	0	0	T2U
264.885	0	0	HU	722.6775	0	0	T2U
264.8851	0	0	HU	722.679	0	0	T2U
264.8854	0	0	HU	728.2244	0	0	HU
272.7747	0	26.9096	HG	728.2251	0	0	HU
272.7771	0	26.9004	HG	728.2267	0	0	HU
272.778	0	26.9032	HG	728.2271	0	0	HU
272.7794	0	26.9084	HG	728.2285	0	0	HU
272.7802	0	26.9159	HG	739.4618	86.9901	0	T1U
300.1357	0	0	GG	739.4627	86.9914	0	T1U
300.1363	0	0	GG	739.4631	86.9929	0	T1U
300.1365	0	0	GG	761.6437	0	0	T1G
300.1369	0	0	GG	761.6462	0	0	T1G
310.4618	42.2257	0	T1U	761.6484	0	0	T1G
310.4636	42.2251	0	T1U	767.9834	0	0	GU
310.4652	42.2271	0	T1U	767.9839	0	0	GU
315.1725	0	7.8285	HG	767.9842	0	0	GU
315.1726	0	7.8317	HG	767.9848	0	0	GU
315.1729	0	7.8327	HG	840.7819	0	12.857	HG
315.1731	0	7.8313	HG	840.7822	0	12.8563	HG
315.1732	0	7.8254	HG	840.7832	0	12.861	HG
320.6667	0	195.2326	AG	840.7842	0	12.8703	HG
346.8368	0	0	T2G	840.7857	0	12.8675	HG
346.8373	0	0	T2G	860.7353	0	0	GG
346.8377	0	0	T2G	860.7355	0	0	GG
362.019	0	0	HU	860.7361	0	0	GG
362.0193	0	0	HU	860.7365	0	0	GG
362.0194	0	0	HU	863.854	0	0	AU
362.0194	0	0	HU	899.1952	25.3171	0	T1U
362.0197	0	0	HU	899.1964	25.3094	0	T1U
417.9115	0	64.6733	AG	899.1971	25.3021	0	T1U
424.5415	2.3832	0	T1U	910.2299	0	0	T2U
424.5418	2.3824	0	T1U	910.2301	0	0	T2U
424.5428	2.3819	0	T1U	910.2313	0	0	T2U
426.8536	0	0	GG	930.6834	0	0	GU
426.8537	0	0	GG	930.6835	0	0	GU
426.854	0	0	GG	930.6838	0	0	GU
426.8544	0	0	GG	930.684	0	0	GU
437.4513	0	0	GU	932.4523	0	0.129	HG
437.4518	0	0	GU	932.4526	0	0.1281	HG
437.452	0	0	GU	932.4527	0	0.1285	HG
437.4522	0	0	GU	932.4529	0	0.1282	HG
446.3233	28.4877	0	T1U	932.4532	0	0.1282	HG
446.3241	28.4874	0	T1U	941.401	0	364.6852	AG

446.3252	28.4874	0	T1U	965.6197	578.653	0	T1U
468.2197	0	0	T1G	965.6214	578.6871	0	T1U
468.2204	0	0	T1G	965.6219	578.6933	0	T1U
468.2208	0	0	T1G	976.9182	0	0	T1G
472.5059	0	0	T2G	976.9188	0	0	T1G
472.5062	0	0	T2G	976.92	0	0	T1G
472.5069	0	0	T2G	980.3572	0	0	GG
490.643	0	15.4443	HG	980.358	0	0	GG
490.6434	0	15.4302	HG	980.3588	0	0	GG
490.6435	0	15.4441	HG	980.3596	0	0	GG
490.6438	0	15.4278	HG	1000.7617	0	0	HU
490.644	0	15.4317	HG	1000.7621	0	0	HU
502.2284	0	0	T2U	1000.7625	0	0	HU
502.2285	0	0	T2U	1000.7627	0	0	HU
502.2286	0	0	T2U	1000.7629	0	0	HU
526.9426	0	0	HU	1011.8201	0	0	HU
526.9439	0	0	HU	1011.8208	0	0	HU
526.9444	0	0	HU	1011.8216	0	0	HU
526.9445	0	0	HU	1011.8224	0	0	HU
526.946	0	0	HU	1011.8229	0	0	HU
545.5868	0	0	HU	1020.9532	0	0	T2U
545.5872	0	0	HU	1020.9545	0	0	T2U
545.5876	0	0	HU	1020.9551	0	0	T2U
545.5878	0	0	HU	1021.5203	0	20.2408	HG
545.5882	0	0	HU	1021.5209	0	20.2417	HG
567.085	0	0	?A	1021.5223	0	20.2391	HG
567.0852	0	0	?A	1021.5224	0	20.2393	HG
567.0854	0	0	?A	1021.5233	0	20.2377	HG
567.086	0	0	?A	1046.1278	0	0	GG
568.0023	0	23.885	?A	1046.1286	0	0	GG
568.0034	0	23.8825	?A	1046.1289	0	0	GG
568.0045	0	23.8833	?A	1046.1298	0	0	GG
568.0049	0	23.8838	?A	1073.9748	0	0	T2G
568.0058	0	23.8786	?A	1073.9754	0	0	T2G
605.6734	0	0	GU	1073.9757	0	0	T2G
605.6736	0	0	GU	1075.2785	0	0	HU
605.6737	0	0	GU	1075.2796	0	0	HU
605.6748	0	0	GU	1075.2799	0	0	HU
610.2049	0	0	T2G	1075.28	0	0	HU
610.205	0	0	T2G	1075.2811	0	0	HU
610.2056	0	0	T2G	1088.4038	0	106.9273	HG
635.3741	0	3.4769	?B	1088.405	0	106.8826	HG
635.3748	0	3.4815	?B	1088.4057	0	106.9017	HG
635.3756	0	3.4773	?B	1088.4064	0	106.9027	HG
635.377	0	3.4823	?B	1088.4075	0	106.9049	HG
635.3771	0	3.4801	?B	1095.5615	0	0	GU
636.2693	0	0	?B	1095.5618	0	0	GU
636.2694	0	0	?B	1095.5639	0	0	GU
636.2704	0	0	?B	1095.5641	0	0	GU

Harmonic vibrational frequencies of C_{60}-I_h at B3LYP/6-31G*							
Frequencies (cm^{-1})	IR (km/mole)	Raman ($Å^4$/amu)	Mode	Frequencies (cm^{-1})	IR (km/mole)	Raman ($Å^4$/amu)	Mode
265.0357	0	22.5813	HG	804.5631	0	0	T2G
265.036	0	22.5776	HG	804.5632	0	0	T2G
265.0365	0	22.5781	HG	840.4414	0	0	T1G
265.037	0	22.5795	HG	840.4422	0	0	T1G
265.0375	0	22.5802	HG	840.4428	0	0	T1G
340.3348	0	0	T2U	966.1879	0	0	AU
340.3351	0	0	T2U	977.7126	0	0	?A
340.3352	0	0	T2U	977.7129	0	0	?A
356.7669	0	0	GU	977.7144	0	0	?A
356.7677	0	0	GU	983.2658	0	0	?A
356.7687	0	0	GU	983.2692	0	0	?A
356.769	0	0	GU	983.2711	0	0	?A
407.8596	0	0	HU	983.2714	0	0	?A
407.8599	0	0	HU	1095.630	0	0	GG
407.8604	0	0	HU	1095.630	0	0	GG
407.8609	0	0	HU	1095.632	0	0	GG
407.8612	0	0	HU	1095.633	0	0	GG
434.8959	0	0.4519	HG	1127.035	0	12.7293	HG
434.896	0	0.4518	HG	1127.037	0	12.7304	HG
434.8962	0	0.4528	HG	1127.038	0	12.726	HG
434.8964	0	0.4517	HG	1127.039	0	12.7283	HG
434.8965	0	0.4519	HG	1127.040	0	12.7317	HG
487.8865	0	0	GG	1202.185	0	0	T2U
487.8866	0	0	GG	1202.185	0	0	T2U
487.8869	0	0	GG	1202.186	0	0	T2U
487.8871	0	0	GG	1214.910	9.0554	0	T1U
497.1464	0	129.1253	AG	1214.911	9.0573	0	T1U
534.4323	28.9007	0	T1U	1214.912	9.0576	0	T1U
534.4325	28.8998	0	T1U	1245.550	0	0	HU
534.4326	28.9	0	T1U	1245.551	0	0	HU
539.4518	0	0	HU	1245.552	0	0	HU
539.4521	0	0	HU	1245.552	0	0	HU
539.4523	0	0	HU	1245.553	0	0	HU
539.4526	0	0	HU	1277.629	0	22.9557	HG
539.4531	0	0	HU	1277.629	0	22.9392	HG
566.4465	0	0	T2G	1277.629	0	22.9537	HG
566.4466	0	0	T2G	1277.629	0	22.9466	HG
566.4467	0	0	T2G	1277.630	0	22.9516	HG
569.3234	0	0	T1G	1303.153	0	0	T1G
569.3237	0	0	T1G	1303.154	0	0	T1G
569.3242	0	0	T1G	1303.155	0	0	T1G
576.0555	0	0	GG	1334.967	0	0	?B
576.0555	0	0	GG	1334.967	0	0	?B
576.0557	0	0	GG	1334.968	0	0	?B
576.0558	0	0	GG	1334.968	0	0	?B
588.0809	10.523	0	T1U	1335.309	0	0	?B
588.0824	10.5235	0	T1U	1335.31	0	0	?B
588.0844	10.5235	0	T1U	1335.310	0	0	?B
678.7523	0	0	HU	1335.311	0	0	?B
678.7528	0	0	HU	1371.706	0	0	HU
678.7532	0	0	HU	1371.706	0	0	HU
678.7535	0	0	HU	1371.707	0	0	HU

678.7538	0	0	HU	1371.707	0	0	HU
716.9258	0	0.4432	HG	1371.708	0	0	HU
716.9264	0	0.4439	HG	1373.092	0	0	T2G
716.927	0	0.4436	HG	1373.093	0	0	T2G
716.9271	0	0.4435	HG	1373.093	0	0	T2G
716.9279	0	0.4433	HG	1455.042	0	2.7377	HG
720.468	0	0	T2U	1455.043	0	2.7334	HG
720.4683	0	0	T2U	1455.043	0	2.7351	HG
720.4686	0	0	T2U	1455.044	0	2.7316	HG
735.2528	0	0	T2G	1455.044	0	2.7381	HG
735.2528	0	0	T2G	1460.672	11.8867	0	T1U
735.2529	0	0	T2G	1460.672	11.8862	0	T1U
740.7703	0	0	HU	1460.673	11.8876	0	T1U
740.7706	0	0	HU	1464.513	0	0	GU
740.7708	0	0	HU	1464.514	0	0	GU
740.771	0	0	HU	1464.515	0	0	GU
740.7713	0	0	HU	1464.515	0	0	GU
750.807	0	0	GU	1503.816	0	408.3615	AG
750.8071	0	0	GU	1537.914	0	0	GG
750.8073	0	0	GU	1537.914	0	0	GG
750.8074	0	0	GU	1537.914	0	0	GG
753.3554	0	0	GG	1537.915	0	0	GG
753.3557	0	0	GG	1566.237	0	0	T2U
753.3558	0	0	GG	1566.237	0	0	T2U
753.3561	0	0	GG	1566.237	0	0	T2U
765.4314	0	0	GU	1607.880	0	0	HU
765.4316	0	0	GU	1607.880	0	0	HU
765.4317	0	0	GU	1607.880	0	0	HU
765.4321	0	0	GU	1607.881	0	0	HU
787.5519	0	8.4433	HG	1607.881	0	0	HU
787.5559	0	8.4436	HG	1617.091	0	50.265	HG
787.5576	0	8.444	HG	1617.091	0	50.2767	HG
787.5594	0	8.4429	HG	1617.092	0	50.258	HG
787.5612	0	8.4442	HG	1617.092	0	50.2715	HG
804.5631	0	0	T2G	1617.092	0	50.2717	HG

A.2 Band structure of B_{32}-tube

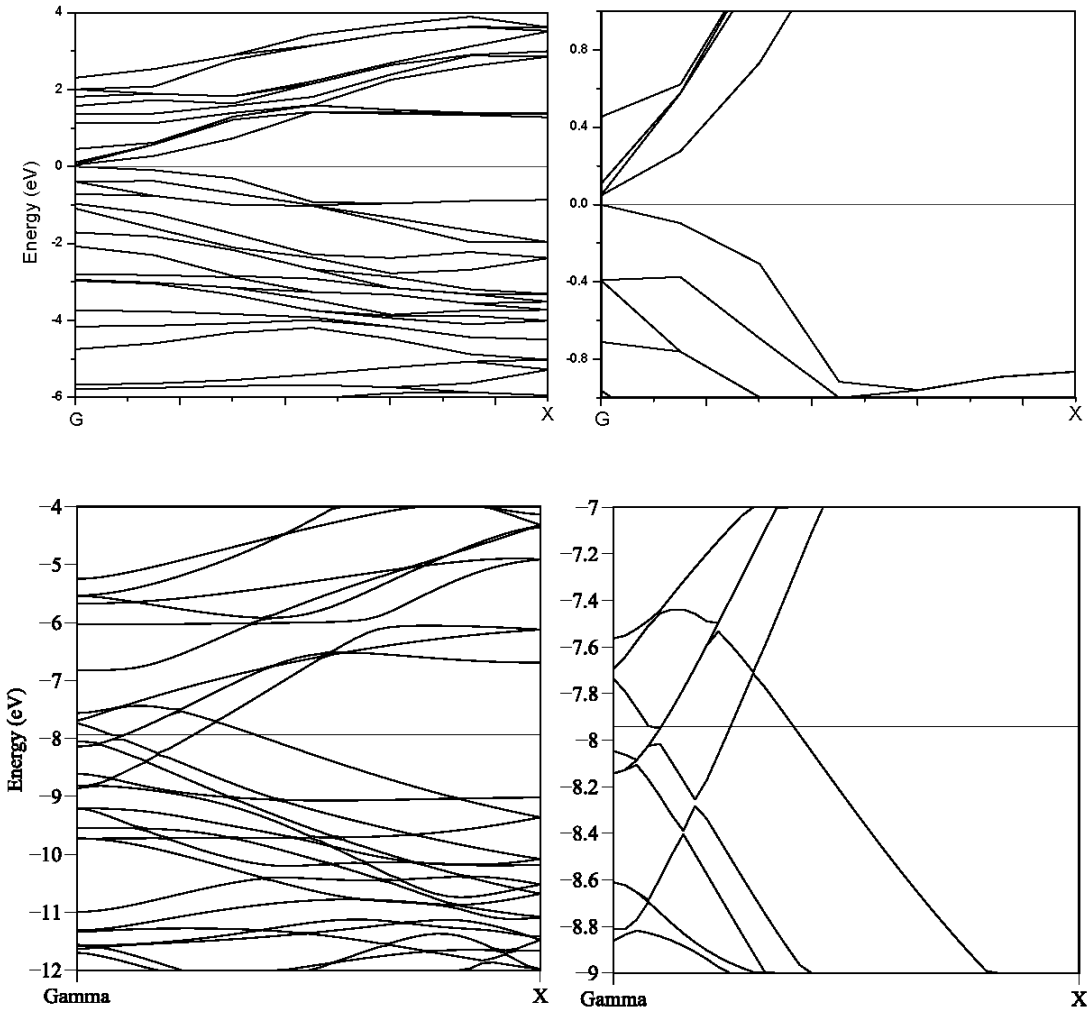

(Top) DFT (LDA/CA-PZ) and (bottom) eH band structure of B_{32}-tube and their expanded band structures are shown in the right.

PUBLICATIONS

Included in Thesis

1. Electronic structure and bonding of β–rhombohedral boron using cluster fragment approach, Dasari L. V. K. Prasad, Musiri M. Balakrishnarajan, and Eluvathingal D. Jemmis, Phys. Rev. B **72**, 195102 (2005).

2. Boron and MgB_2 analogs of fullerenes and carbon nanotubes: A density functional theory study, Dasari L. V. K. Prasad and Eluvathingal D. Jemmis, J. Mol. Struct. (Theochem) **771**, 111 (2006).

3. Icosahedral B_{12}, macropolyhedral boranes, β–rhombohedral boron and boron-rich solids, Eluvathingal D. Jemmis and Dasari L. V. K. Prasad, J. Solid State Chem. **179**, 2768 (2006).

4. Stuffing improves the stability of fullerenelike boron clusters, Dasari L. V. K. Prasad and Eluvathingal D. Jemmis, Phys. Rev. Lett. **100**, 165504 (2008). [Also published in the May 5, 2008 issue of Virtual Journal of Nanoscale Science & Technology].

5. Stuffed fullerene-like boron carbide clusters, Dasari L. V. K. Prasad and Eluvathingal D. Jemmis, (to be submitted).

6. Electronic structure of boron sheets and nanotubes in view of graphene and carbon nanotubes, Dasari L. V. K. Prasad and Eluvathingal D. Jemmis, (to be submitted).

7. Mechanical stability and properties of boron allotropes and boron-rich solids, Dasari L. V. K. Prasad and Eluvathingal D. Jemmis, (to be submitted).

Not Included in Thesis

1. Electronic structure and bonding studies on triple-decker sandwich complexes with a P_6 middle ring, Dandamudi Usharani, Dasari L. V. K. Prasad, John F. Nixon, and Eluvathingal D. Jemmis, J. Comp. Chem. **28**, 310 (2007).

2. $Si_xC_{1-x}O_2$ alloys: A possible route to stabilize carbon-based silica-like solids? Shobhana Narasimhan et al., Solid State Comm. **144**, 273 (2007).

Pedagogical Articles

1. Unknowns in the chemistry of boron, Eluvathingal D. Jemmis and Dasari L. V. K. Prasad, Current Science **95**, 1277 (2008).

Presentations

1. Boron fullerenes and MgB_2 nanotubes, Dasari L. V. K. Prasad and Eluvathingal D. Jemmis, NCSCA-2003, IIT-Delhi, Delhi, India.

2. Is MgB_2 unique?, Eluvathingal D. Jemmis and Dasari L. V. K. Prasad, Annual in-house symposiums-2003, School of Chemistry, University of Hyderabad, India.

3. Design of materials based on chemical binding: Boron-rich solids, Dasari L. V. K. Prasad and Eluvathingal D. Jemmis, ICTP – summer school and workshop on "Electronic Structure Methods and Their Applications", 2006, JNCASR, Bangalore, India.

4. Studies of clusters and solids: A comparison between boron and carbon, Eluvathingal D. Jemmis and Dasari L. V. K. Prasad, NANO-2006, IISc, Bangalore, India.

5. *Ab initio* studies on electronic, elastic and dynamical behavior of graphite and graphene analogues of boron, Dasari L. V. K. Prasad and Eluvathingal D. Jemmis, 11^{th} V. A. Fock-Meeting, September-2007, Anapa, Russia.

6. Carbon analogues of boron nanomaterials, Dasari L. V. K. Prasad and Eluvathingal D. Jemmis, October 9^{th}, 2007, Moscow State University, Moscow, Russia.

“It would be possible to describe everything scientifically, but it would make no sense; it would be without meaning, as if you described a Beethoven symphony as a variation of wave pressure.”

- Albert Einstein